Supporting Information for

Structural factors determining thermal stability limits of ionic liquid/MOF composites: Imidazolium ionic liquids combined with CuBTC and ZIF-8

Muhammad Zeeshan, [†,‡] Vahid Nozari,[†,‡] Seda Keskin,[*,†,‡] and Alper Uzun[*,†,‡,ξ]

[†]*Department of Chemical and Biological Engineering, Koç University, Rumelifeneri Yolu, 34450 Sariyer, Istanbul, Turkey*

[‡]*Koç University TÜPRAŞ Energy Center (KUTEM), Koç University, Rumelifeneri Yolu, 34450 Sariyer, Istanbul, Turkey*

[ξ]*Koç University Surface Science and Technology Center (KUYTAM), Koç University, Rumelifeneri Yolu, Sariyer, 34450 Istanbul, Turkey;*

Table S1. Names and molecular structures of the imidazolium based ILs considered in this work.

Name of IL	Cation	Anion	Molecular structure
1-Ethyl-3-methylimidazolium hexafluorophosphate	[EMIM]	[PF_6]	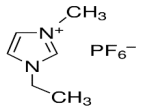
1,3-Dimethoxyimidazolium bis(trifluoromethyl-sulfonyl)imide	[$(MeO)_2$IM]	[NTf_2]	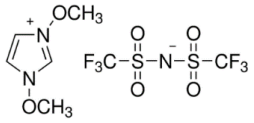
1,3-Dimethoxy-2-methylimidazolium bis(trifluoromethylsulfonyl)imide	[$(MeO)_2$MIM]	[NTf_2]	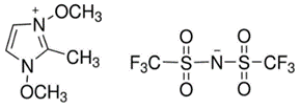
1-(3-Cyanopropyl)-3-methylimidazolium bis(trifluoromethylsulfonyl)imide	[CPMIM]	[NTf_2]	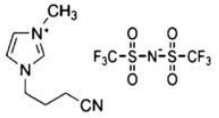
1,3-Dihydroxyimidazolium bis(trifluoromethylsulfonyl)imide	[$(OH)_2$IM]	[NTf_2]	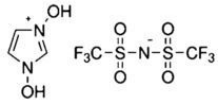
1-Allyl-3-methylimidazolium bis(trifluoromethylsulfonyl)imide	[AllylMIM]	[NTf_2]	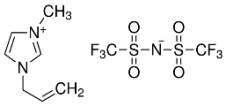
1,3-Diethoxyimidazolium bis(trifluoromethylsulfonyl)imide	[$(EtO)_2$IM]	[NTf_2]	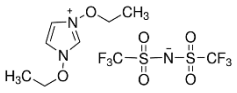
1-Butyl-3-methylimidazolium thiocyanate	[BMIM]	[SCN]	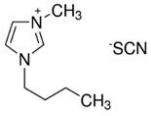
1-Butyl-3-methylimidazolium hexafluoroantimonate	[BMIM]	[SbF_6]	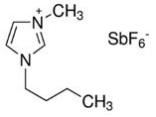
1-Butyl-3-methylimidazolium bis(trifluoromethylsulfonyl)imide	[BMIM]	[NTf_2]	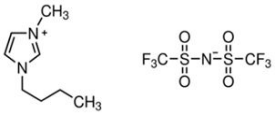

1-Butyl-3-methylimidazolium methanesulfonate	[BMIM]	[$MeSO_3$]	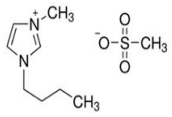
1-Butyl-3-methylimidazolium methyl sulfate	[BMIM]	[$MeSO_4$]	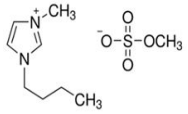
1-Butyl-3-methylimidazolium Octyl sulfate	[BMIM]	[$OcSO_4$]	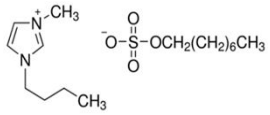
1-Butyl-3-methylimidazolium trifluoromethanesulfonate	[BMIM]	[CF_3SO_3]	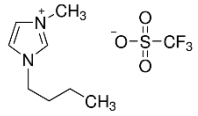
1-Butyl-3methylimidazolium dicyanamide	[BMIM]	[DCA]	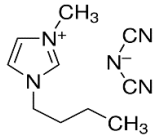
1-Ethyl-3-Methylimidazolium dicyanamide	[EMIM]	[DCA]	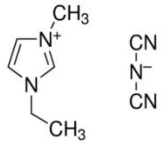
1-Methyl-3-propylimidazolium bis(trifluoromethylsulfonyl)imide	[MPMIM]	[NTf_2]	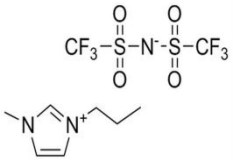
1-Butyl-2.3-dimethylimidazolium hexafluorophosphate	[BMMIM]	[PF_6]	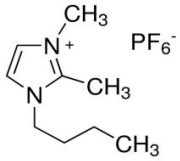
1-Butyl-3-methylimidazolium hexafluorophophate	[BMIM]	[PF_6]	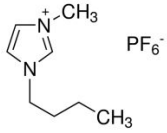

1-Butyl-3-methylimidazolium dibutylphosphate	[BMIM]	[DBP]	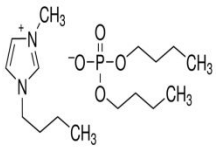
1-Butyl-3-methylimidazolium trifluoracetate	[BMIM]	[TFA]	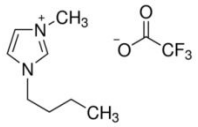
1-Ethyl-3-methylimidazolium methylsulfate	[EMIM]	[$MESO_4$]	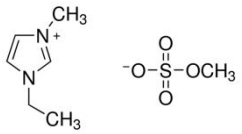
1-Butyl-3-methylimidazolium acetate	[BMIM]	[AC]	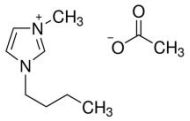
1-Ethyl-3-methylimidazolium diethyl phosphate	[EMIM]	[DEP]	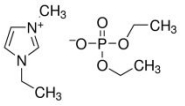
1,3-Dimethylimidazolium dimethyl phosphate	[DMIM]	[DMP]	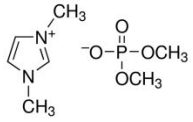
1-Hexyl-3-methylimidazolium tetrafluoroborate	[HMIM]	[BF_4]	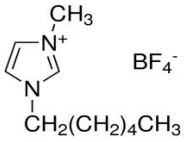
1-Ethyl-3-methylimidazolium thiocyanate	[EMIM]	[SCN]	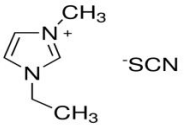
1-Decyl-3-methylimidazolium tetrafluoroborate	[C_{10}MIM]	[BF_4]	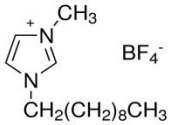
1-Butyl-3-methylimidazolium tetrafluoroborate	[BMIM]	[BF_4]	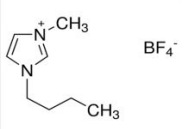

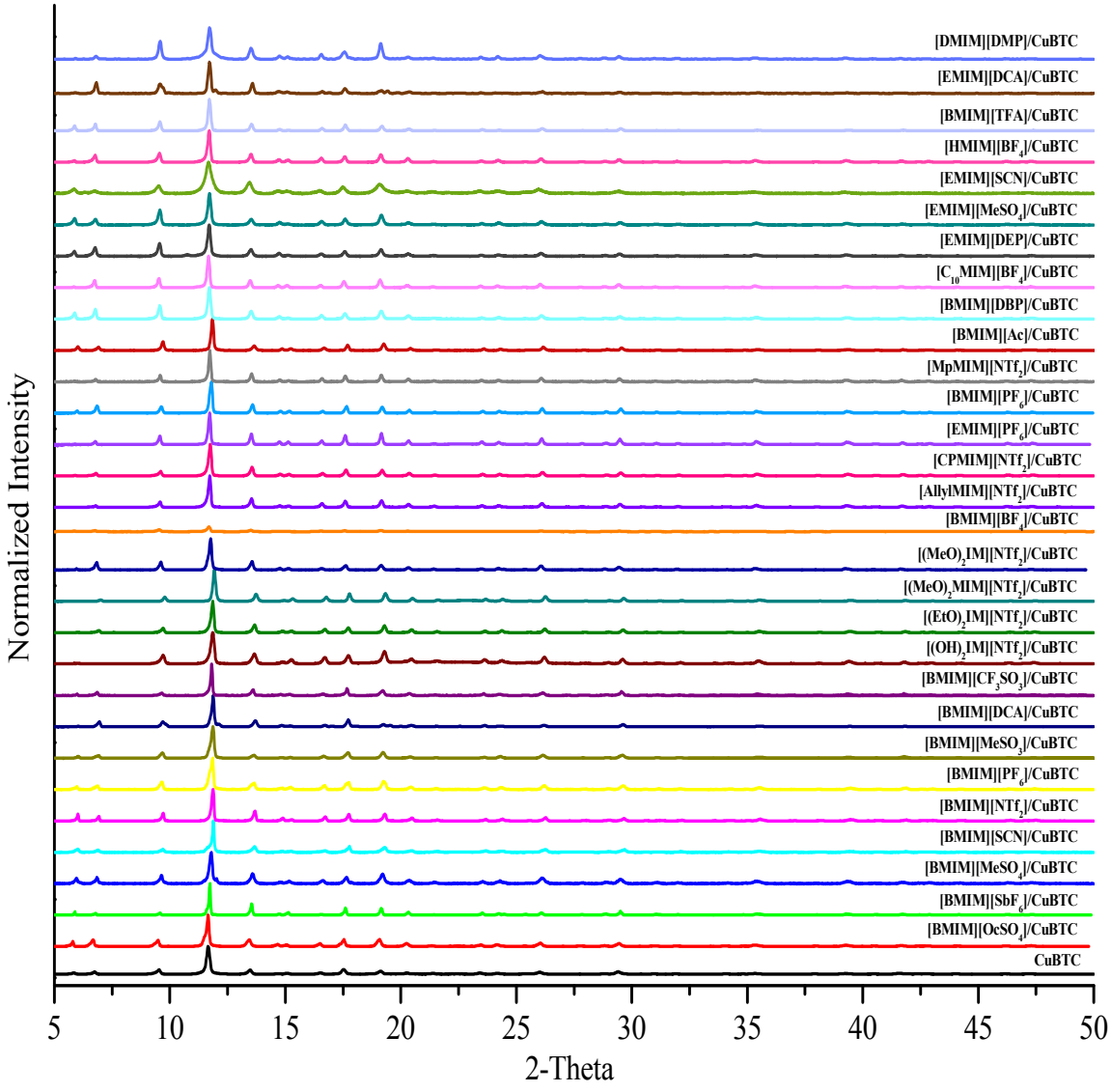

Figure S1. XRD patterns of pristine CuBTC and IL/CuBTC composites.

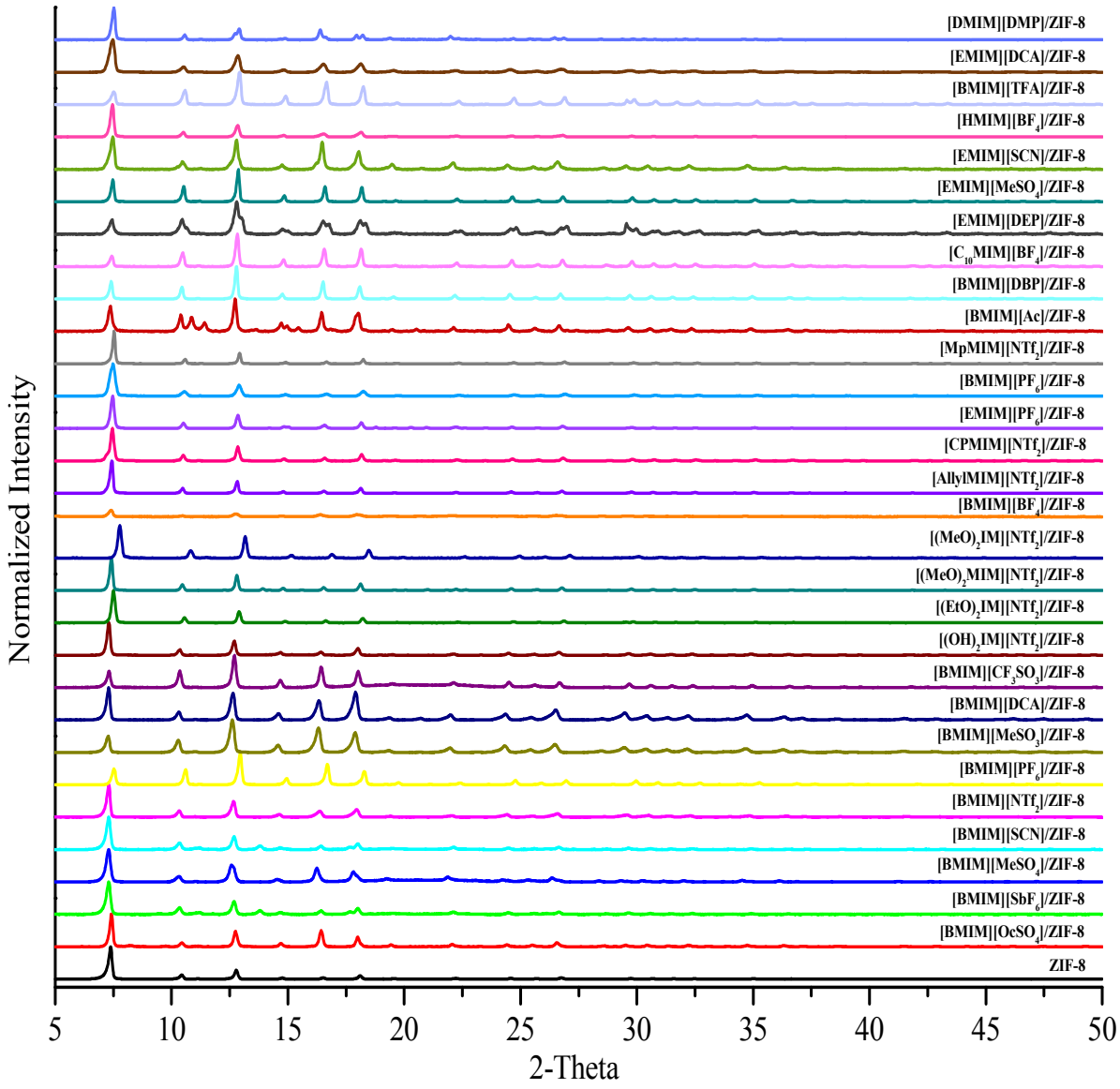

Figure S2. XRD patterns of pristine ZIF-8 and IL/ZIF-8 composites.

Table S2. BET surface area and pore volume of pristine MOFs.

Pristine MOFs	S_{BET} (m^2/g)	Pore volume (cm^3/g)
CuBTC	1324	0.52
ZIF-8	1208	0.63

Table S3. BET Surface area and pore volume of IL/MOF composites.

Cation	Anion	IL/CuBTC Composites		IL/ZIF-8 Composites	
		S_{BET} (m^2/g)	Pore volume (cm^3/g)	S_{BET} (m^2/g)	Pore volume (cm^3/g)
[EMIM]	[PF_6]	238.10	0.03	308	0.19
[$(MeO)_2$IM]	[NTf_2]	53	0.10	631	0.34
[$(MeO)_2$MIM]	[NTf_2]	344	0.16	568	0.32
[CPMIM]	[NTf_2]	601	0.28	726	0.39
[$(OH)_2$IM]	[NTf_2]	6	0.02	83	0.06
[AllylMIM]	[NTf_2]	487	0.22	0.86	0.03
[BMIM]	[BF_4]	247*,1	0.002*1	177*,2	0.11*,2
[$(EtO)_2$IM]	[NTf_2]	399	0.18	509	0.29
[BMIM]	[SCN]	88*,3	0.07*,3	48*,4	0.02*,4
[BMIM]	[SbF_6]	601*,3	0.32*,3	221	0.01
[BMIM]	[NTf_2]	319*,3	0.14*,3	2.6	0.01
[BMIM]	[$MeSO_3$]	128*,3	0.06*,3	195	0.03
[BMIM]	[$MeSO_4$]	339*,3	0.15*,3	233	0.02
[BMIM]	[$OcSO_4$]	142*,3	0.06*,3	195	0.03
[BMIM]	[CF_3SO_3]	357*,3	0.16*,3	362	0.04
[BMIM]	[DCA]	54	0.03	55	0.03
[EMIM]	[DCA]	16	0.01	51	0.01
[MPMIM]	[NTf_2]	390	0.18	4.99	0.002
[BMMIM]	[PF_6]	306	0.14	766	0.42
[BMIM]	[PF_6]	364*,5	0.06*,5	415*,6	0.22*,6
[BMIM]	[DBP]	374	0.17	167	0.07
[BMIM]	[TFA]	131	0.06	491	0.30
[EMIM]	[$MESO_4$]	114	0.05	329	0.21
[BMIM]	[AC]	0.77	0.01	15	0.02
[EMIM]	[DEP]	131	0.06	238	0.15
[DMIM]	[DMP]	0.94	0.003	276	0.16
[HMIM]	[BF_4]	404	0.18	107	0.14
[EMIM]	[SCN]	3.4	0..02	129	0.12
[C_{10}MIM]	[BF_4]	225	0.09	261	0.26

*BET surface area and pore volume values were obtained from the previous published works of our group.

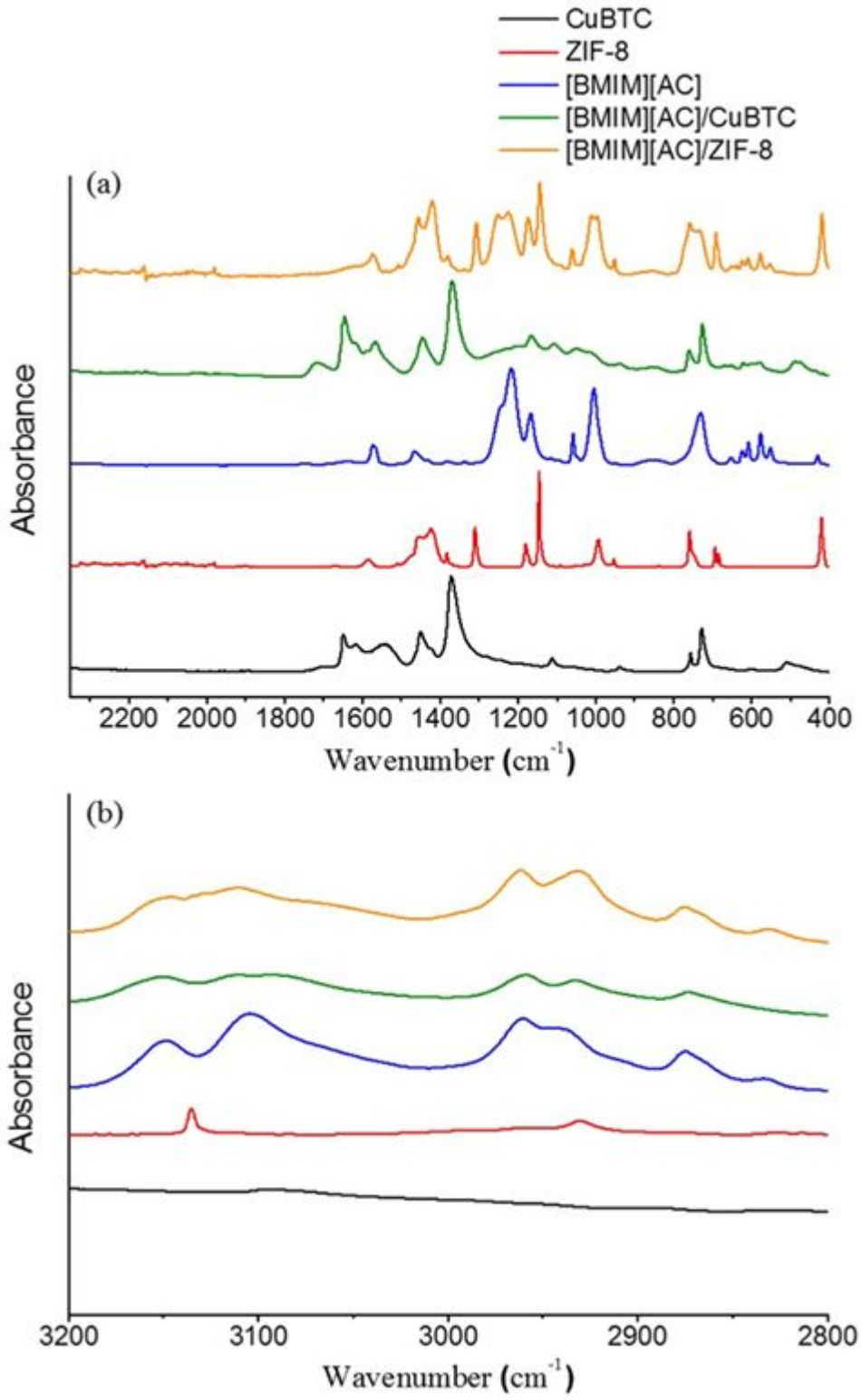

Figure S3. FTIR spectra of CuBTC, ZIF-8, [BMIM][AC], [BMIM][AC]/CuBTC, and [BMIM][AC]/ZIF-8 (a) 400-2250 cm^{-1} and (b) 2800-3200 cm^{-1}.

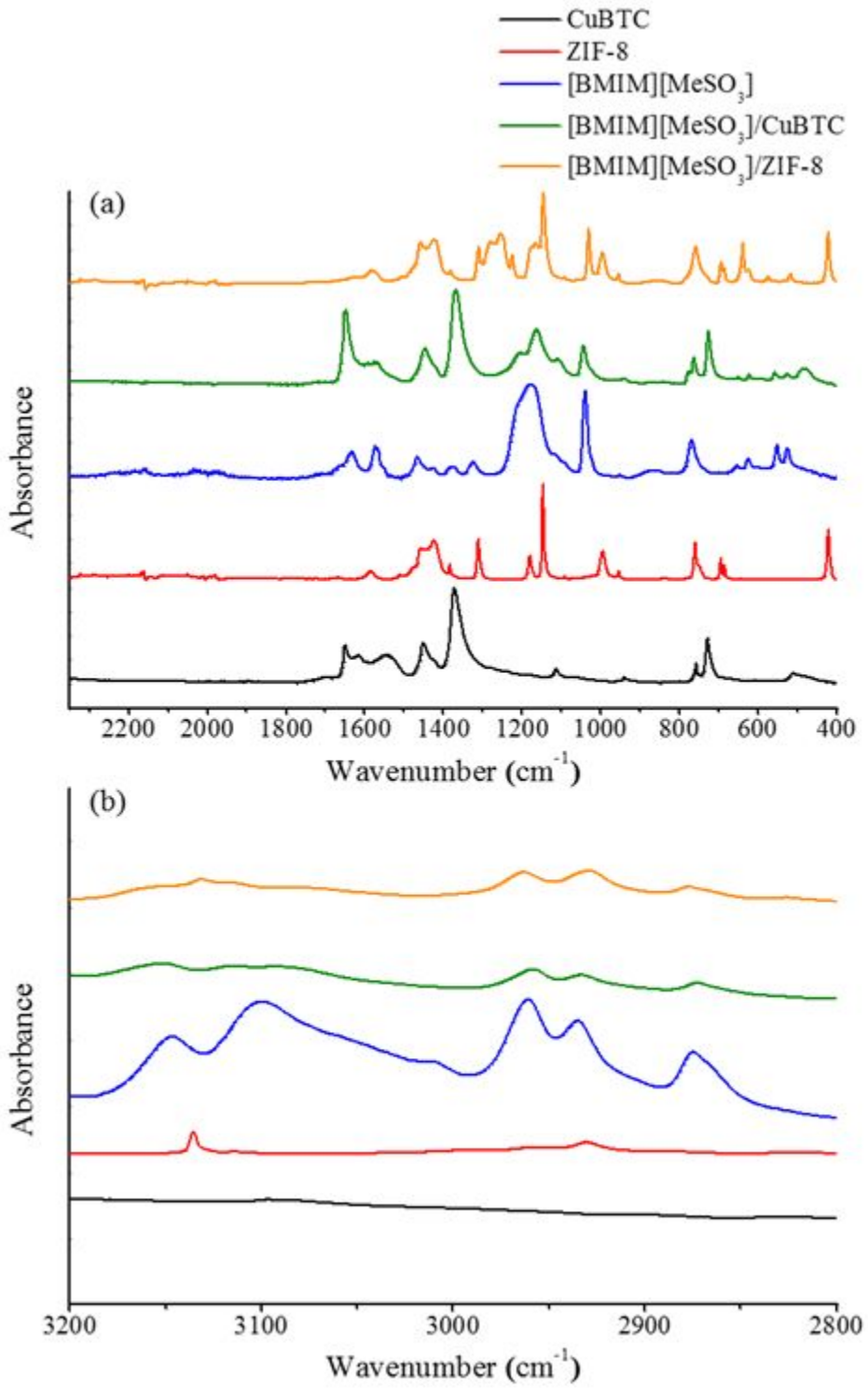

Figure S4. FTIR spectra of CuBTC, ZIF-8, [BMIM][$MeSO_3$], [BMIM][$MeSO_3$]/CuBTC, and [BMIM][$MeSO_3$]/ZIF-8 (a) 400-2250 cm^{-1} and (b) 2800-3200 cm^{-1}.

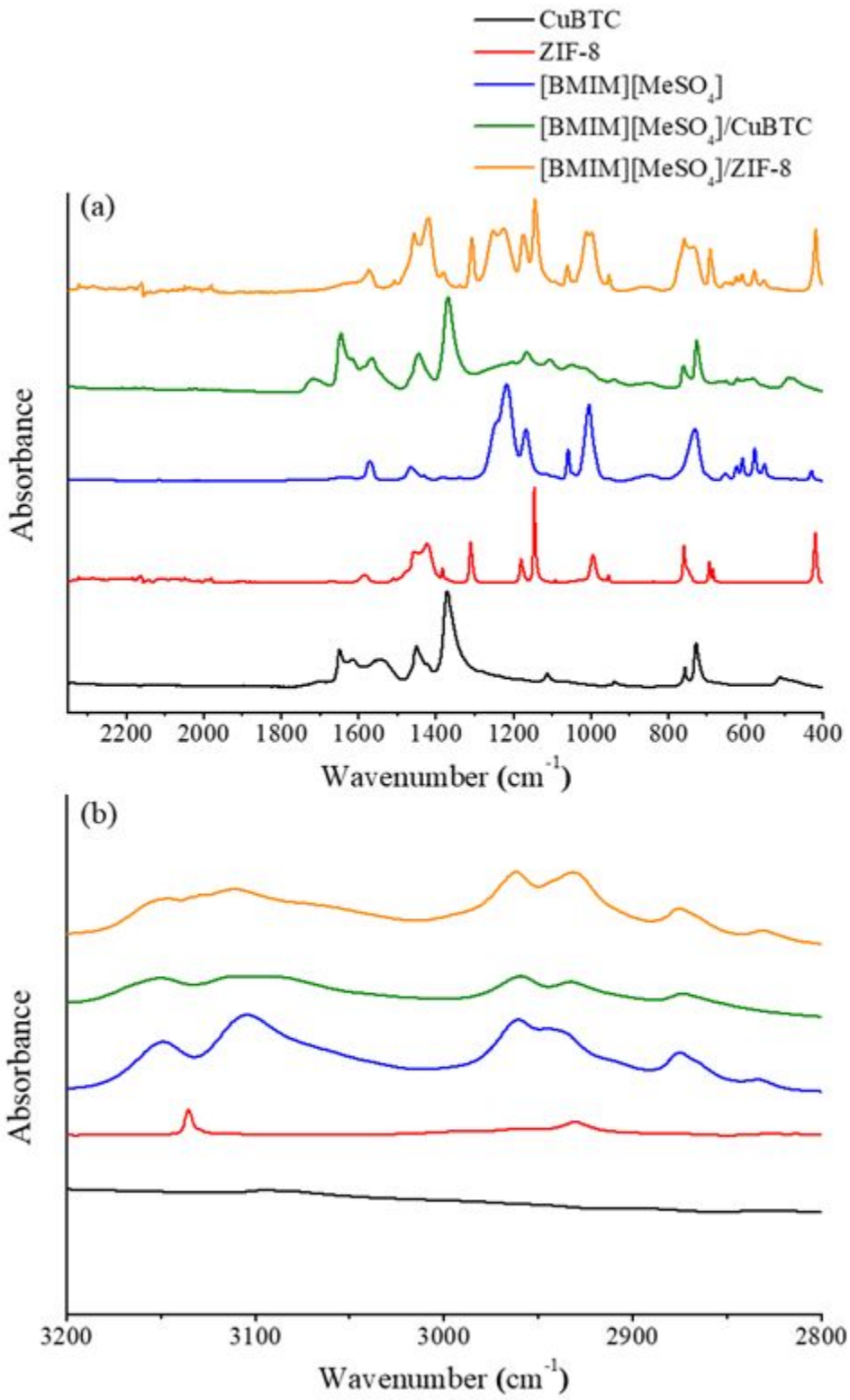

Figure S5. FTIR spectra of CuBTC, ZIF-8, [BMIM][$MeSO_4$], [BMIM][$MeSO_4$]/CuBTC, and [BMIM][$MeSO_4$]/ZIF-8 (a) 400-2250 cm^{-1} and (b) 2800-3200 cm^{-1}.

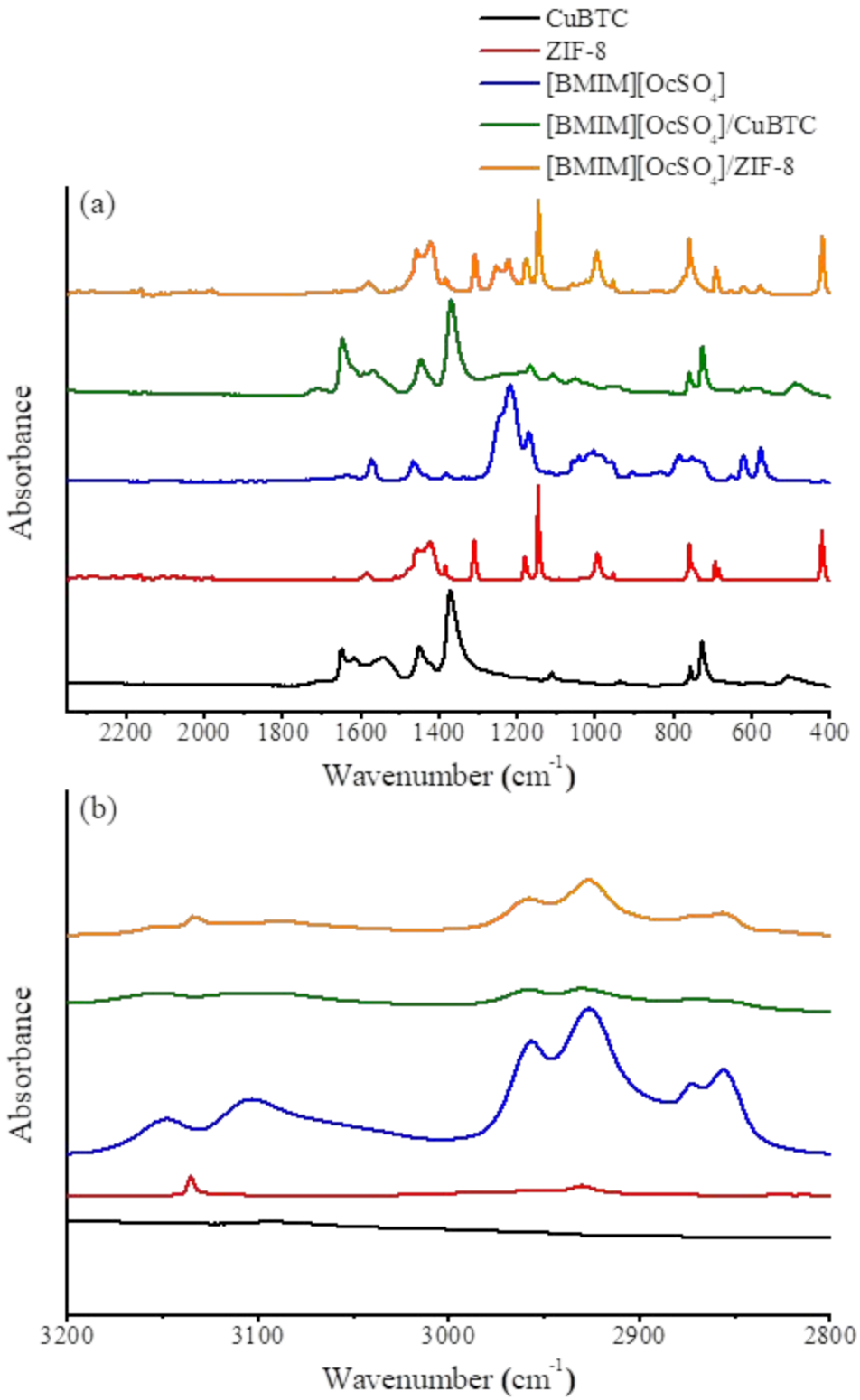

Figure S6. FTIR spectra of CuBTC, ZIF-8, [BMIM][$OcSO_4$], [BMIM][$OcSO_4$]/CuBTC, and [BMIM][$OcSO_4$]/ZIF-8 (a) 400-2250 cm^{-1} and (b) 2800-3200 cm^{-1}.

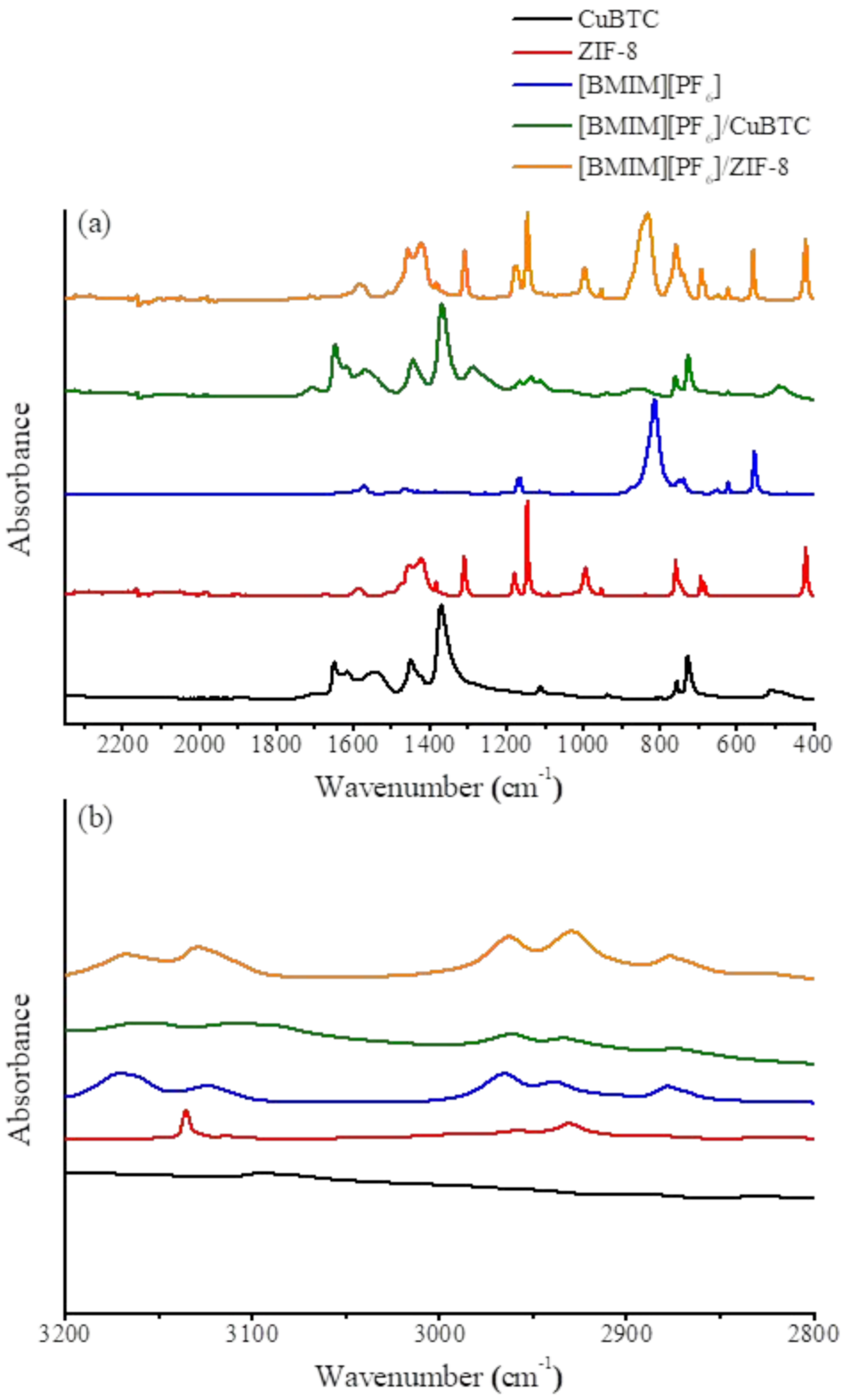

Figure S7. FTIR spectra of CuBTC, ZIF-8, [BMIM][PF_6], [BMIM][PF_6]/CuBTC, and [BMIM][PF_6]/ZIF-8 (a) 400-2250 cm^{-1} and (b) 2800-3200 cm^{-1}.

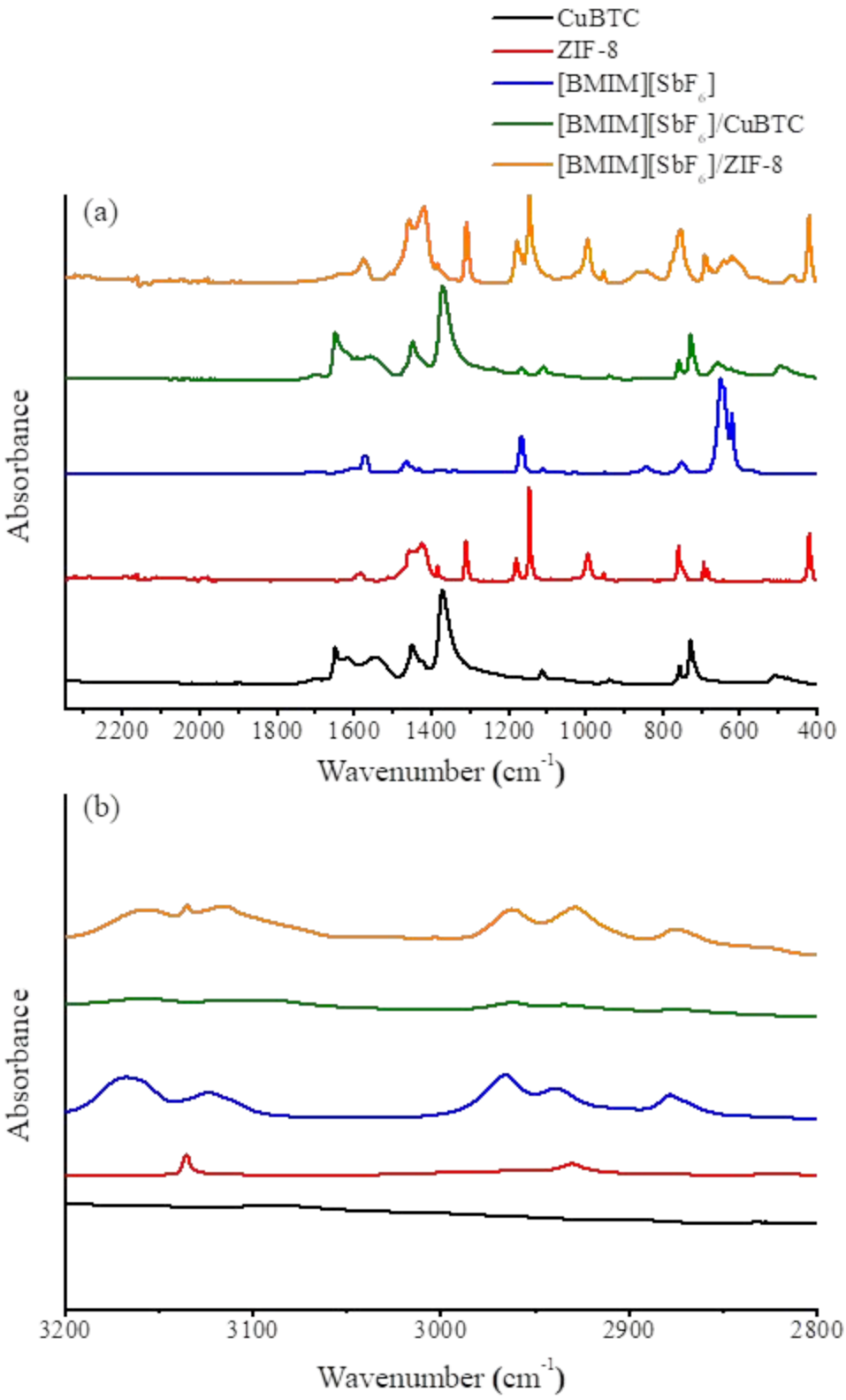

Figure S8. FTIR spectra of CuBTC, ZIF-8, [BMIM][SbF_6], [BMIM][SbF_6]/CuBTC, and [BMIM][SbF_6]/ZIF-8 (a) 400-2250 cm^{-1} and (b) 2800-3200 cm^{-1}.

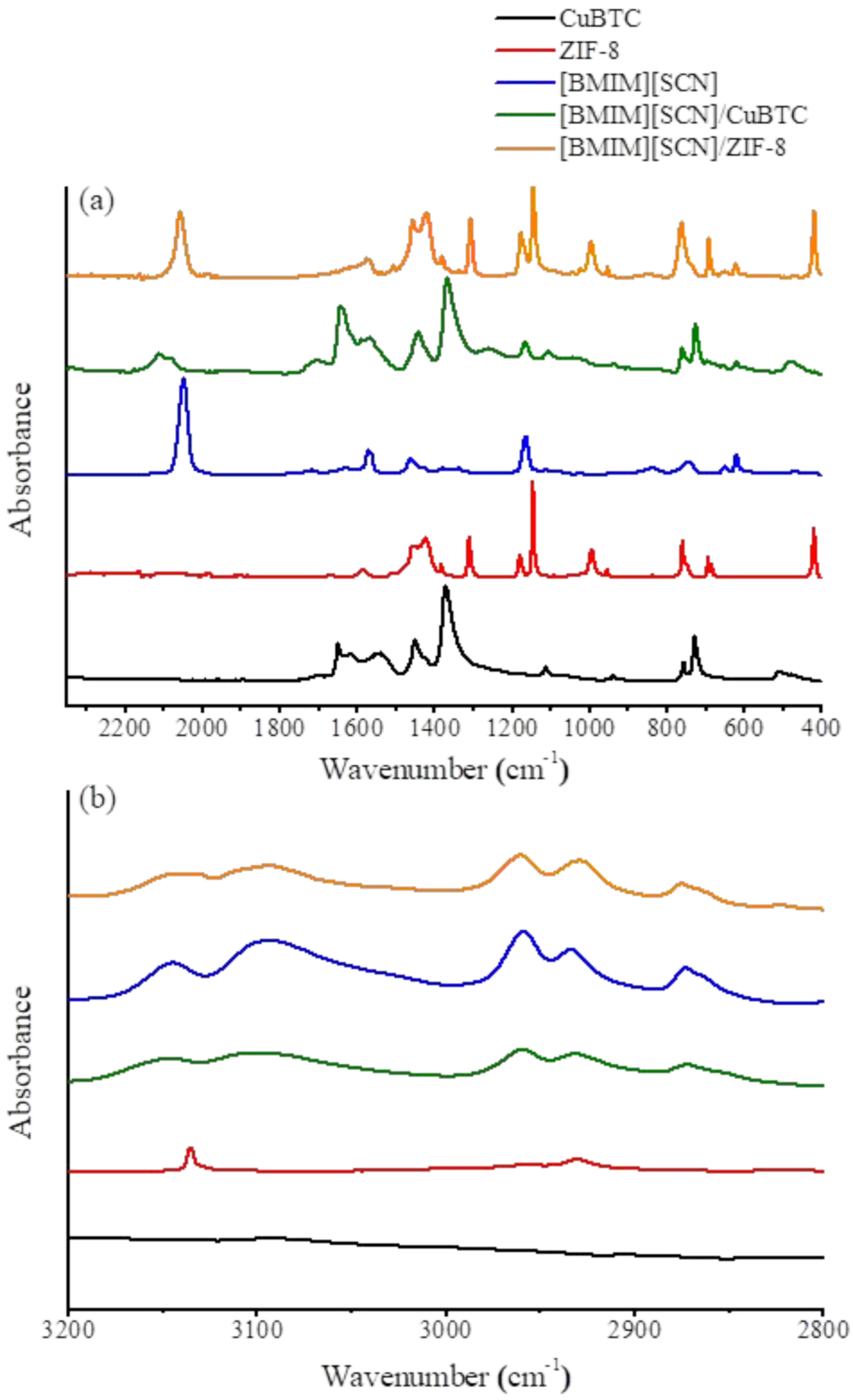

Figure S9. FTIR spectra of CuBTC, ZIF-8, [BMIM][SCN], [BMIM][SCN]/CuBTC, and [BMIM][SCN]/ZIF-8 (a) 400-2250 cm^{-1} and (b) 2800-3200 cm^{-1}.

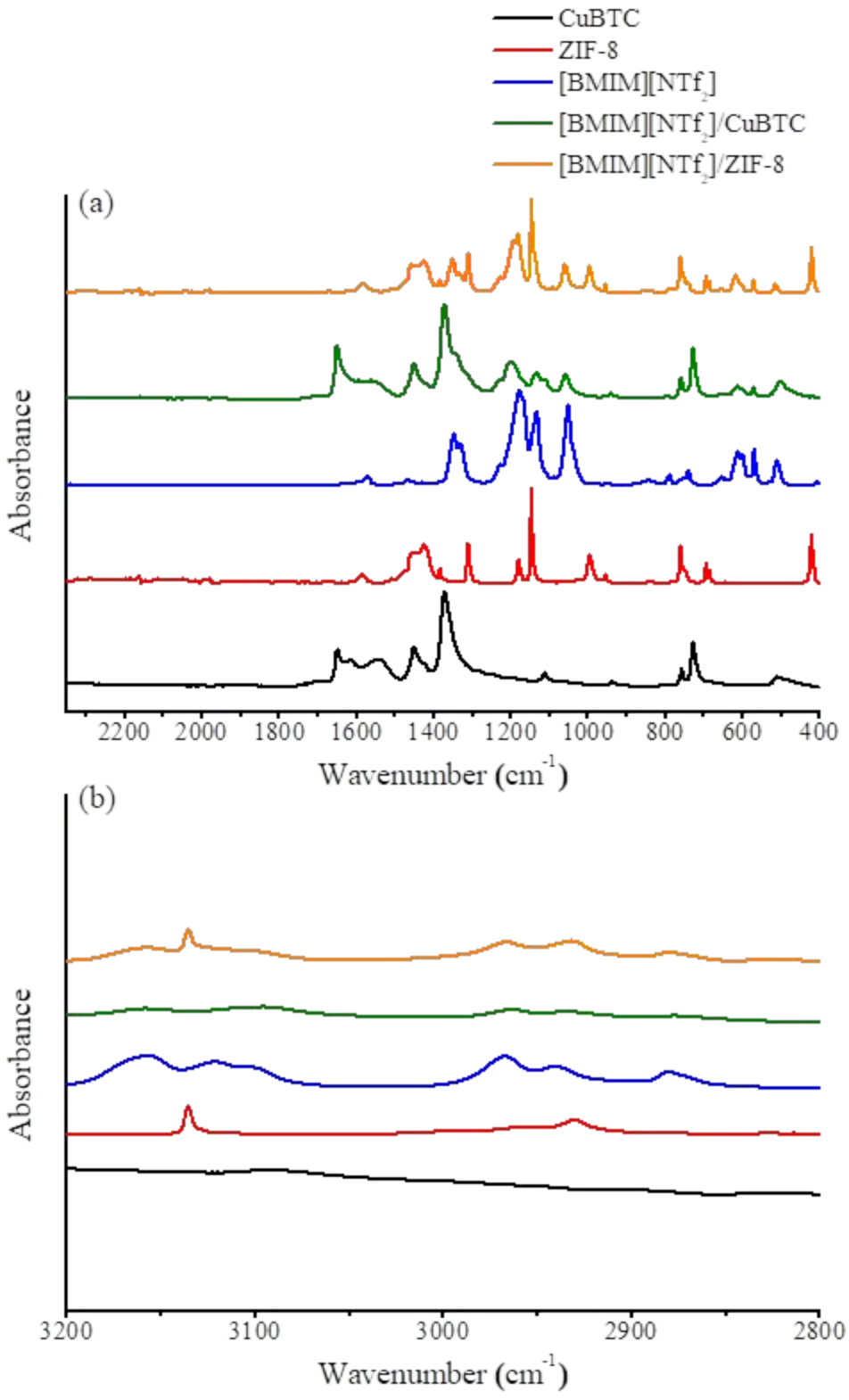

Figure S10. FTIR spectra of CuBTC, ZIF-8, [BMIM][NTf_2], [BMIM][NTf_2]/CuBTC, and [BMIM][NTf_2]/ZIF-8 (a) 400-2250 cm^{-1} and (b) 2800-3200 cm^{-1}.

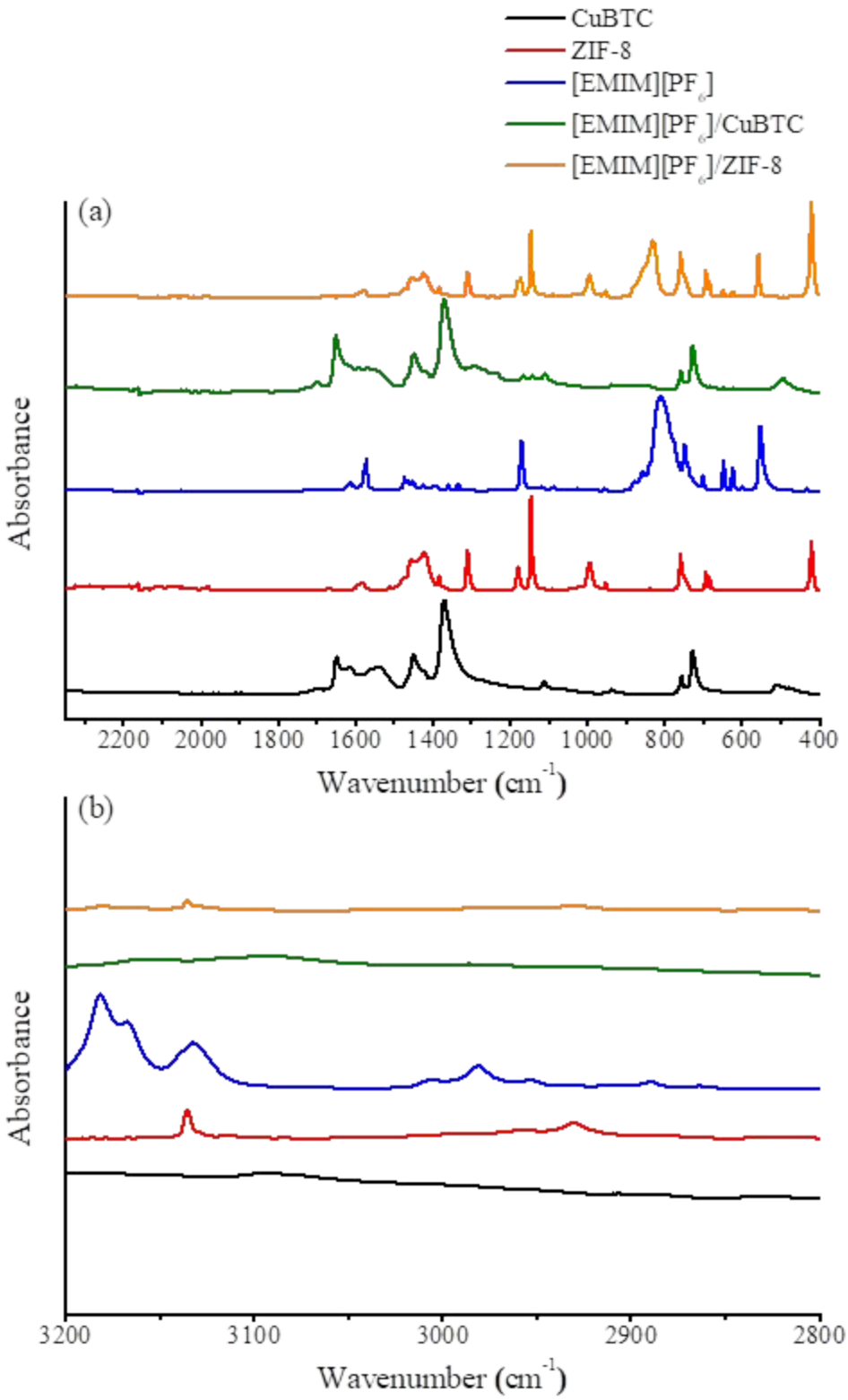

Figure S11. FTIR spectra of CuBTC, ZIF-8, [EMIM]PF_6], [EMIM]PF_6]/CuBTC, and [EMIM]PF_6]/ZIF-8 (a) 400-2250 cm^{-1} and (b) 2800-3200 cm^{-1}.

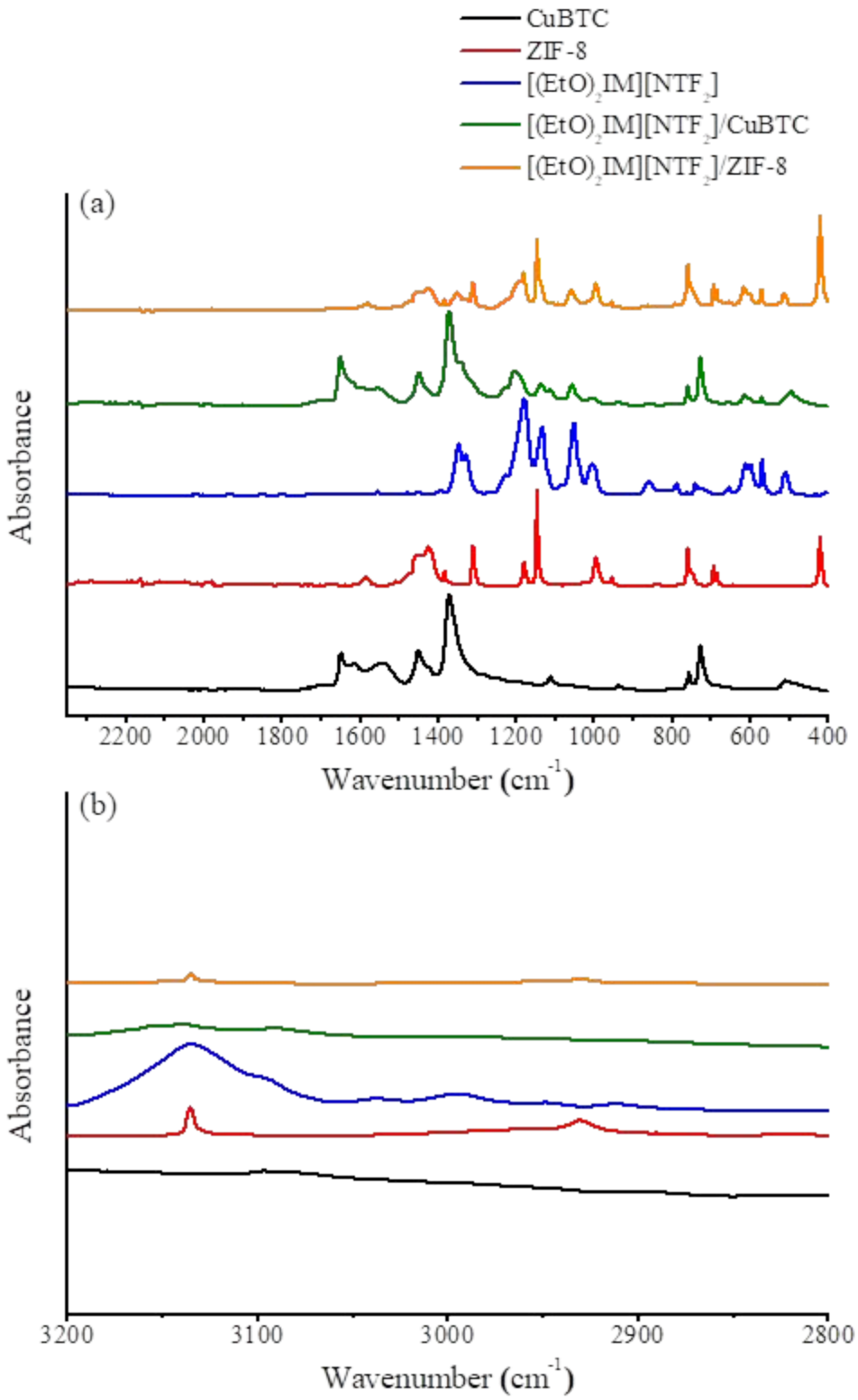

Figure S12. FTIR spectra of CuBTC, ZIF-8, $[(EtO)_2IM][NTF_2]$, $[(EtO)_2IM][NTF_2]$/CuBTC, and $[(EtO)_2IM][NTF_2]$/ZIF-8 (a) 400-2250 cm^{-1} and (b) 2800-3200 cm^{-1}.

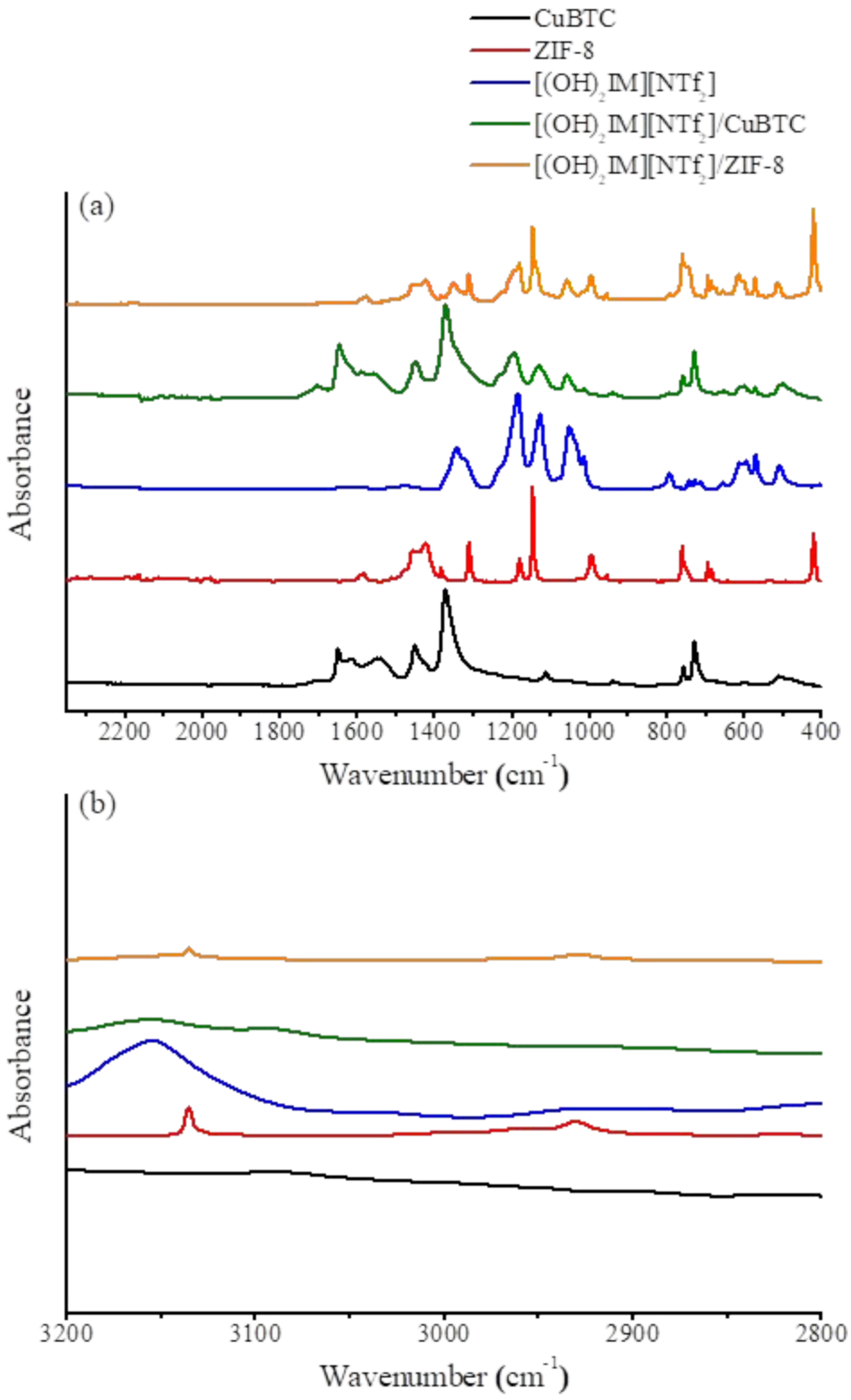

Figure S13. FTIR spectra of CuBTC, ZIF-8, $[(OH)_2IM][NTf_2]$, $[(OH)_2IM][NTf_2]$/CuBTC, and $[(OH)_2IM][NTf_2]$/ZIF-8 (a) 400-2250 cm^{-1} and (b) 2800-3200 cm^{-1}.

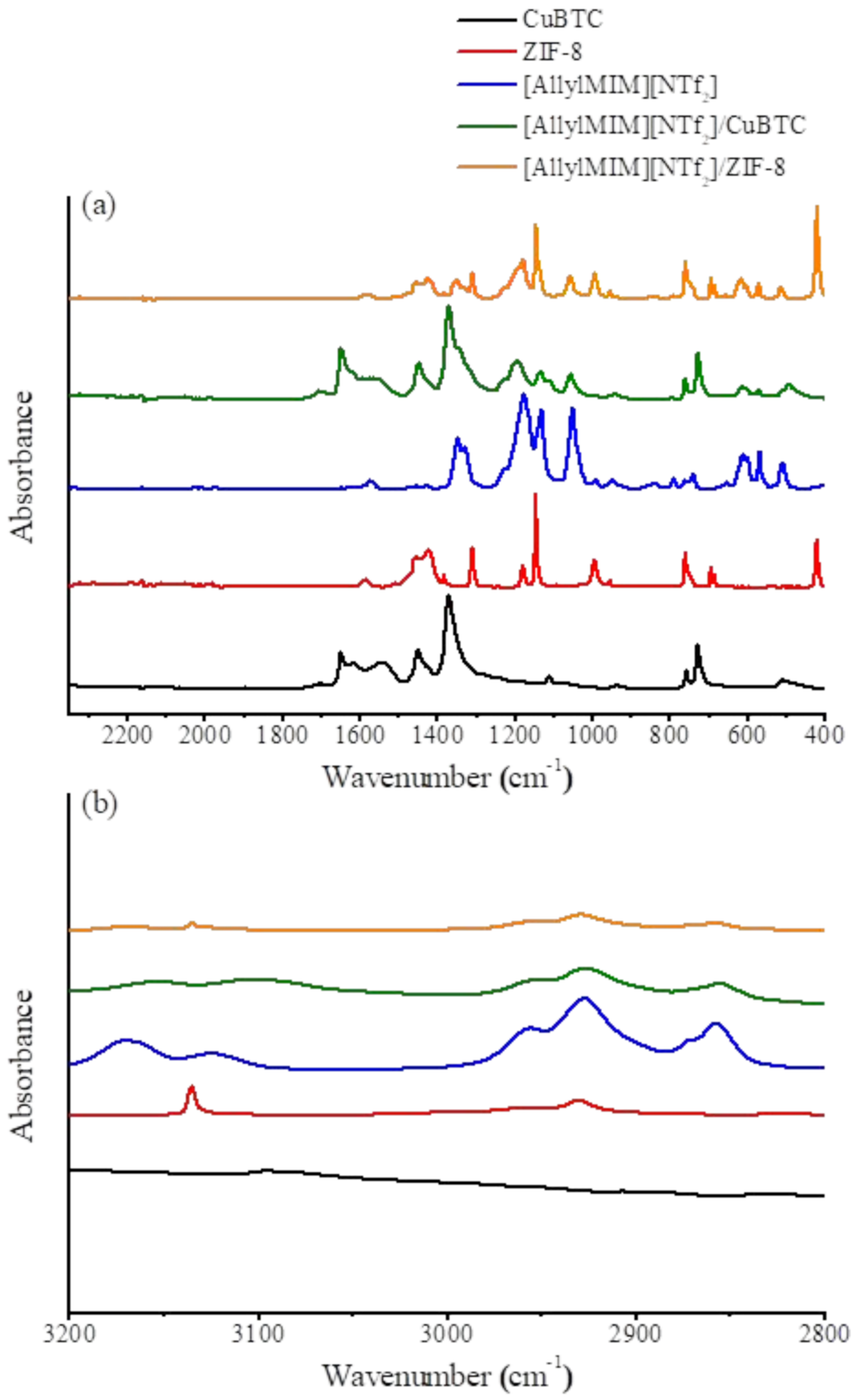

Figure S14. FTIR spectra of CuBTC, ZIF-8, [AllylIIM][NTf_2], [AllylIIM][NTf_2]/CuBTC, and [AllylIIM][NTf_2]/ZIF-8 (a) 400-2250 cm^{-1} and (b) 2800-3200 cm^{-1}.

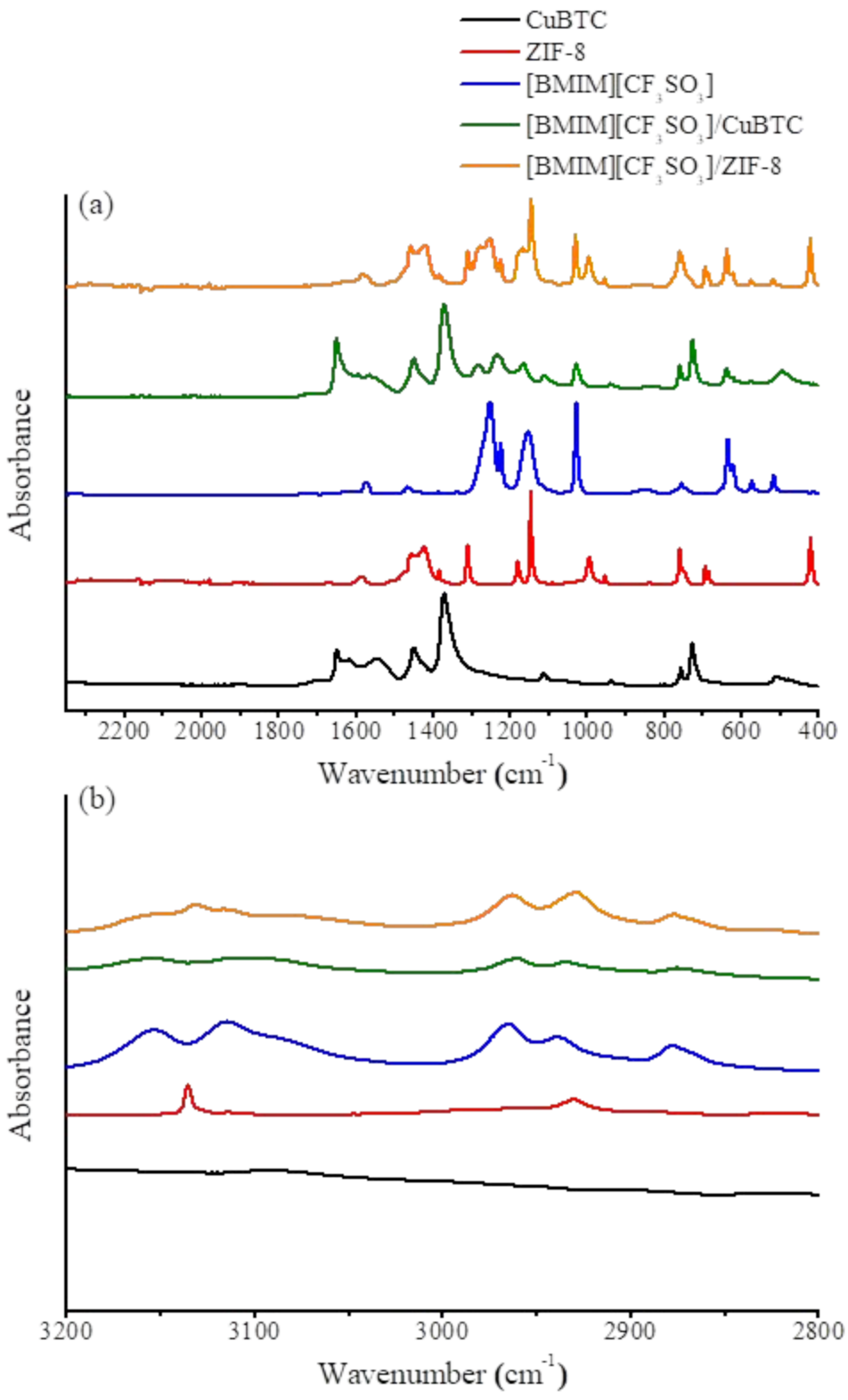

Figure S15. FTIR spectra of CuBTC, ZIF-8, [BMIM][CF_3SO_3], [BMIM][CF_3SO_3]/CuBTC, and [BMIM][CF_3SO_3]/ZIF-8 (a) 400-2250 cm^{-1} and (b) 2800-3200 cm^{-1}.

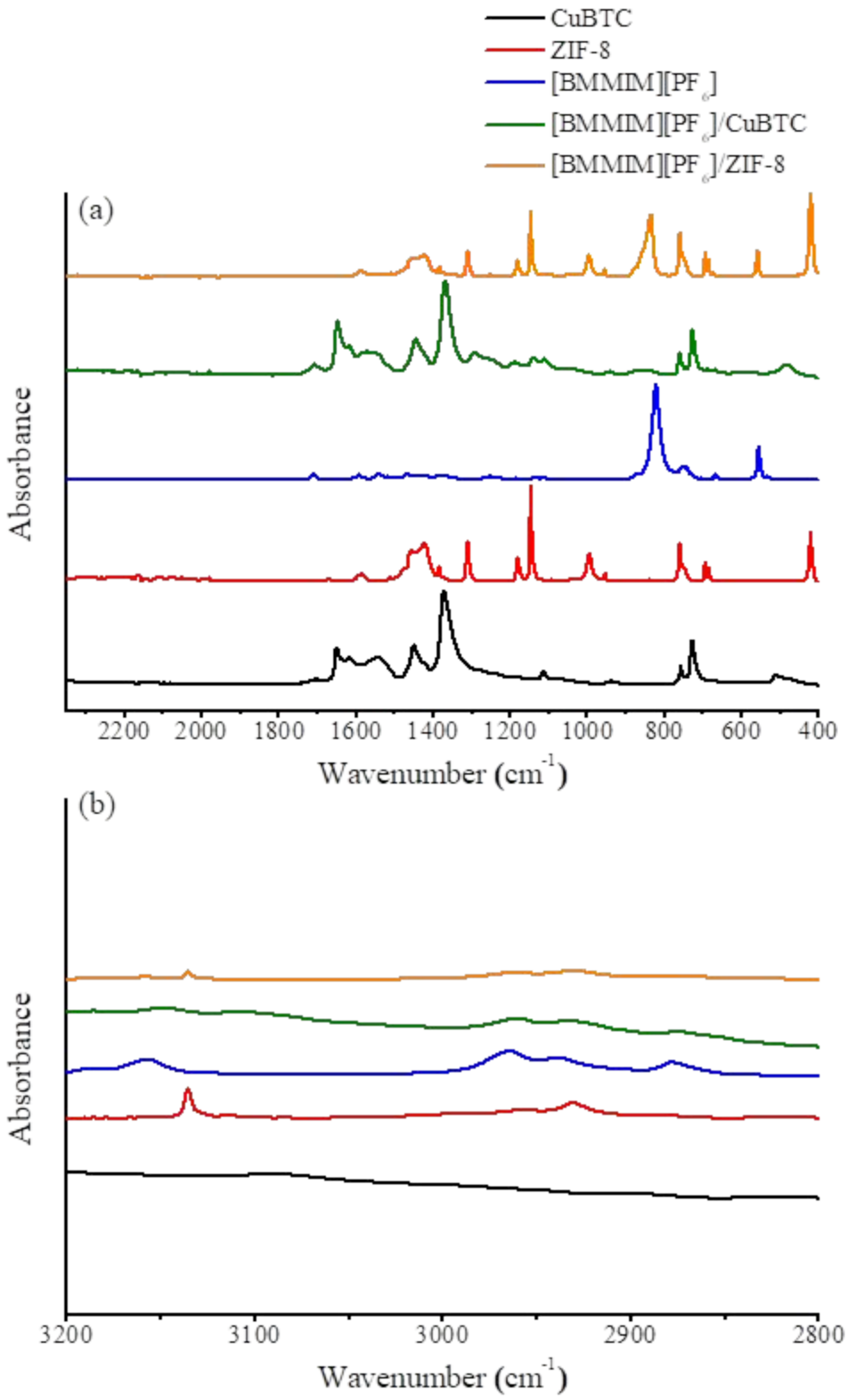

Figure S16. FTIR spectra of CuBTC, ZIF-8, [BMMIM][PF_6], [BMMIM][PF_6]/CuBTC, and [BMMIM][PF_6]/ZIF-8 (a) 400-2250 cm^{-1} and (b) 2800-3200 cm^{-1}.

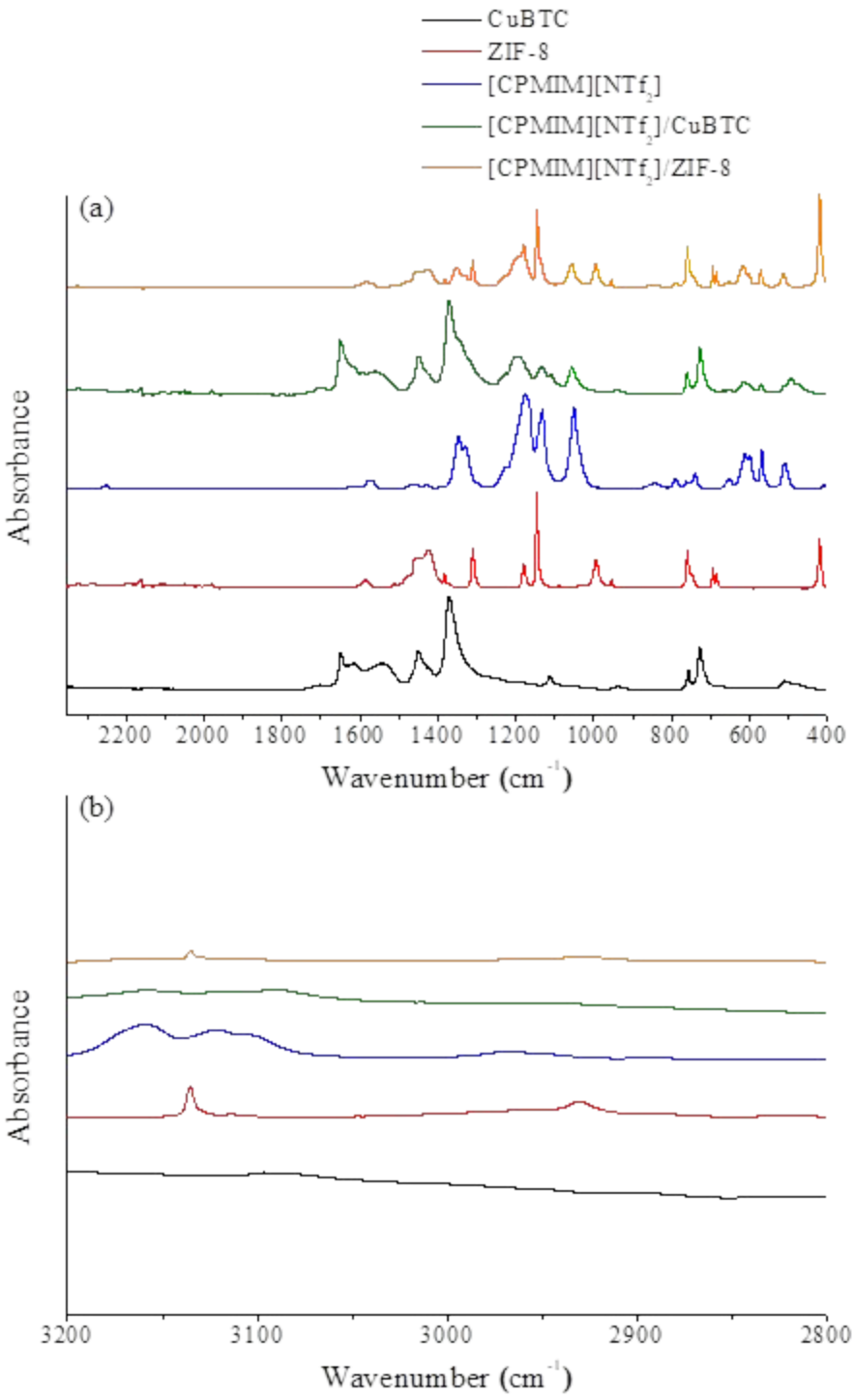

Figure S17. FTIR spectra of CuBTC, ZIF-8, [CPMIM][NTf_2], [(CPMIM][NTf_2]/CuBTC, and [CPMIM][NTf_2]/ZIF-8 (a) 400-2250 cm^{-1} and (b) 2800-3200 cm^{-1}.

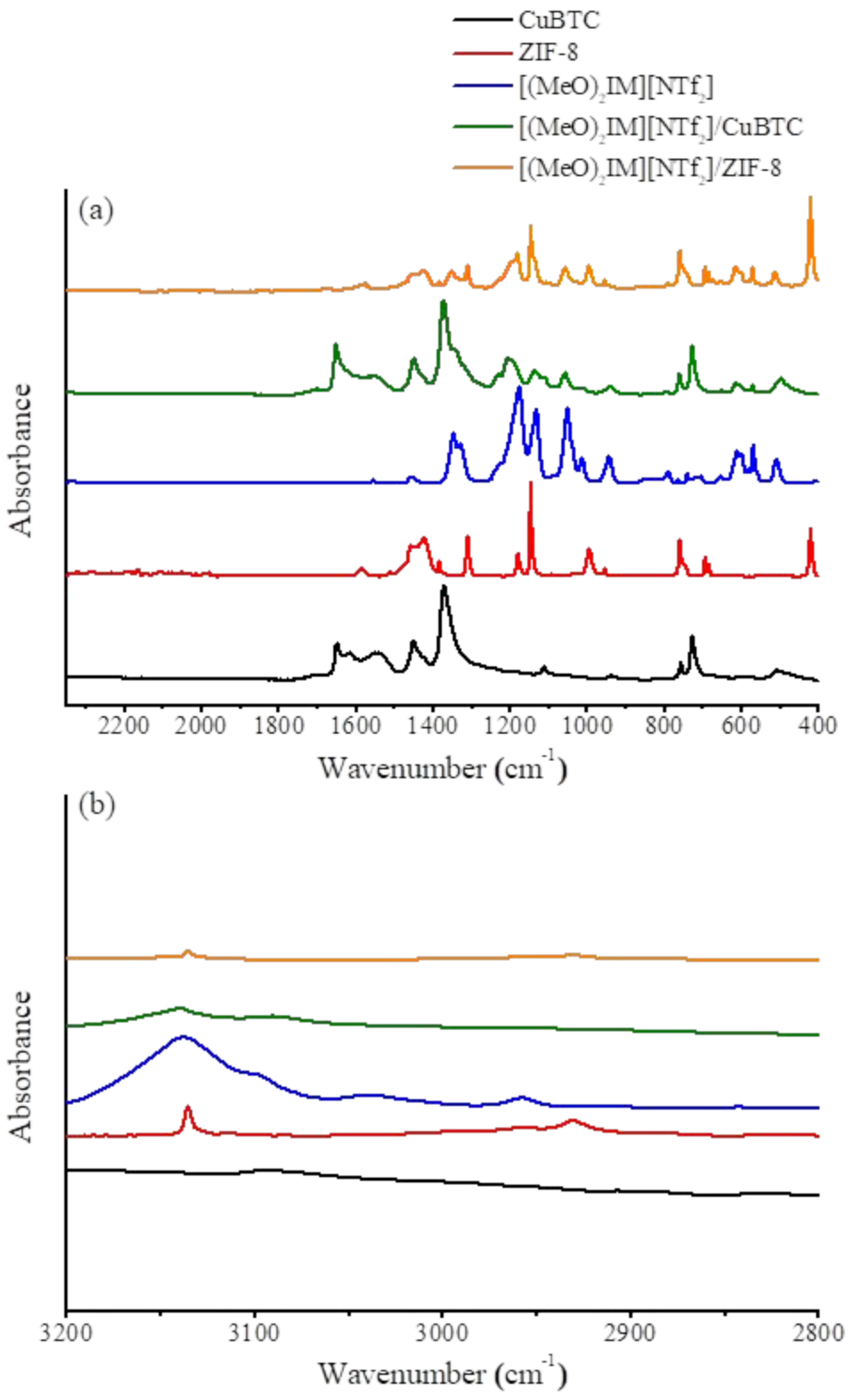

Figure S18. FTIR spectra of CuBTC, ZIF-8, $[(MeO)_2IM][NTf_2]$, $[(MeO)_2IM][NTf_2]$/CuBTC, and $[(MeO)_2IM][NTf_2]$/ZIF-8 (a) 400-2250 cm^{-1} and (b) 2800-3200 cm^{-1}.

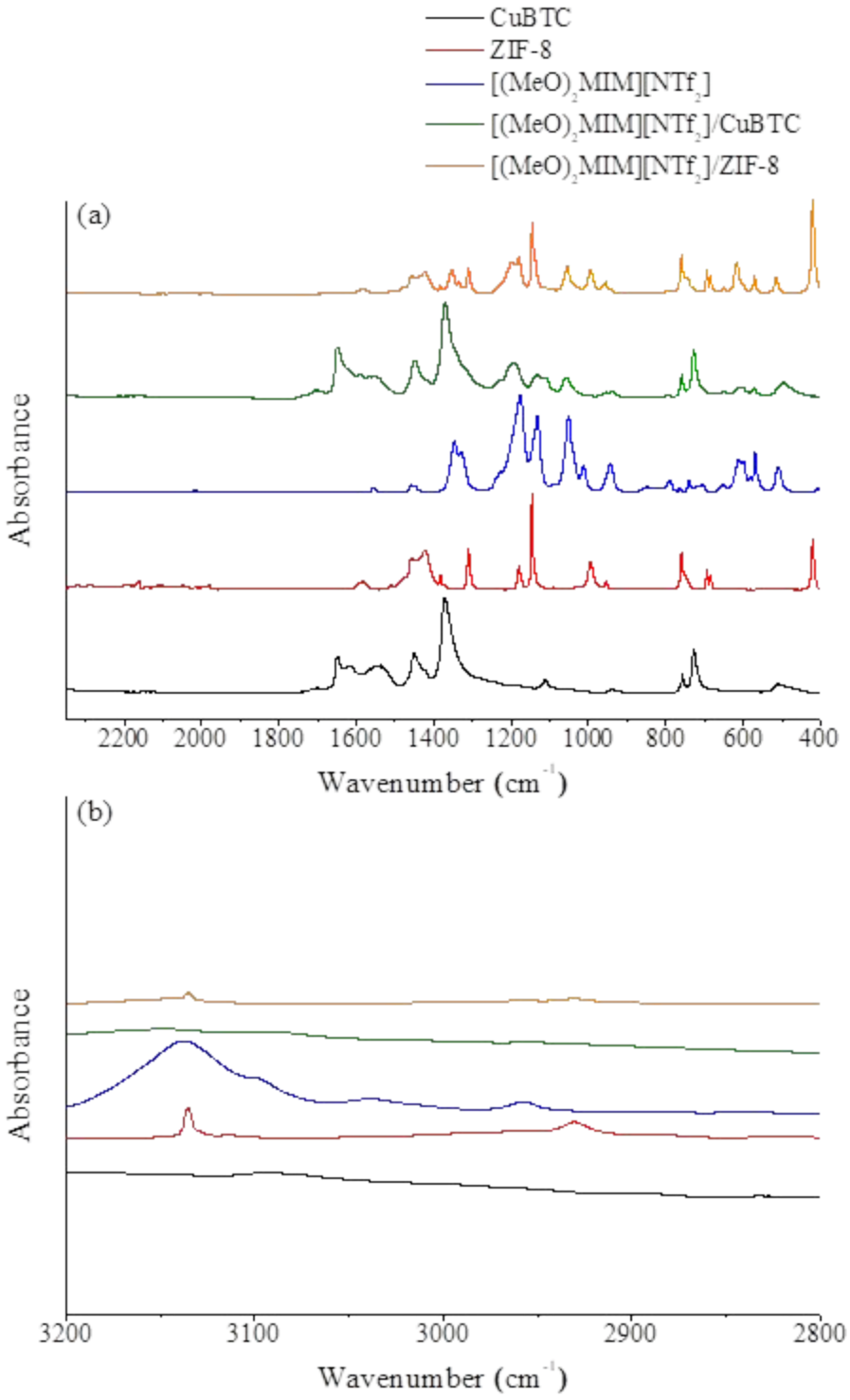

Figure S19. FTIR spectra of CuBTC, ZIF-8, $[(MeO)_2MIM][NTf_2]$, $[(MeO)_2MIM][NTf_2]$/CuBTC, and $[(MeO)_2MIM][NTf_2]$/ZIF-8 (a) 400-2250 cm^{-1} and (b) 2800-3200 cm^{-1}.

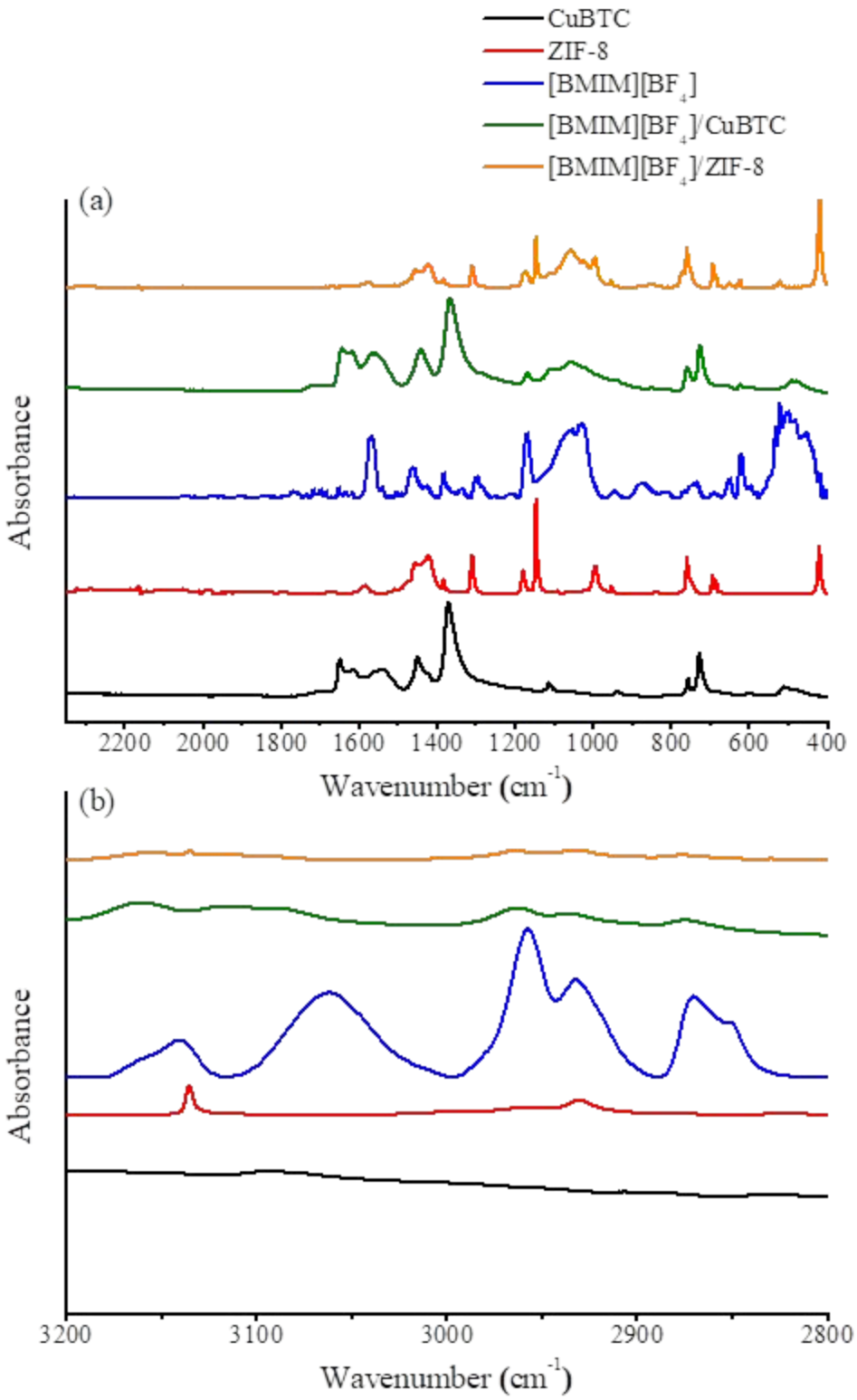

Figure S20. FTIR spectra of CuBTC, ZIF-8, [BMIM][BF_4], [BMIM][BF_4]/CuBTC, and [BMIM][BF_4]/ZIF-8 (a) 400-2250 cm^{-1} and (b) 2800-3200 cm^{-1}.

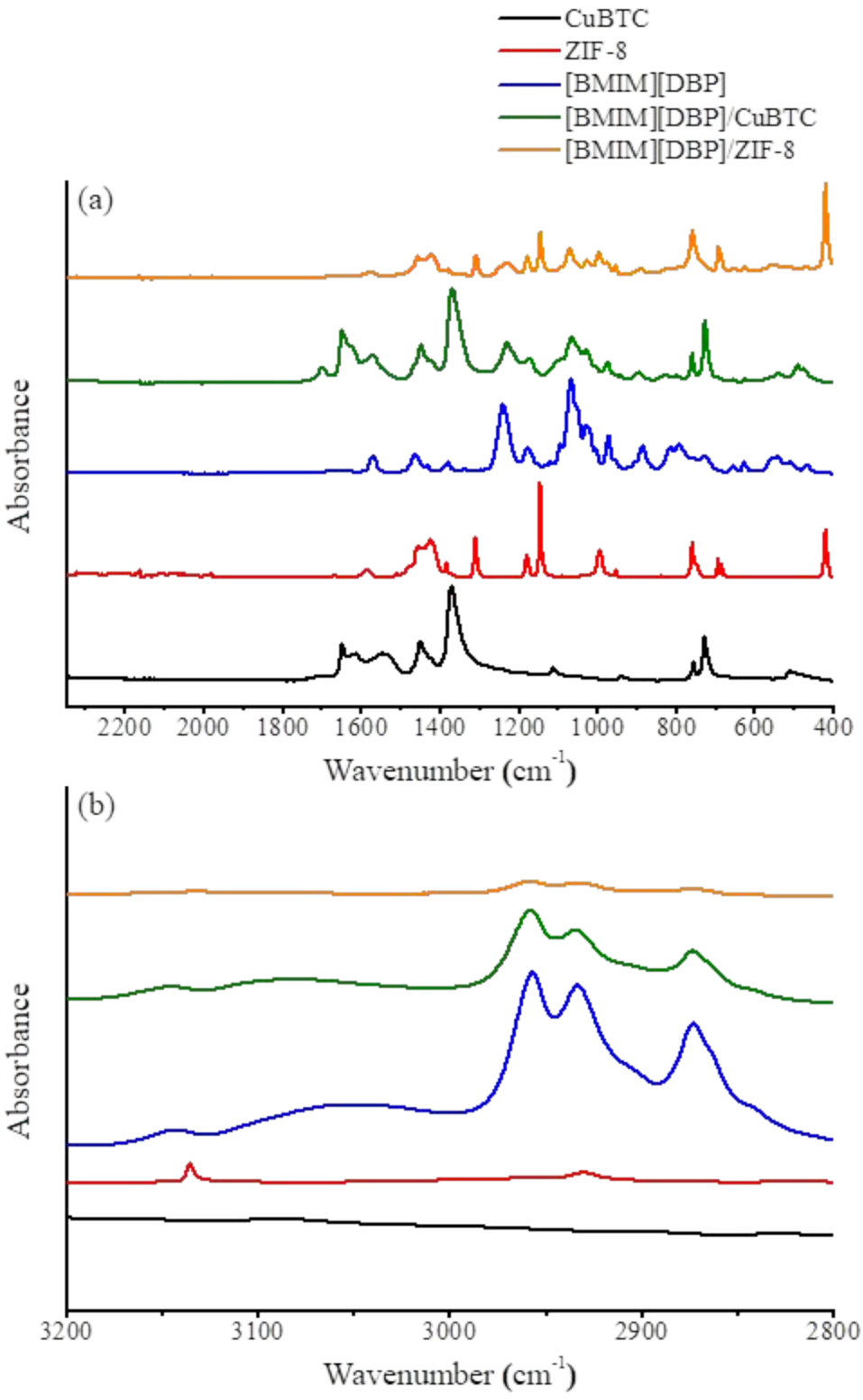

Figure S21. FTIR spectra of CuBTC, ZIF-8, [BMIM][DBP], [BMIM][DBP]/CuBTC, and [BMIM][DBP]/ZIF-8 (a) 400-2250 cm^{-1} and (b) 2800-3200 cm^{-1}.

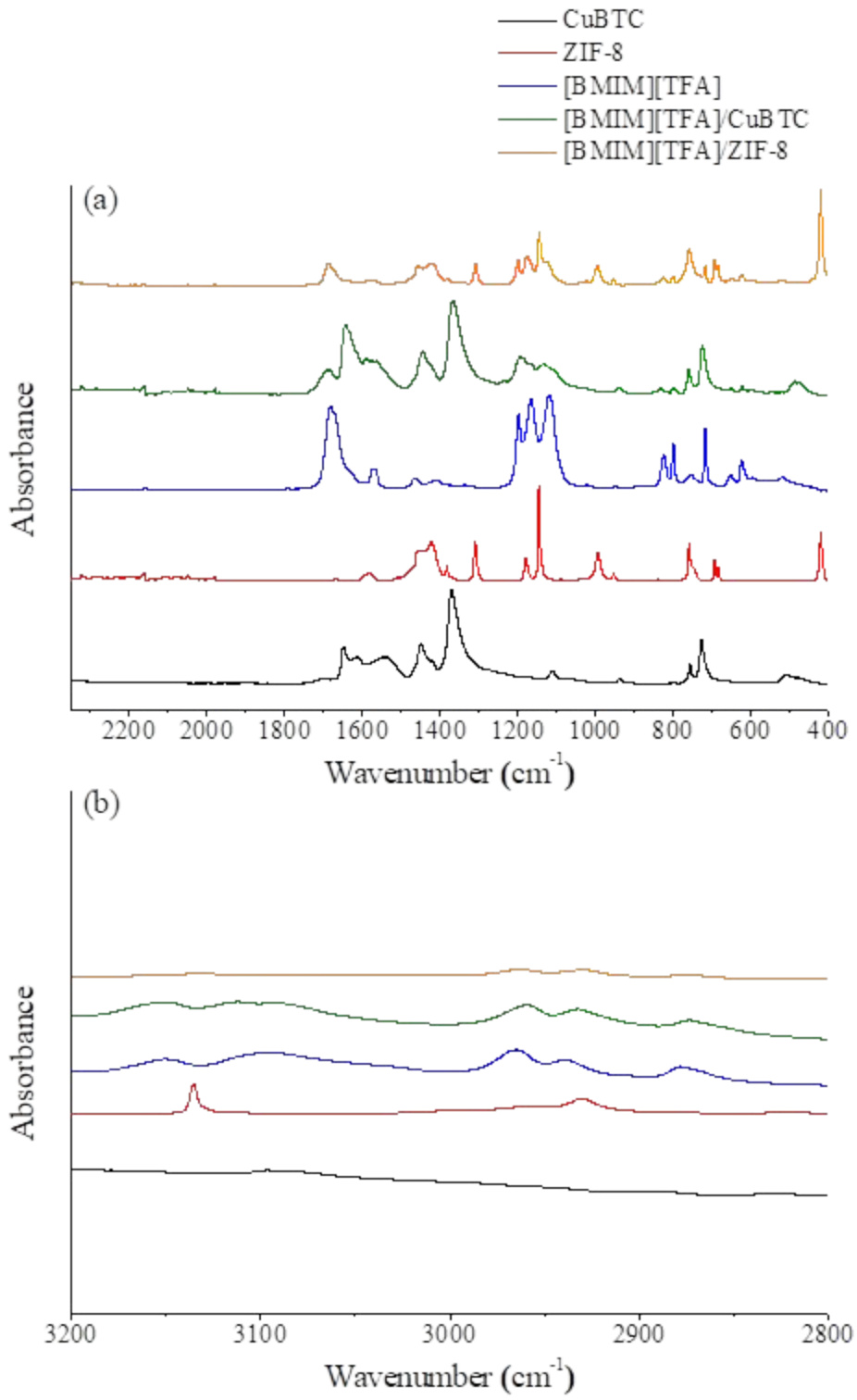

Figure S22. FTIR spectra of CuBTC, ZIF-8, [BMIM][TFA], [BMIM][TFA]/CuBTC, and [BMIM][TFA]/ZIF-8 (a) 400-2250 cm^{-1} and (b) 2800-3200 cm^{-1}.

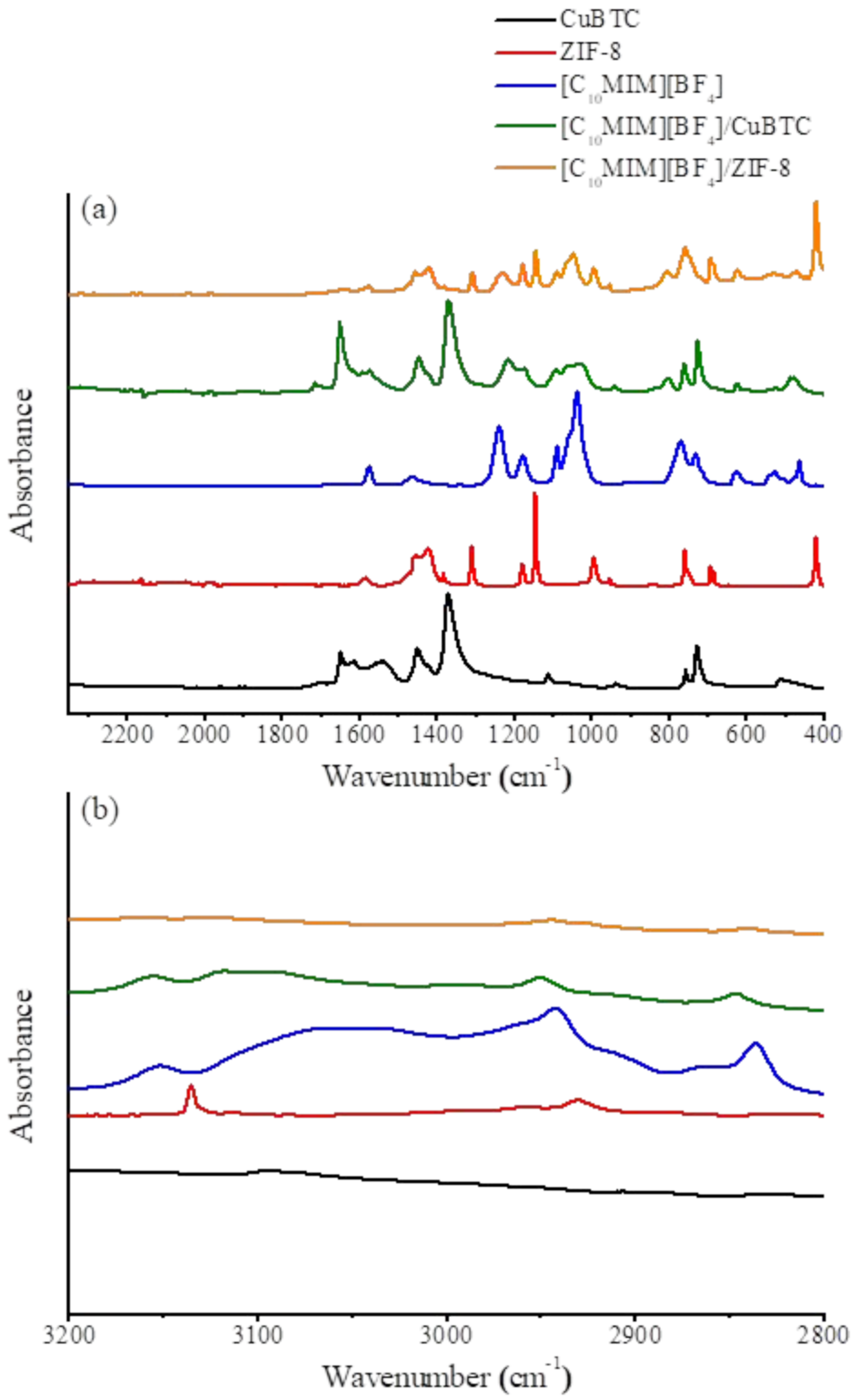

Figure S23. FTIR spectra of CuBTC, ZIF-8, $[C_{10}MIM][BF_4]$, $[C_{10}MIM][BF_4]$/CuBTC, and $[C_{10}MIM][BF_4]$/ZIF-8 (a) 400-2250 cm^{-1} and (b) 2800-3200 cm^{-1}.

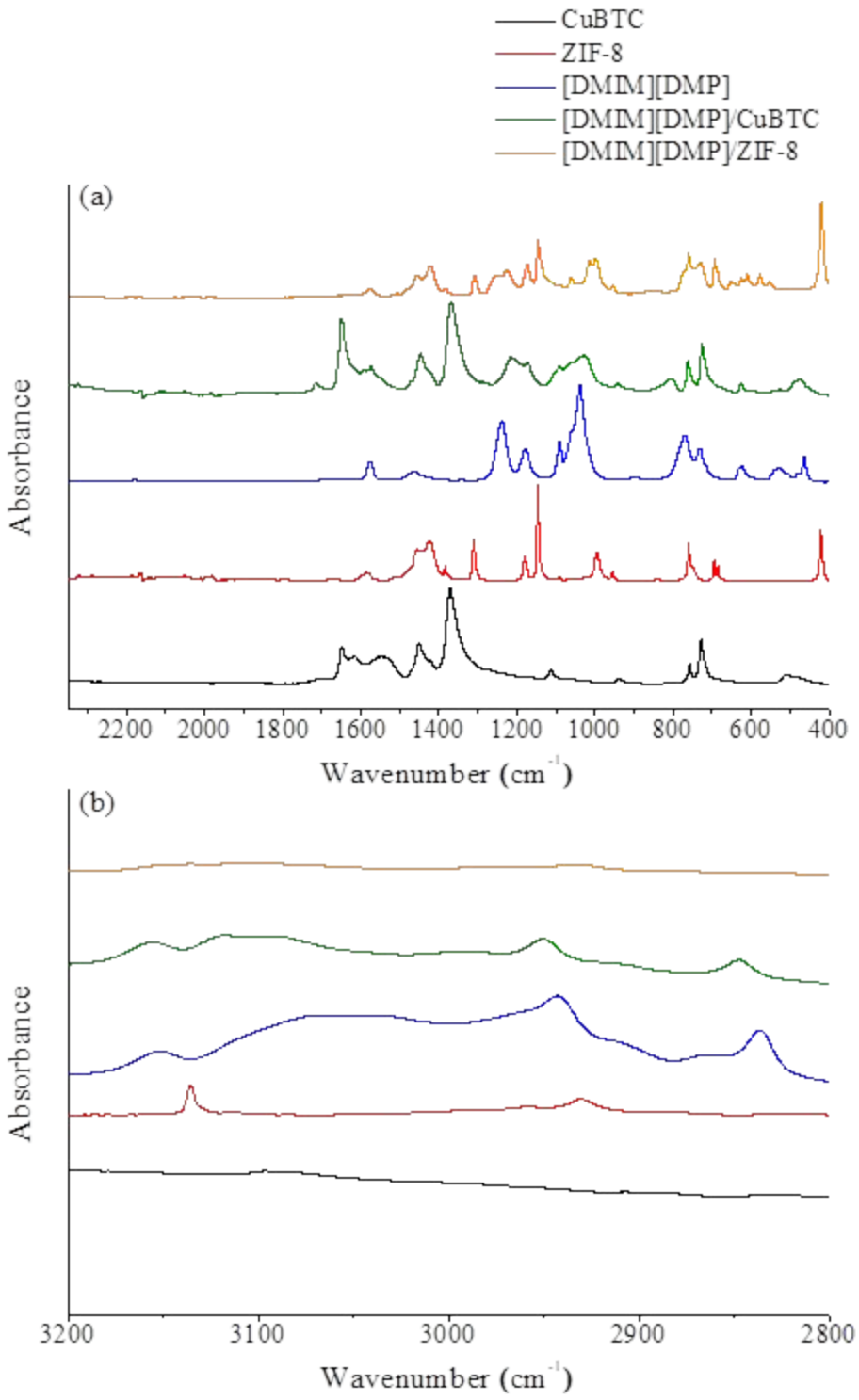

Figure S24. FTIR spectra of CuBTC, ZIF-8, [DMIM][DMP], [DMIM][DMP]/CuBTC, and [DMIM][DMP]/ZIF-8 (a) 400-2250 cm^{-1} and (b) 2800-3200 cm^{-1}.

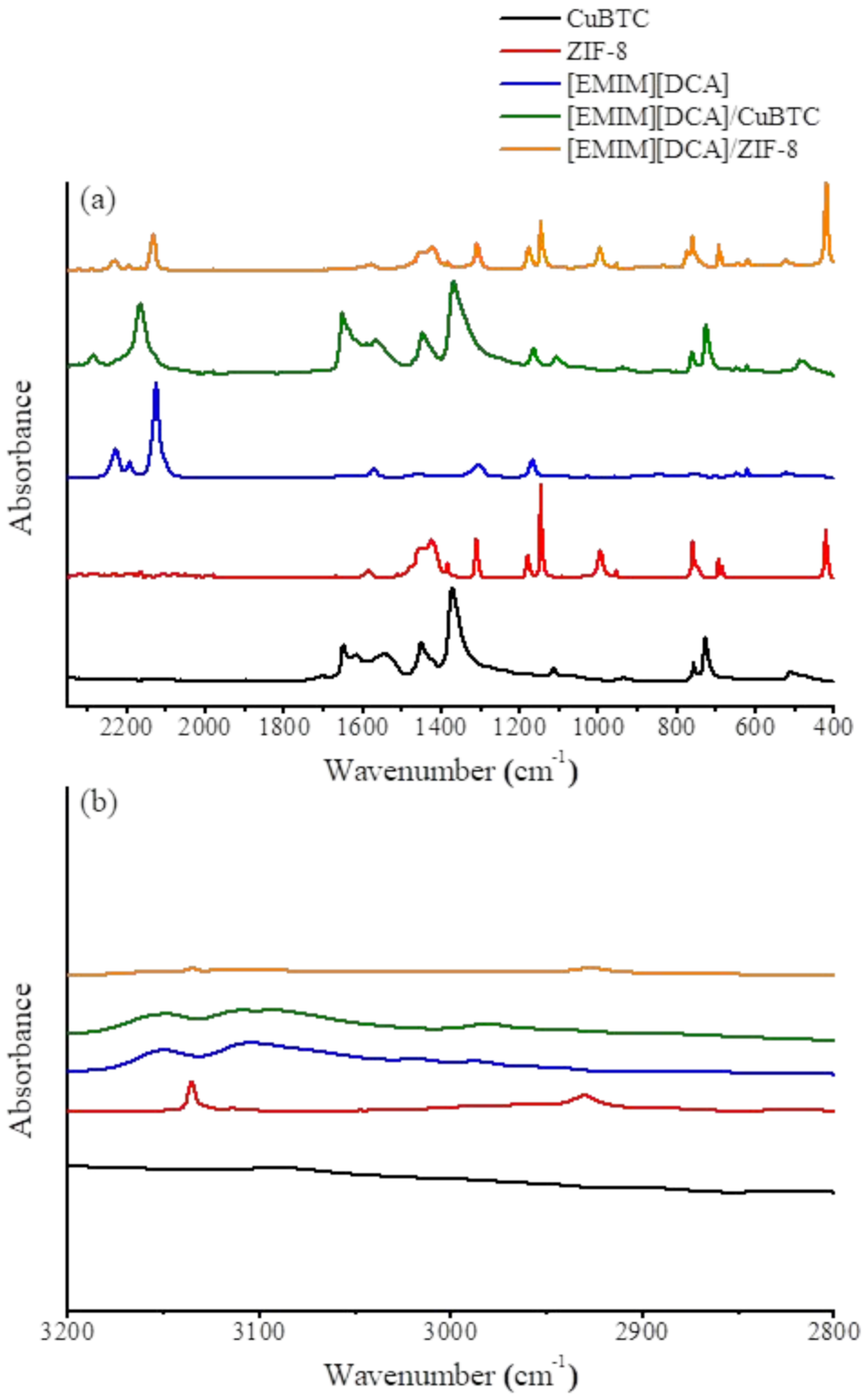

Figure S25. FTIR spectra of CuBTC, ZIF-8, [EMIM][DCA], [EMIM][DCA]/CuBTC, and [EMIM][DCA]/ZIF-8 (a) 400-2250 cm^{-1} and (b) 2800-3200 cm^{-1}.

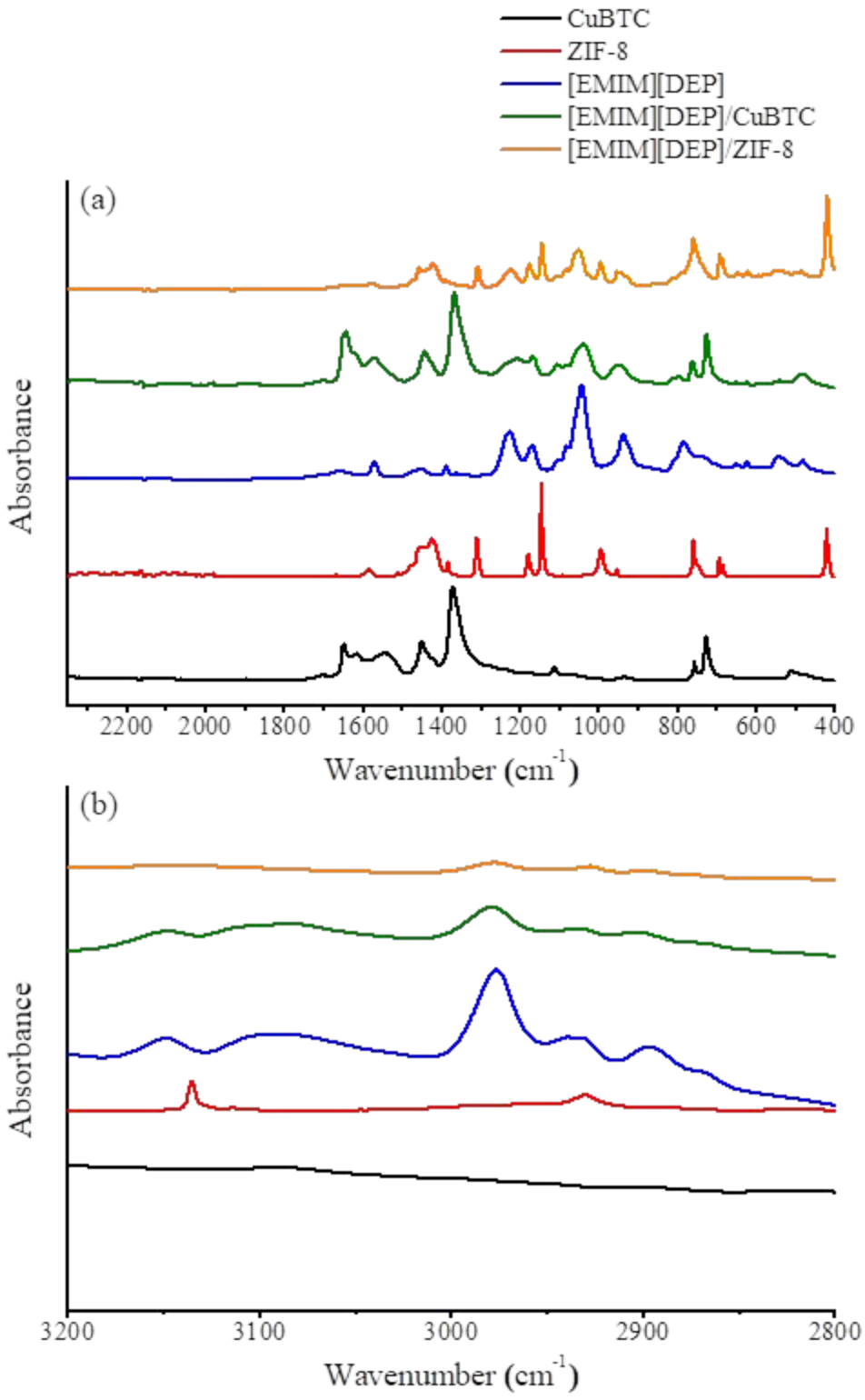

Figure S26. FTIR spectra of CuBTC, ZIF-8, [EMIM][DEP], [EMIM][DEP]/CuBTC, and [EMIM][DEP]/ZIF-8 (a) 400-2250 cm^{-1} and (b) 2800-3200 cm^{-1}.

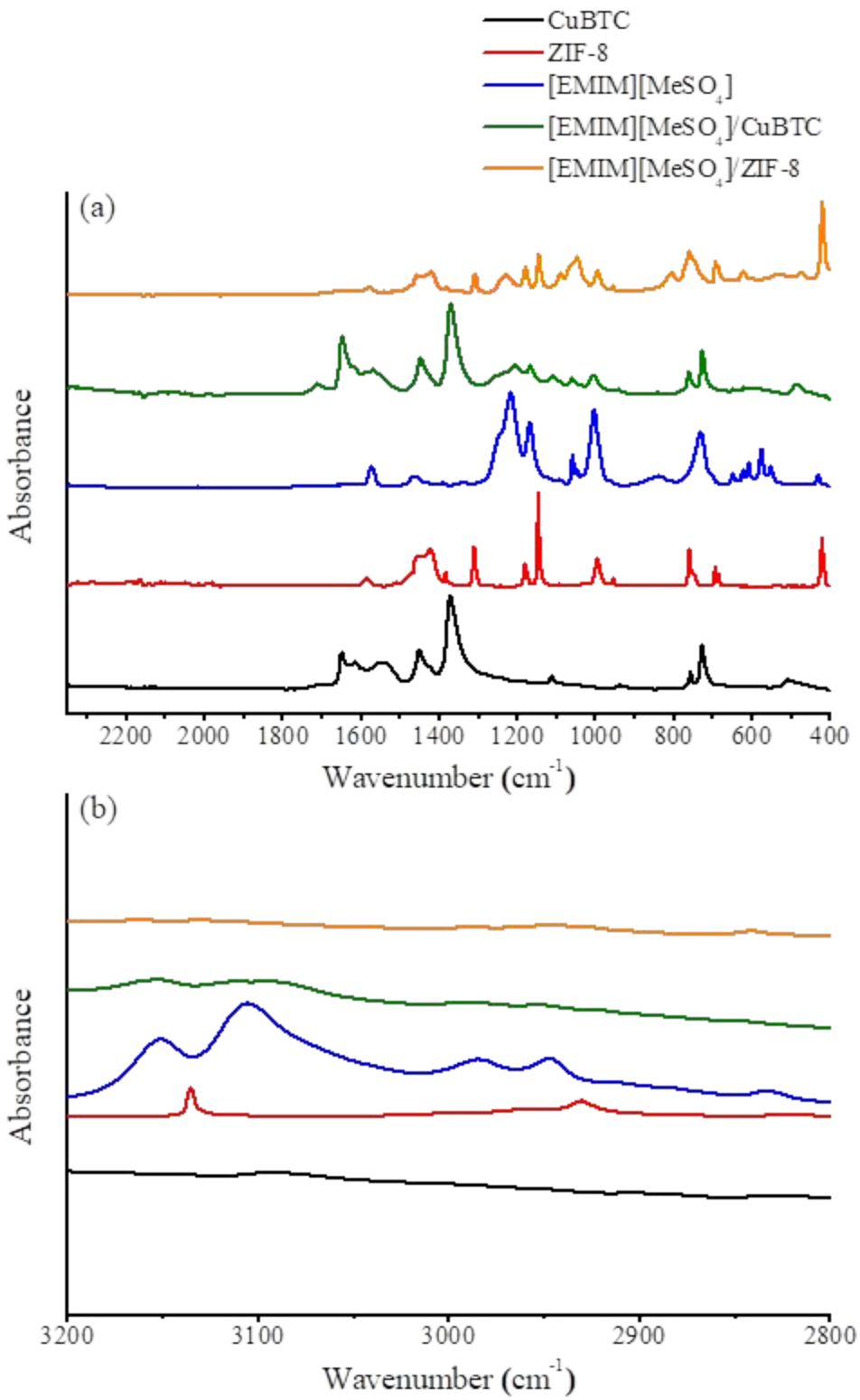

Figure S27. FTIR spectra of CuBTC, ZIF-8, [EMIM][$MeSO_4$], [EMIM][$MeSO_4$]/CuBTC, and [EMIM][$MeSO_4$]/ZIF-8 (a) 400-2250 cm^{-1} and (b) 2800-3200 cm^{-1}.

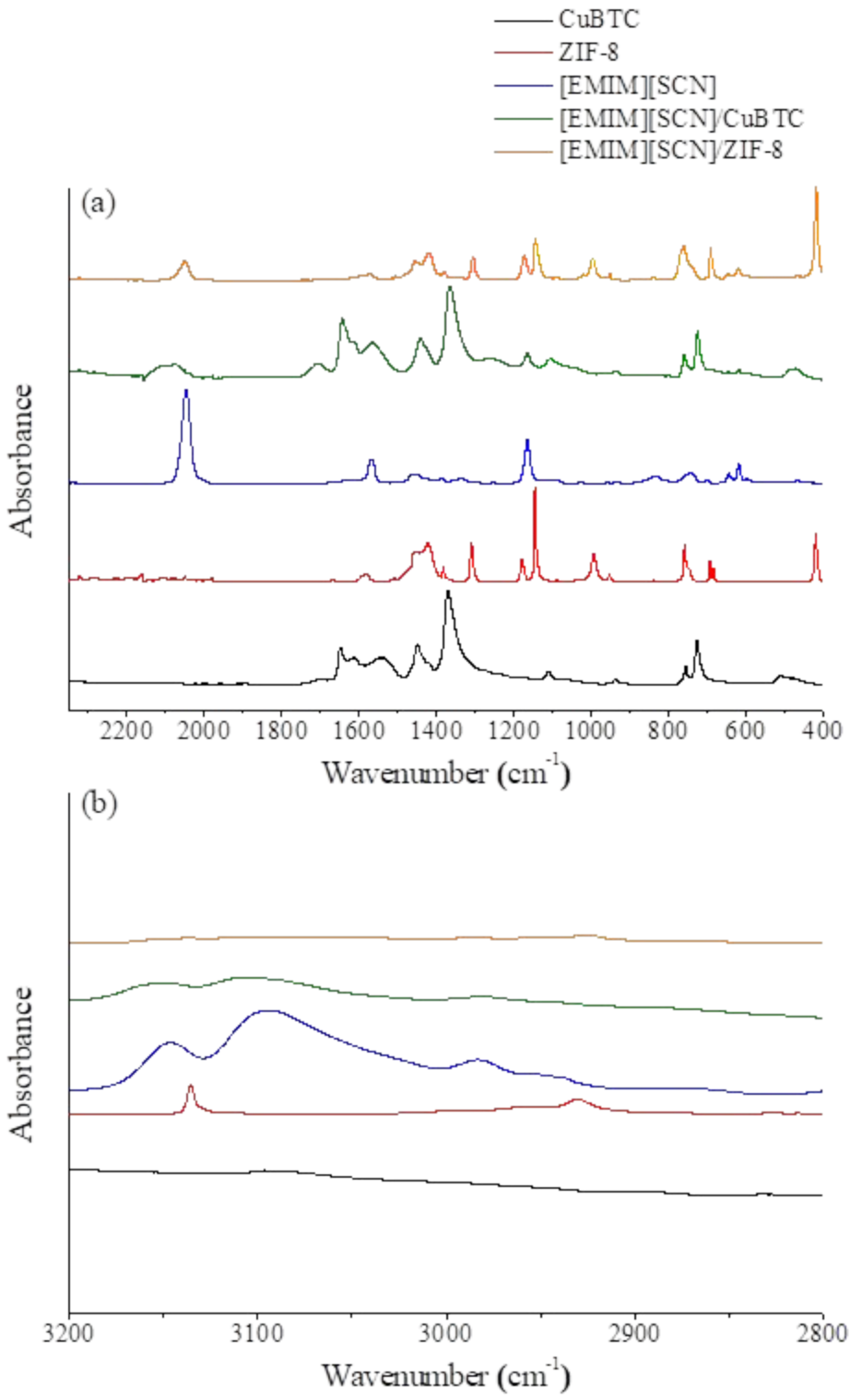

Figure S28. FTIR spectra of CuBTC, ZIF-8, [EMIM][SCN], [EMIM][SCN]/CuBTC, and [EMIM][SCN]/ZIF-8 (a) 400-2250 cm^{-1} and (b) 2800-3200 cm^{-1}.

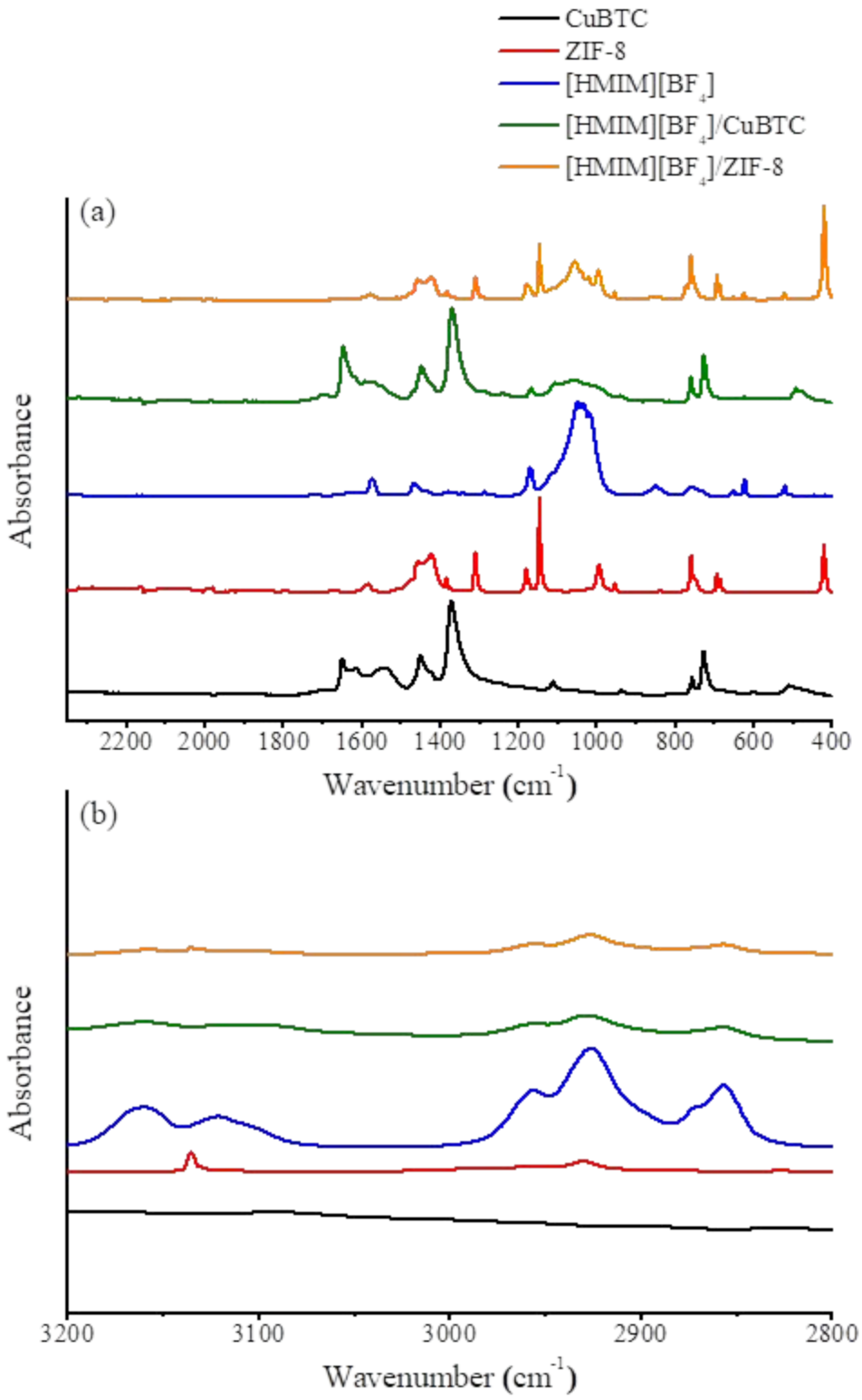

Figure S29. FTIR spectra of CuBTC, ZIF-8, [HMIM][BF_4], [HMIM][BF_4]/CuBTC, and [HMIM][BF_4]/ZIF-8 (a) 400-2250 cm^{-1} and (b) 2800-3200 cm^{-1}.

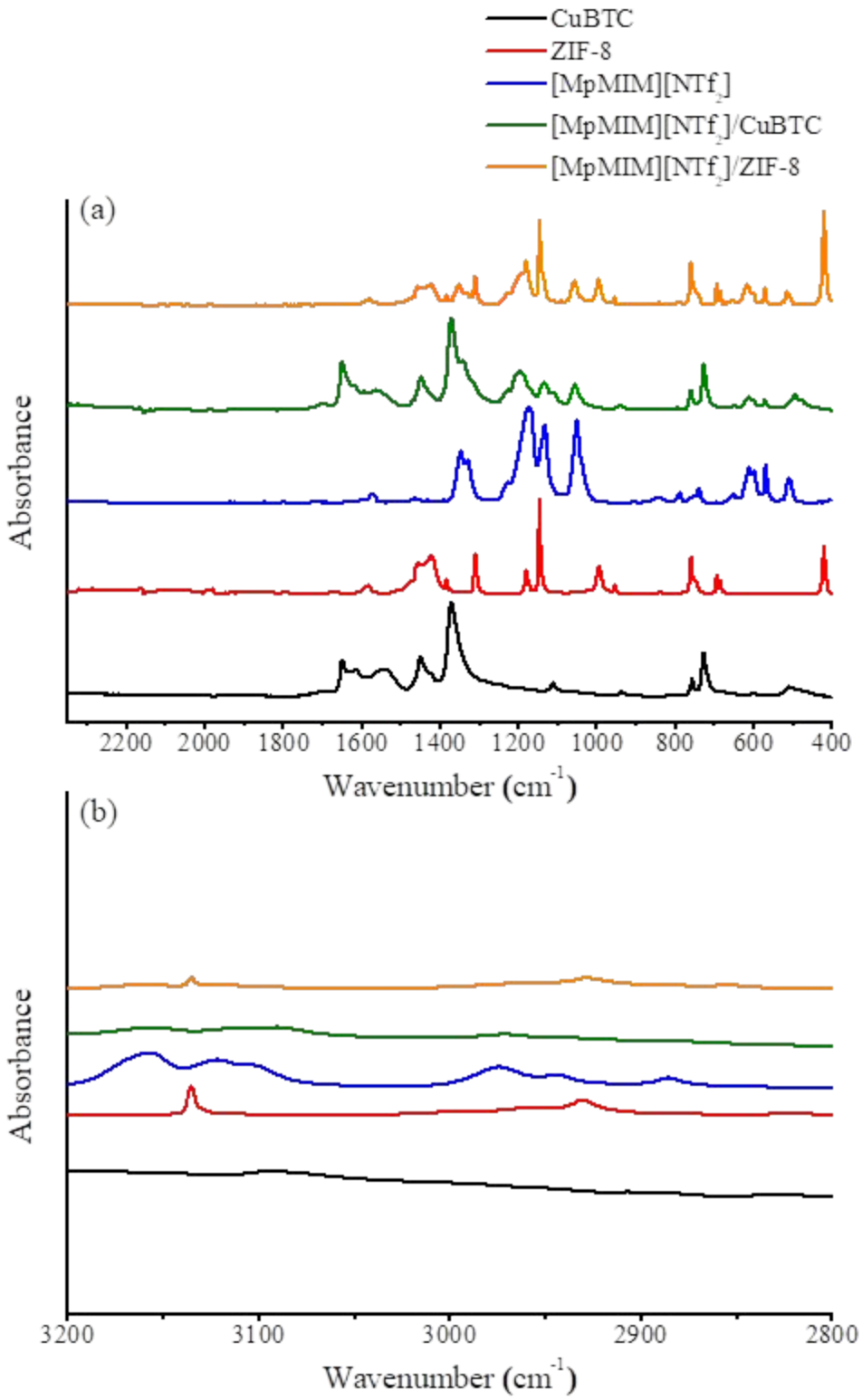

Figure S30. FTIR spectra of CuBTC, ZIF-8, [MpMIM][NTf_2], [MpMIM][NTf_2]/CuBTC, and [MpMIM][NTf_2]/ZIF-8 (a) 400-2250 cm^{-1} and (b) 2800-3200 cm^{-1}.

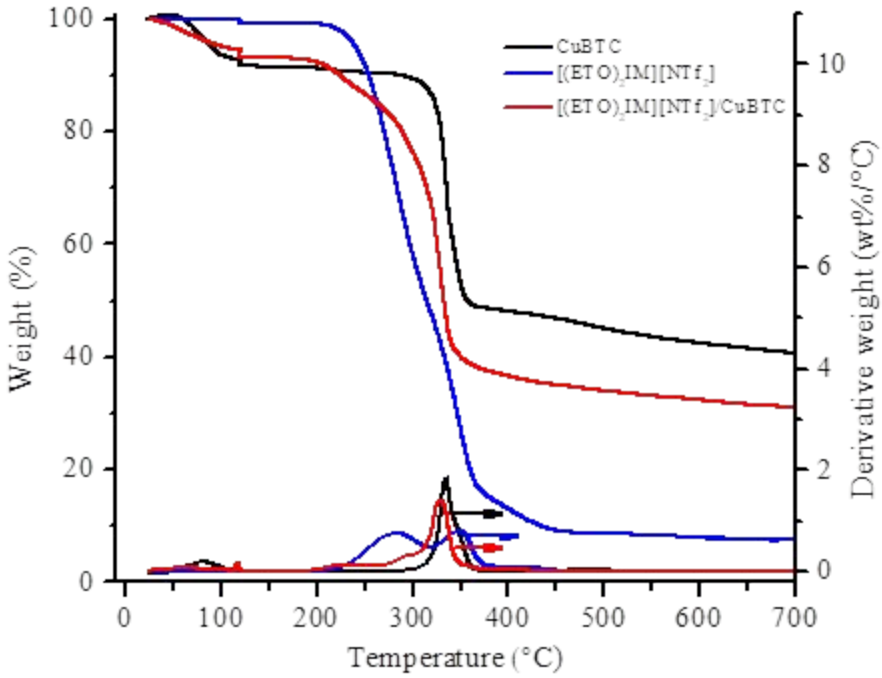

Figure S31. Thermal stability of pristine CuBTC, bulk $[(ETO)_2IM][NTf_2]$, and $[(ETO)_2IM][NTf_2]$/CuBTC.

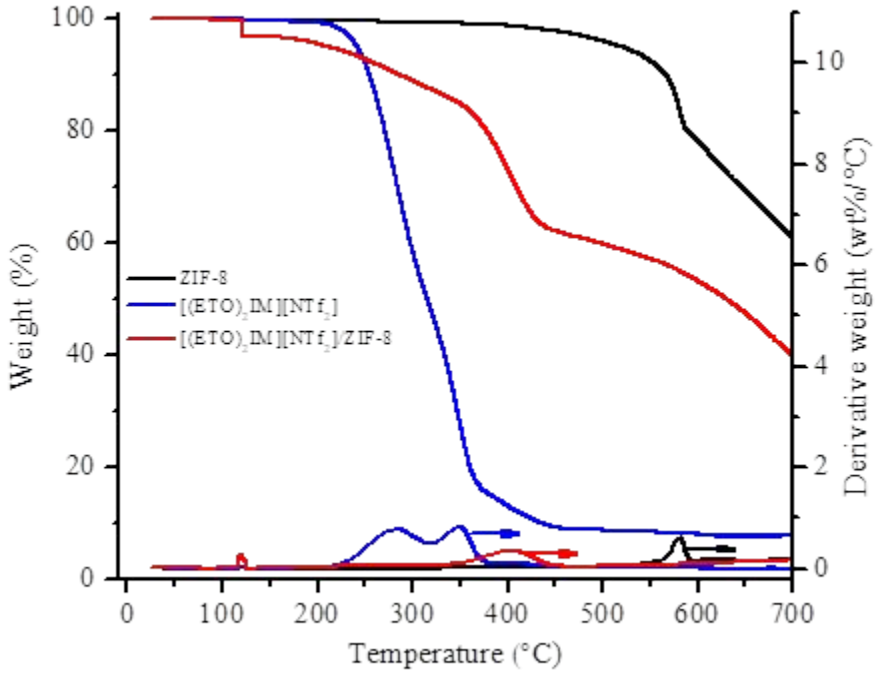

Figure S32. Thermal stability of pristine ZIF-8, bulk $[(ETO)_2IM][NTf_2]$, and $[(ETO)_2IM][NTf_2]$/ZIF-8.

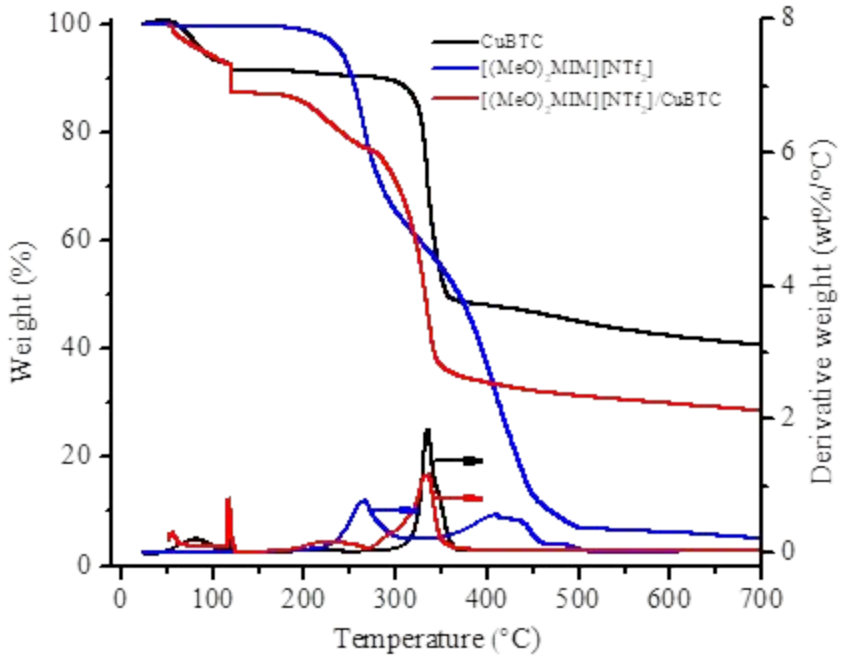

Figure S33. Thermal stability of pristine CuBTC, bulk $[(MeO)_2MIM][NTf_2]$, and $[(MeO)_2MIM][NTf_2]$/CuBTC.

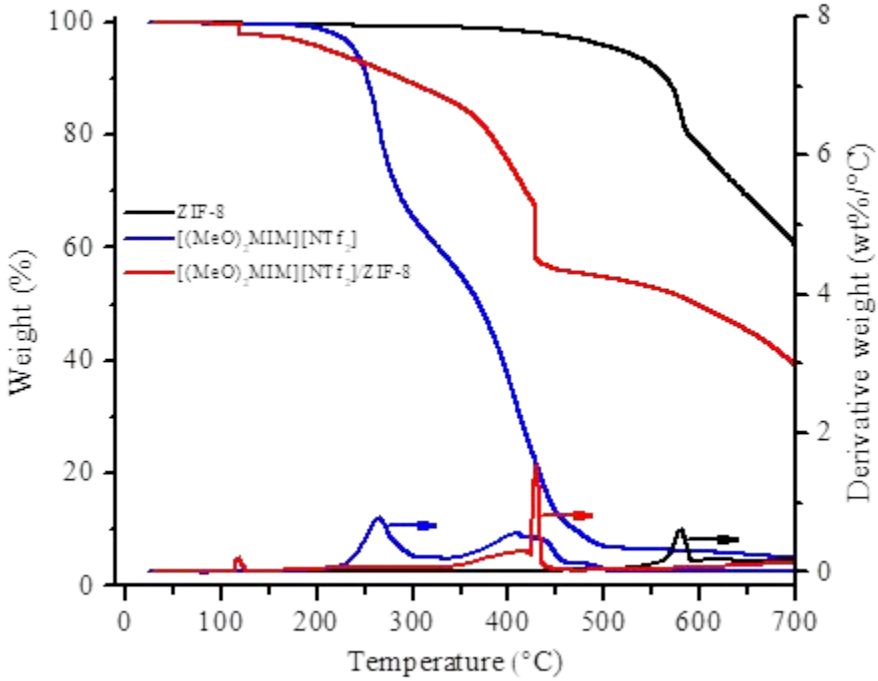

Figure S34. Thermal stability of pristine ZIF-8, bulk $[(MeO)_2MIM][NTf_2]$, and $[(MeO)_2MIM][NTf_2]$/ZIF-8.

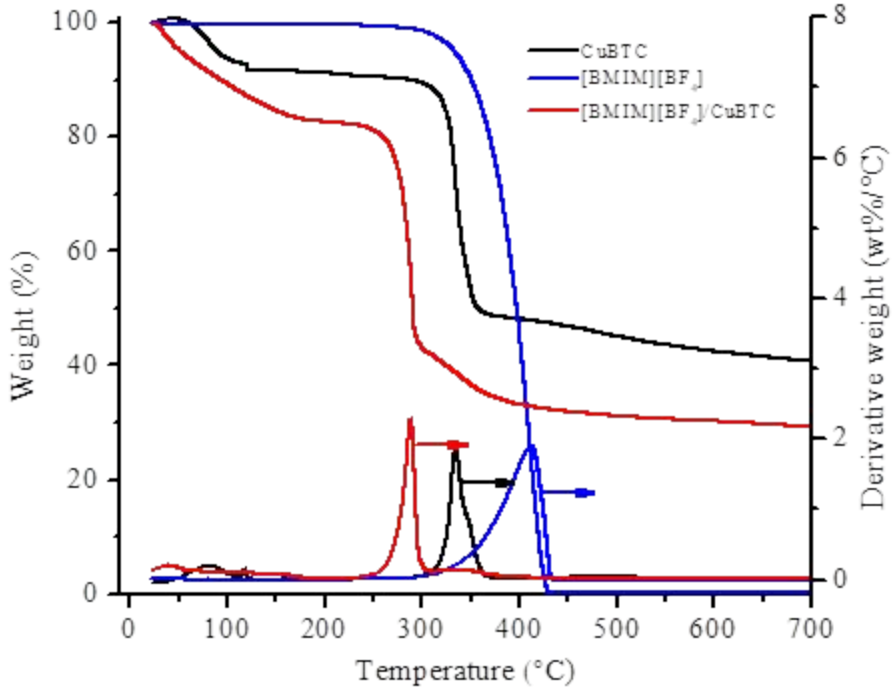

Figure S35. Thermal stability of pristine CuBTC, bulk [BMIM][BF_4], and [BMIM][BF_4]/CuBTC.

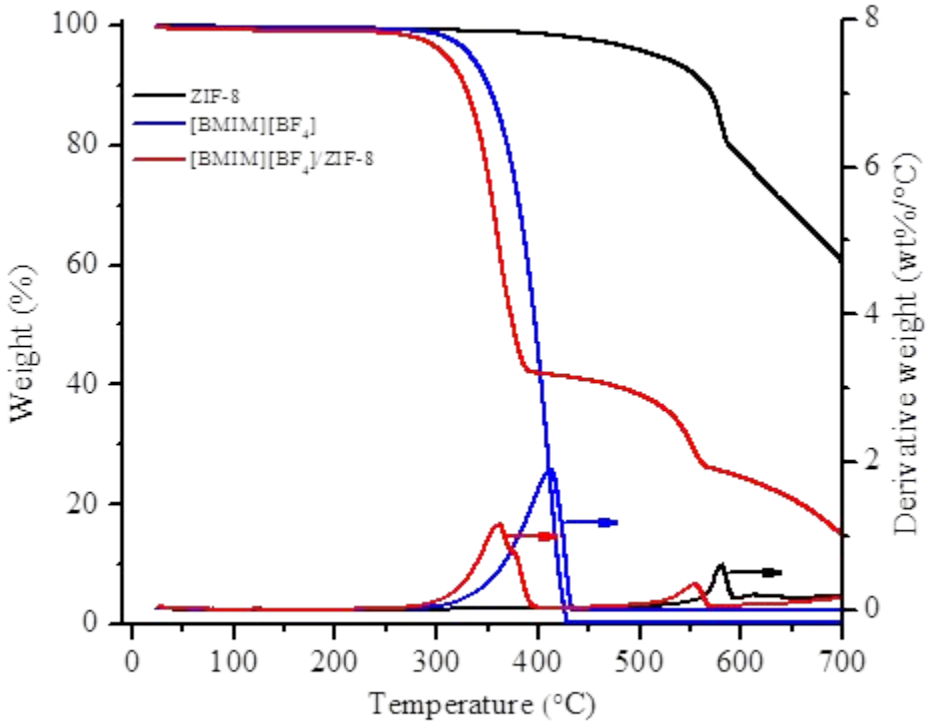

Figure S36. Thermal stability of pristine ZIF-8, bulk [BMIM][BF_4], and [BMIM][BF_4]/ZIF-8.

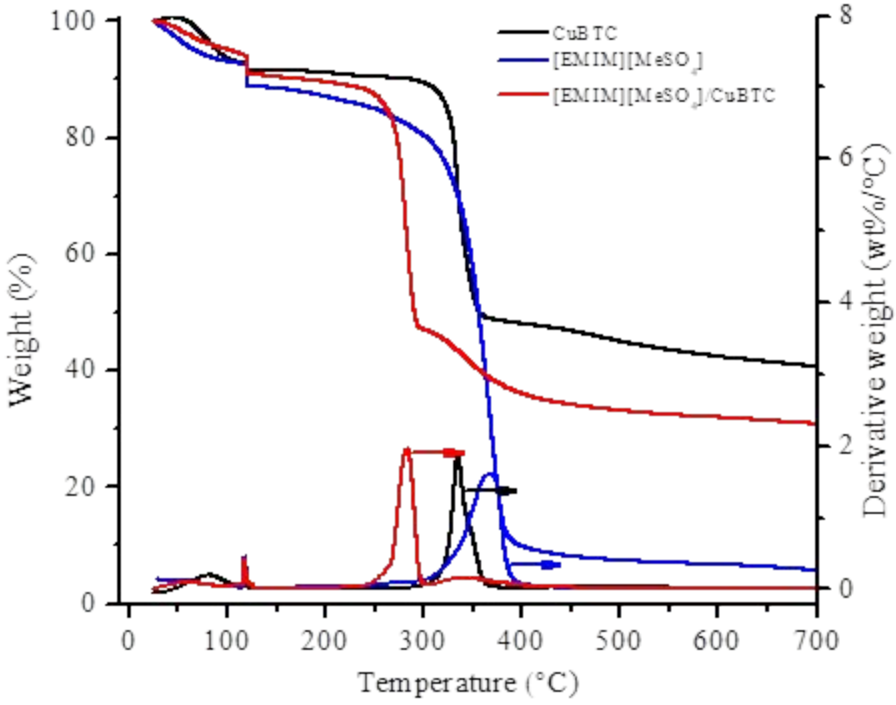

Figure S37. Thermal stability of pristine CuBTC, bulk [EMIM][$MeSO_4$], and [EMIM][$MeSO_4$]/CuBTC.

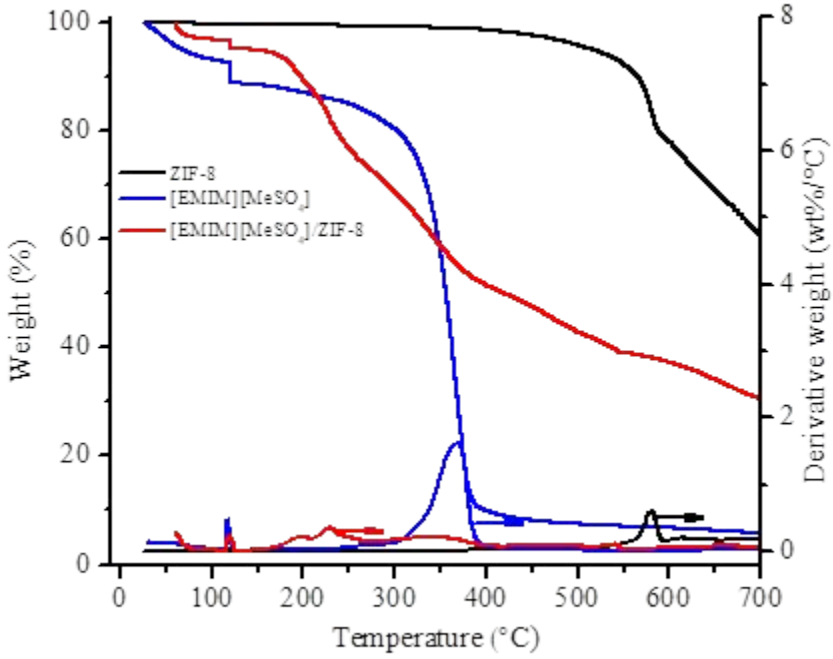

Figure S38. Thermal stability of pristine ZIF-8, bulk [EMIM][$MeSO_4$], and [EMIM][$MeSO_4$]/ZIF-8.

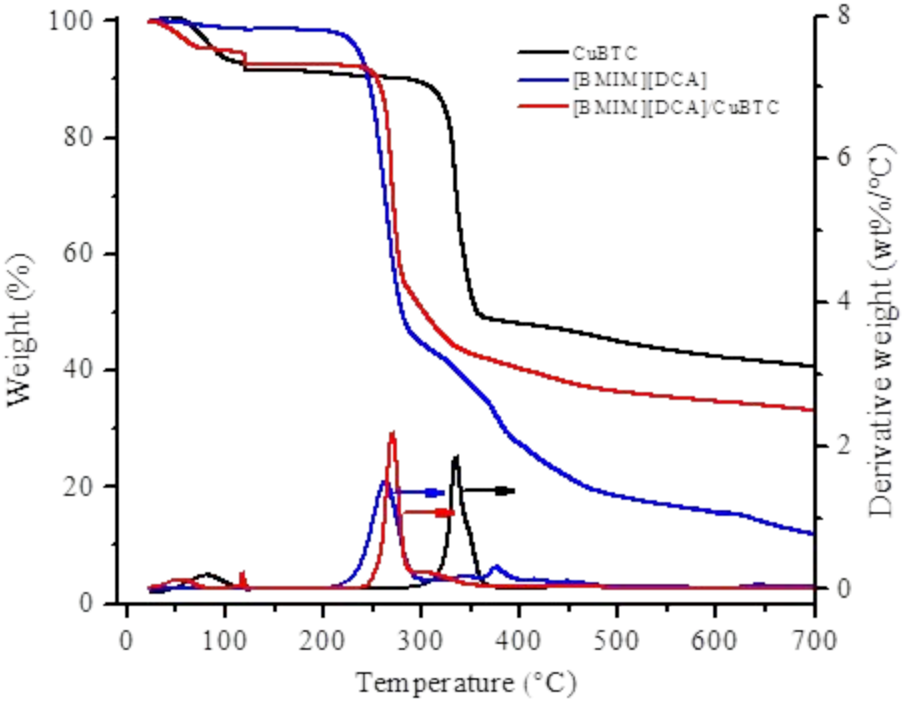

Figure S39. Thermal stability of pristine CuBTC, bulk [BMIM][DCA], and [BMIM][DCA]/CuBTC.

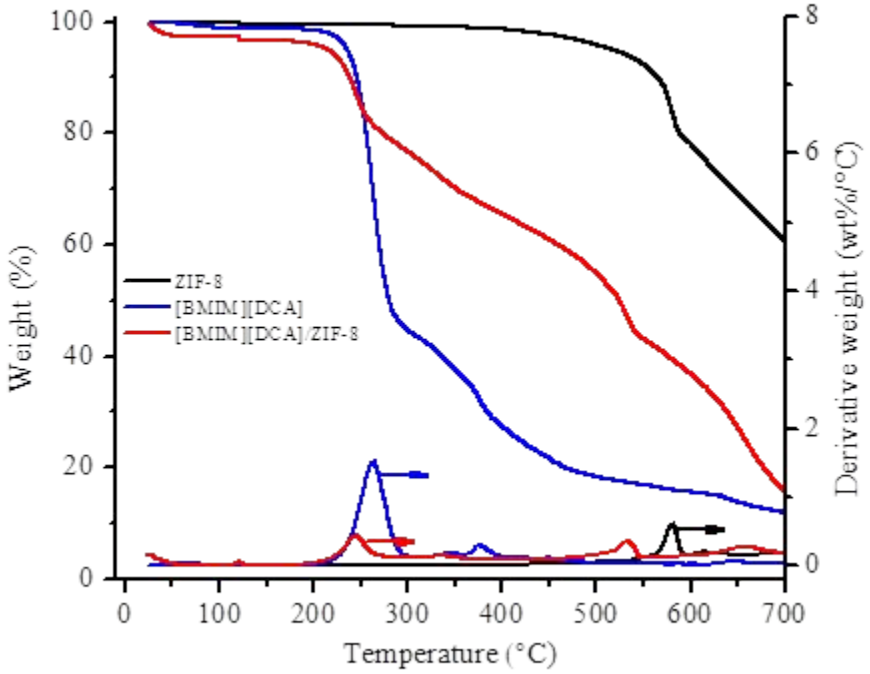

Figure S40. Thermal stability of pristine ZIF-8, bulk [BMIM][DCA], and [BMIM][DCA]/ZIF-8.

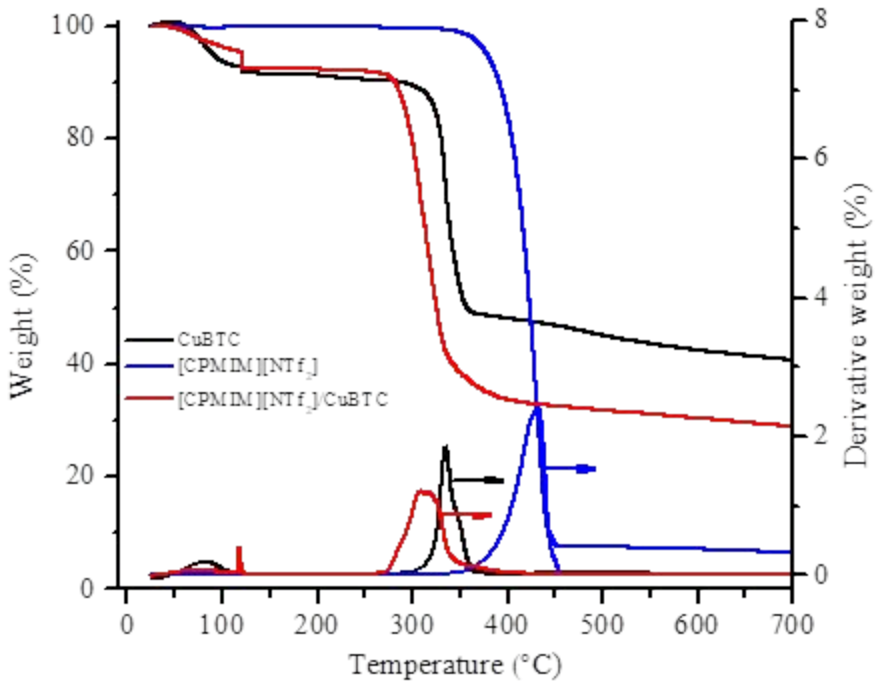

Figure S41. Thermal stability of pristine CuBTC, bulk [CPMIM][NTf_2], and [CPMIM][NTf_2]/CuBTC.

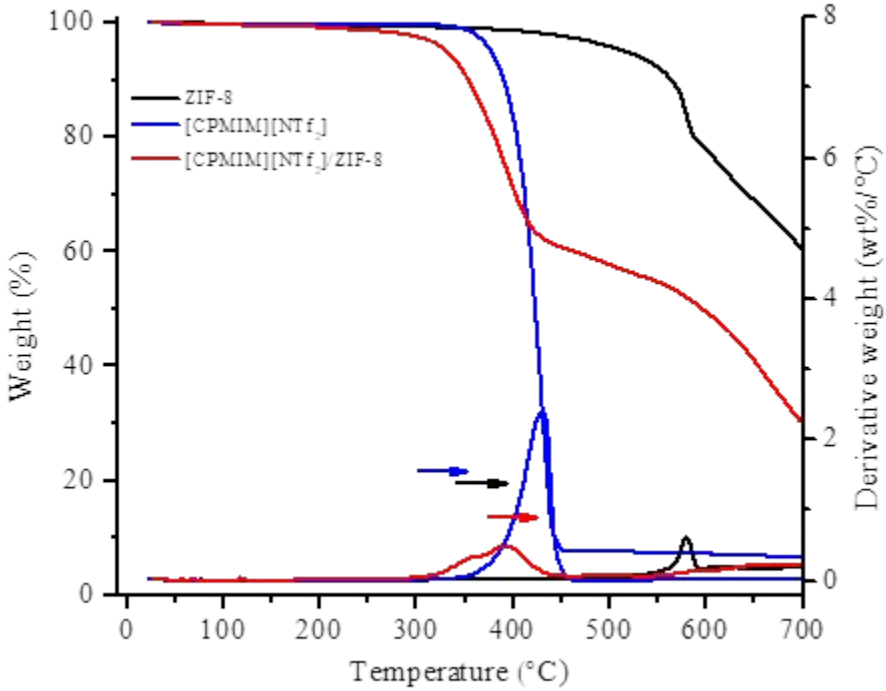

Figure S42. Thermal stability of pristine ZIF-8, bulk [CPMIM][NTf_2], and [CPMIM][NTf_2]/ZIF-8.

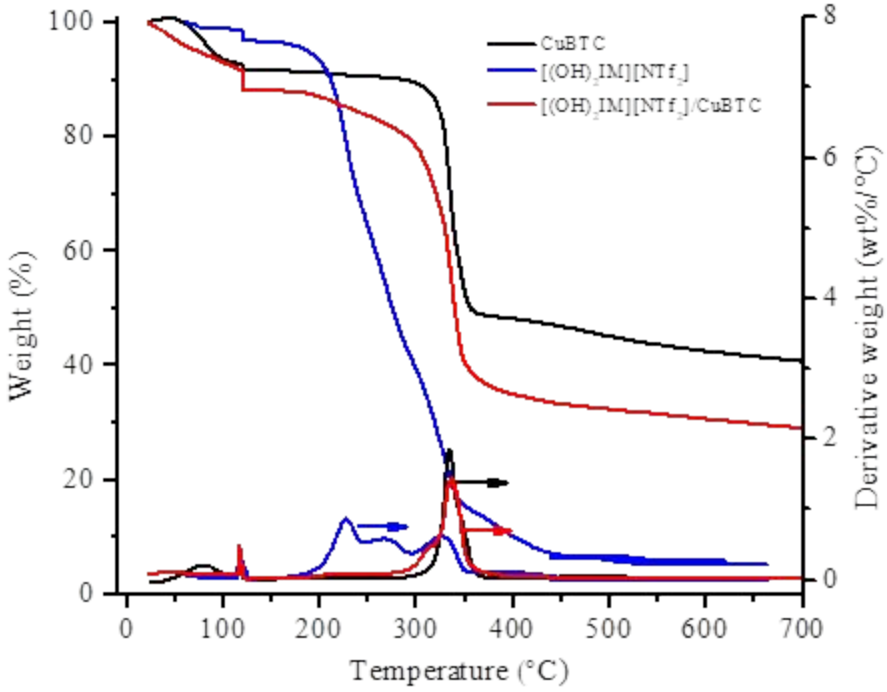

Figure S43. Thermal stability of pristine CuBTC, bulk $[(OH)_2IM][NTf_2]$, and $[(OH)_2IM][NTf_2]$/CuBTC.

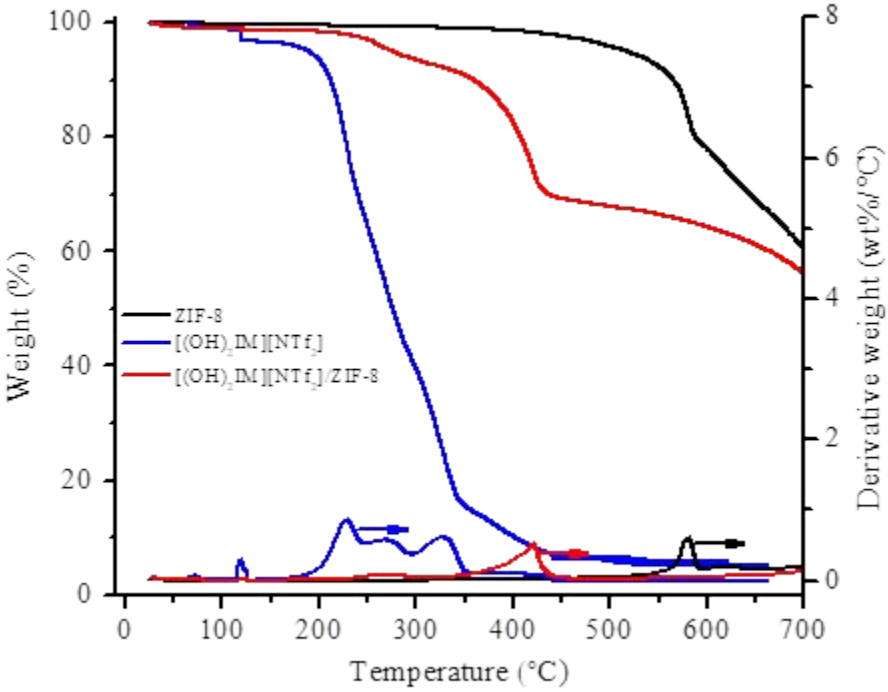

Figure S44. Thermal stability of pristine ZIF-8, bulk $[(OH)_2IM][NTf_2]$, and $[(OH)_2IM][NTf_2]$/ZIF-8.

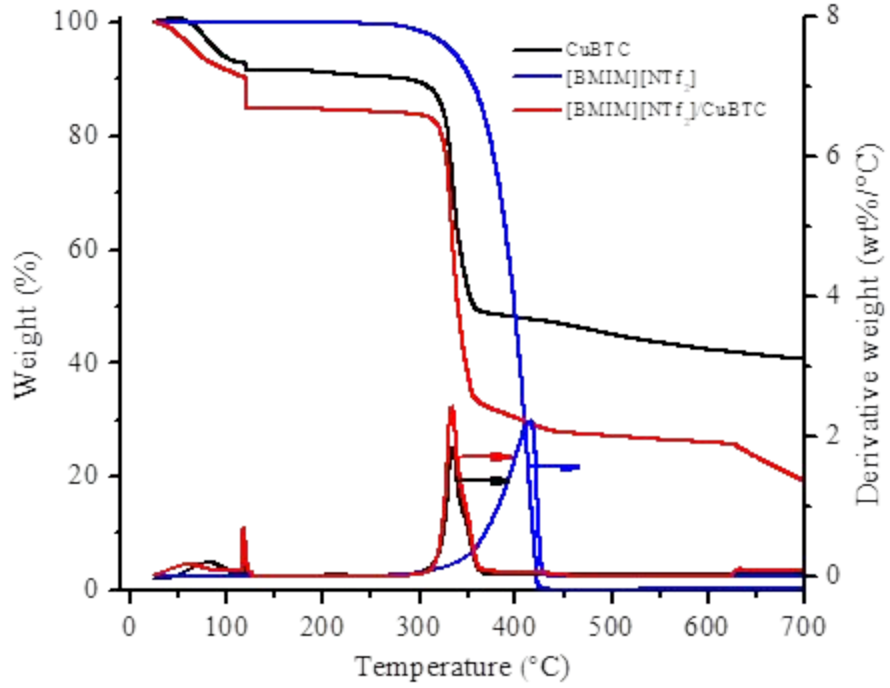

Figure S45. Thermal stability of pristine CuBTC, bulk [BMIM][NTf_2], and [BMIM][NTf_2]/CuBTC.

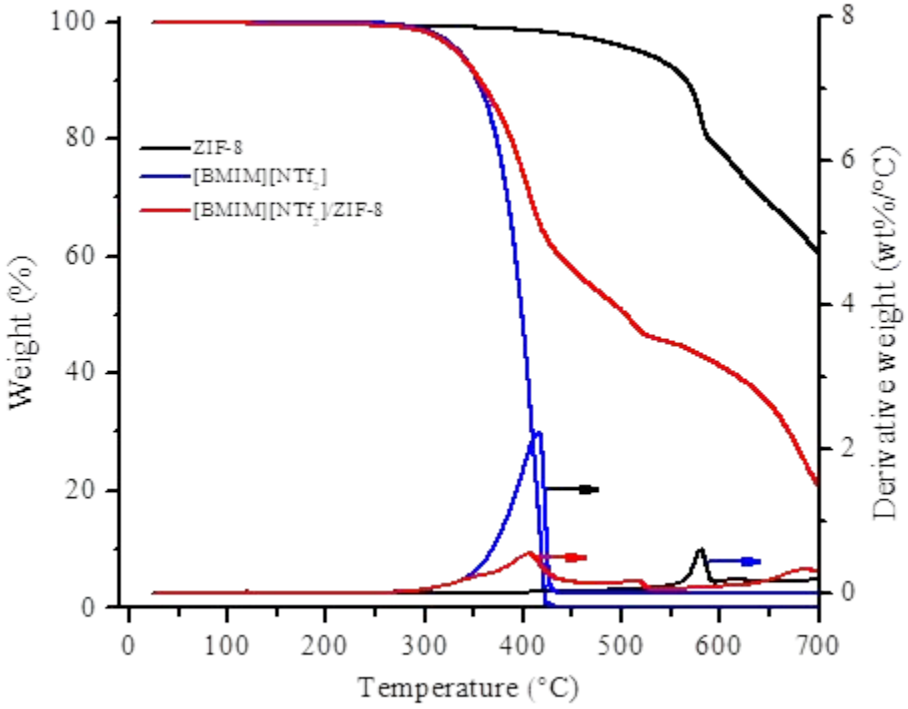

Figure S46. Thermal stability of pristine ZIF-8, bulk [BMIM][NTf_2], and [BMIM][NTf_2]/ZIF-8.

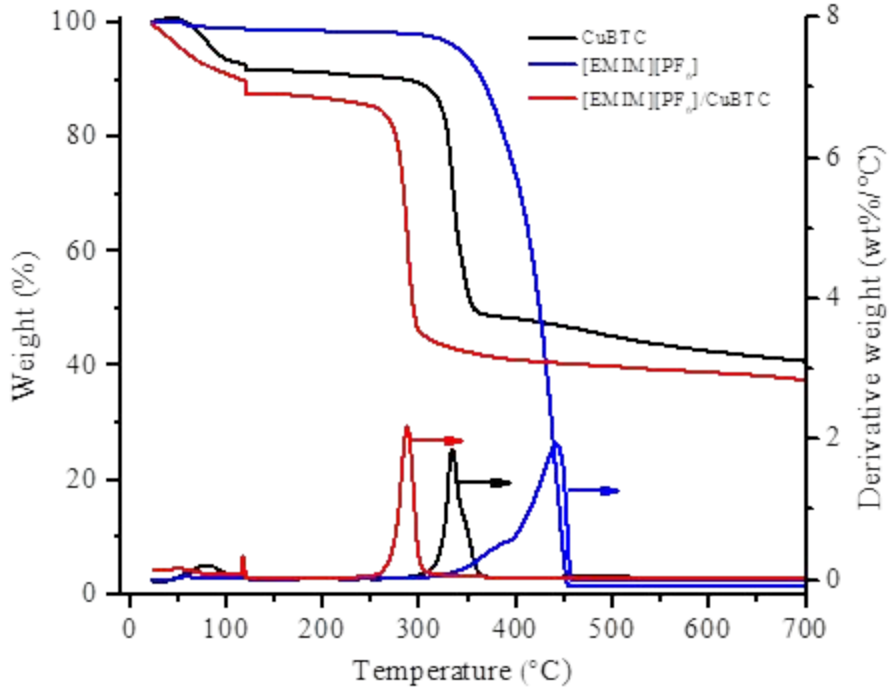

Figure S47. Thermal stability of pristine CuBTC, bulk [EMIM][PF_6], and [EMIM][PF_6]/CuBTC.

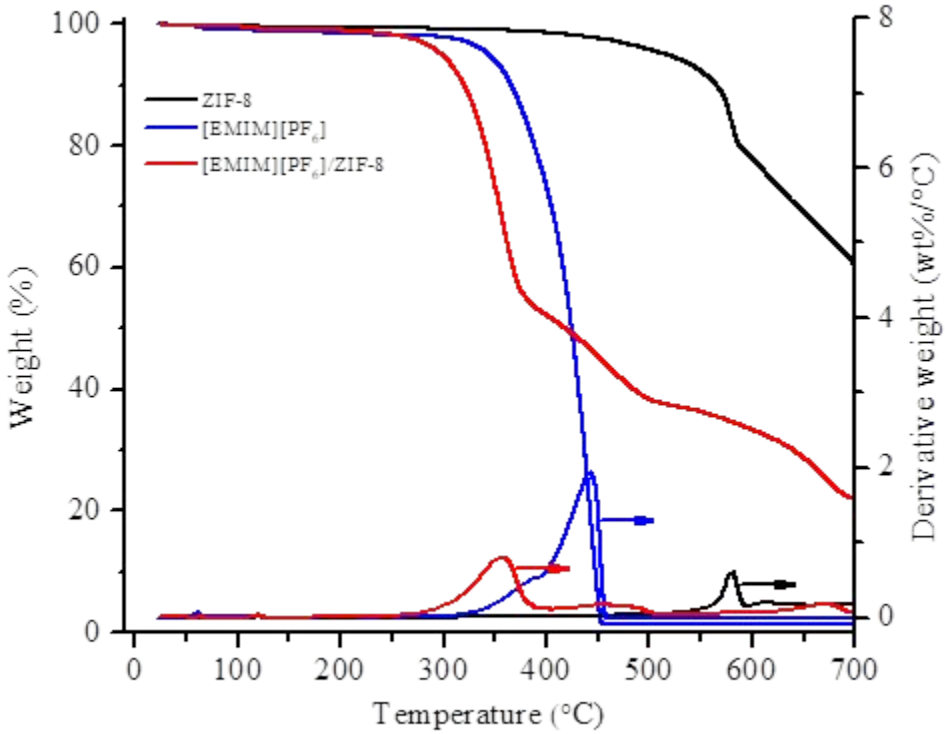

Figure S48. Thermal stability of pristine ZIF-8, bulk [EMIM][PF_6], and [EMIM][PF_6]/ZIF-8.

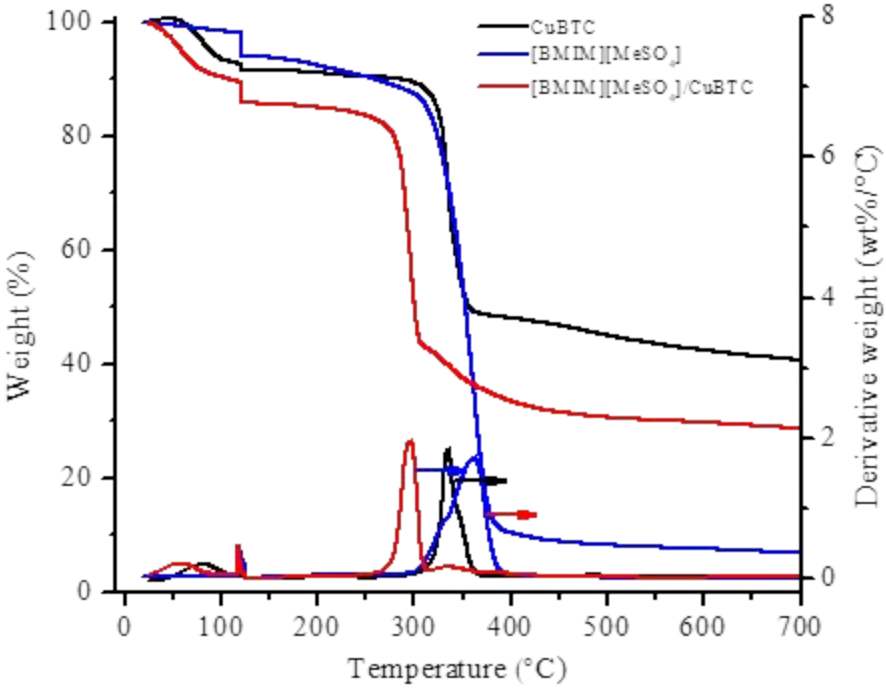

Figure S49. Thermal stability of pristine CuBTC, bulk [BMIM][$MeSO_4$], and [BMIM][$MeSO_4$]/CuBTC.

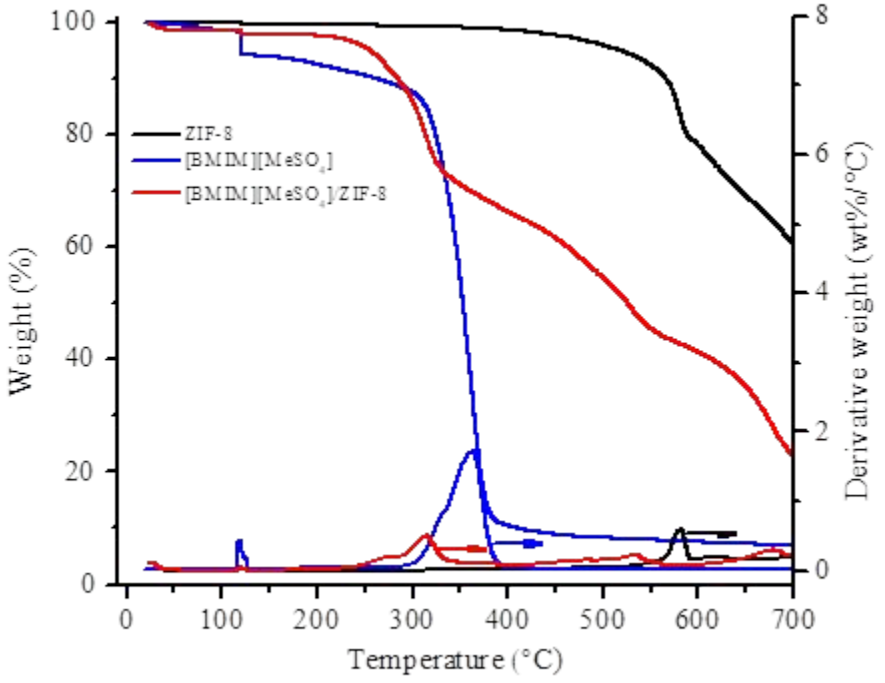

Figure S50. Thermal stability of pristine ZIF-8, bulk [BMIM][$MeSO_4$], and [BMIM][$MeSO_4$]/ZIF-8.

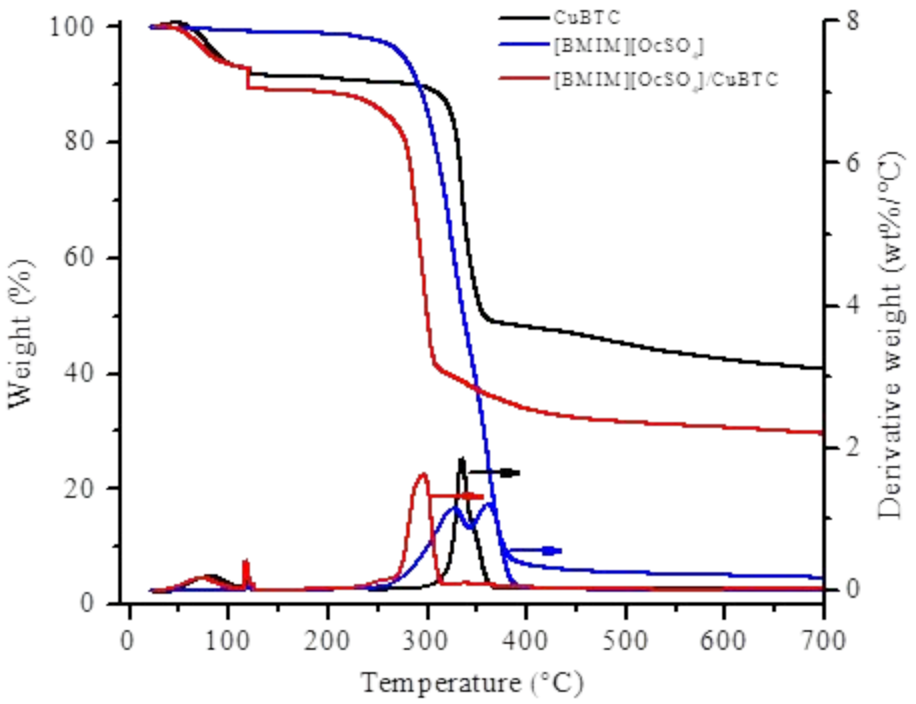

Figure S51. Thermal stability of pristine CuBTC, bulk [BMIM][$OcSO_4$], and [BMIM][$OcSO_4$]/CuBTC.

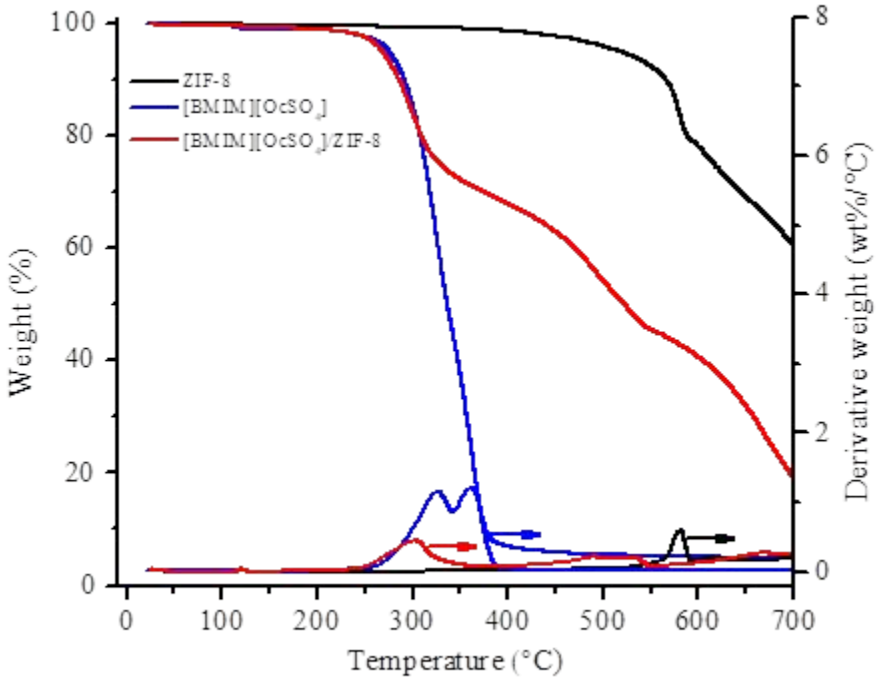

Figure S52. Thermal stability of pristine ZIF-8, bulk [BMIM][$OcSO_4$], and [BMIM][$OcSO_4$]/ZIF-8.

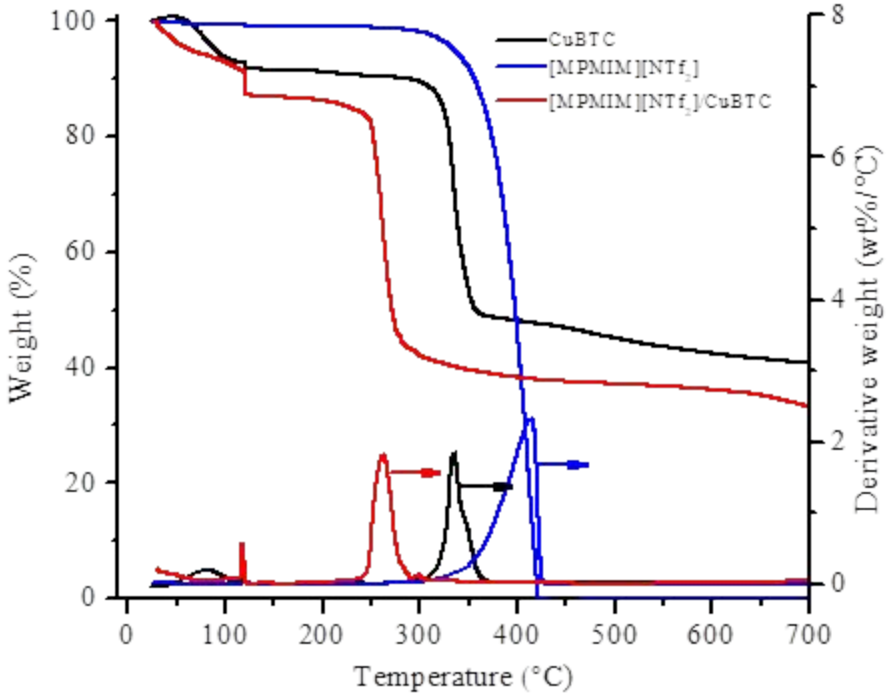

Figure S53. Thermal stability of pristine CuBTC, bulk [MPMIM][NTf_2], and [MPMIM][NTf_2]/CuBTC.

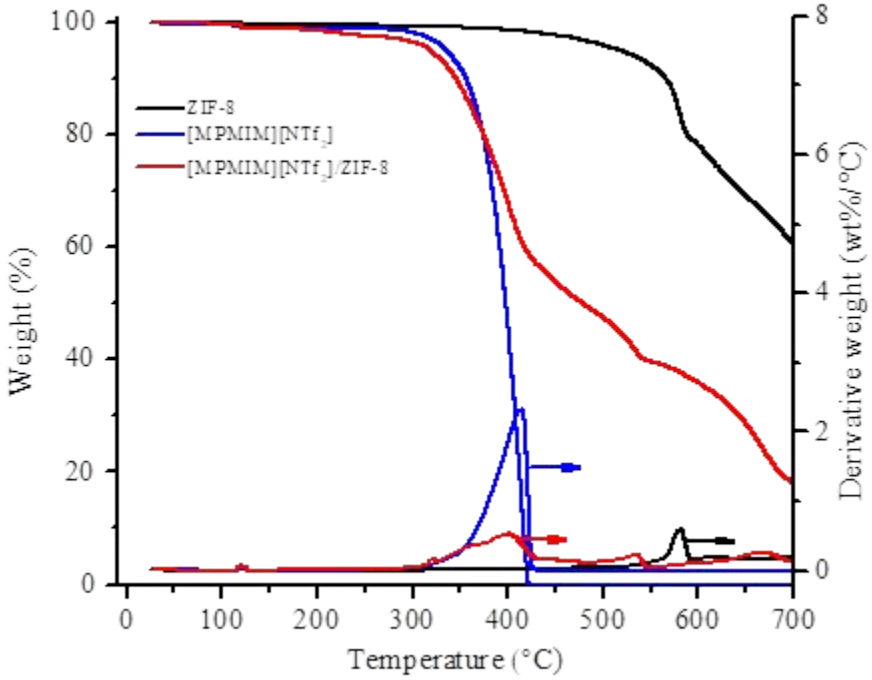

Figure S54. Thermal stability of pristine ZIF-8, Bulk [MPMIM][NTf_2], and [MPMIM][NTf_2]/ZIF-8.

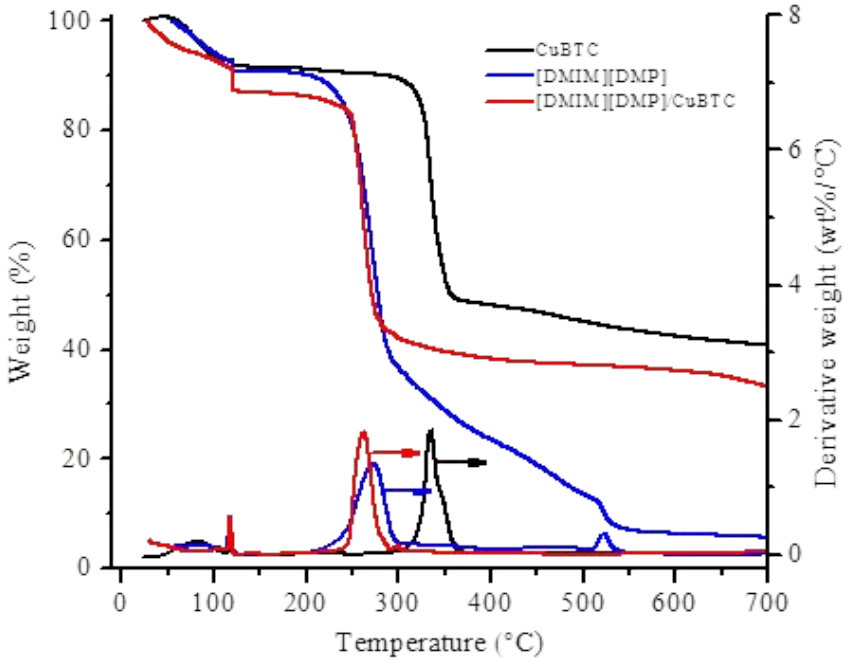

Figure S55. Thermal stability of pristine CuBTC, bulk [DMIM][DMP], and [DMIM][DMP]/CuBTC.

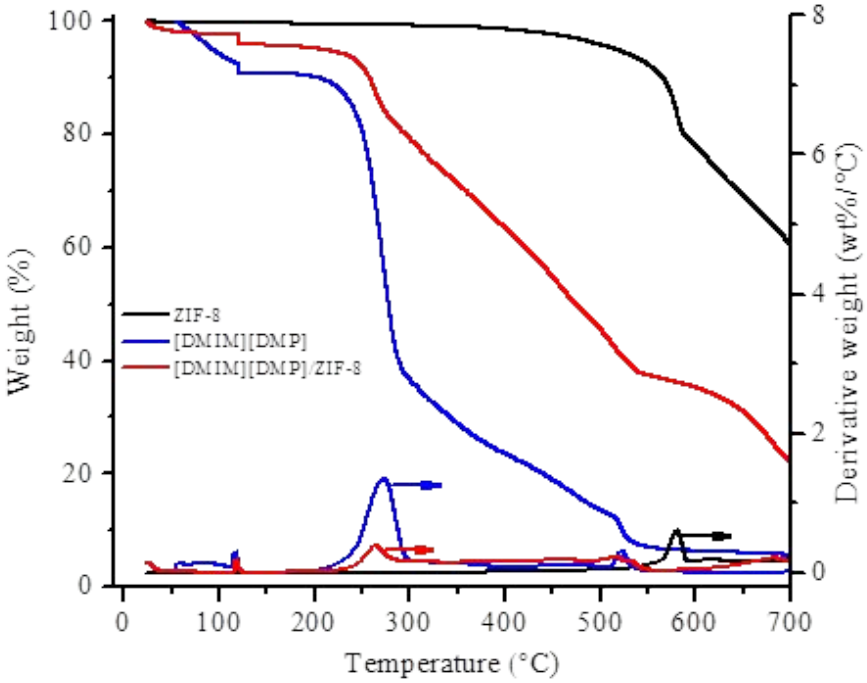

Figure S56. Thermal stability of pristine ZIF-8, bulk [DMIM][DMP], and [DMIM][DMP]/ZIF-8.

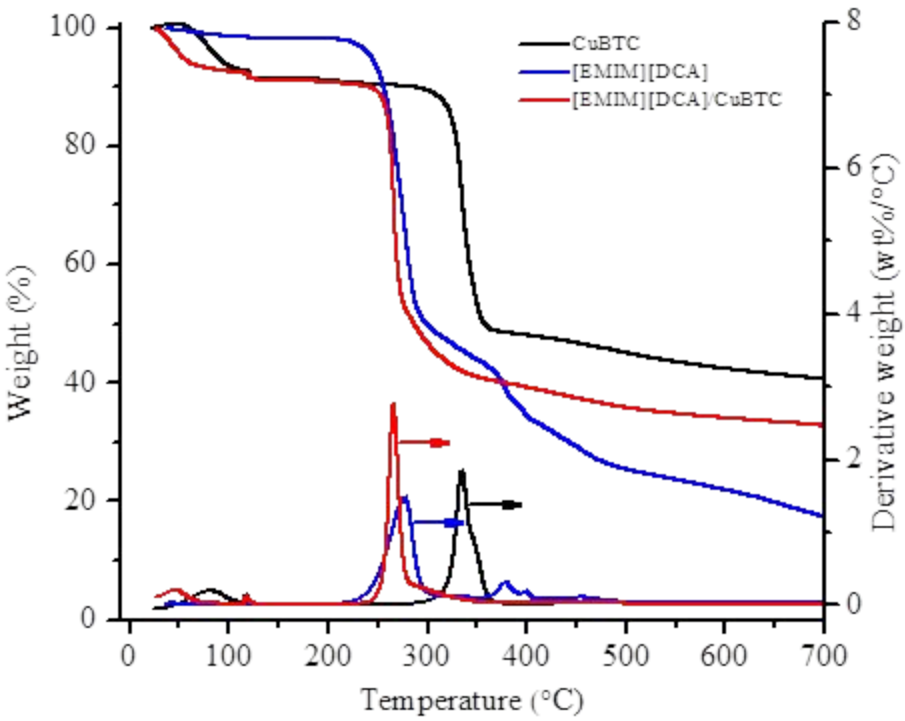

Figure S57. Thermal stability of pristine CuBTC, bulk [EMIM][DCA], and [EMIM][DCA]/CuBTC.

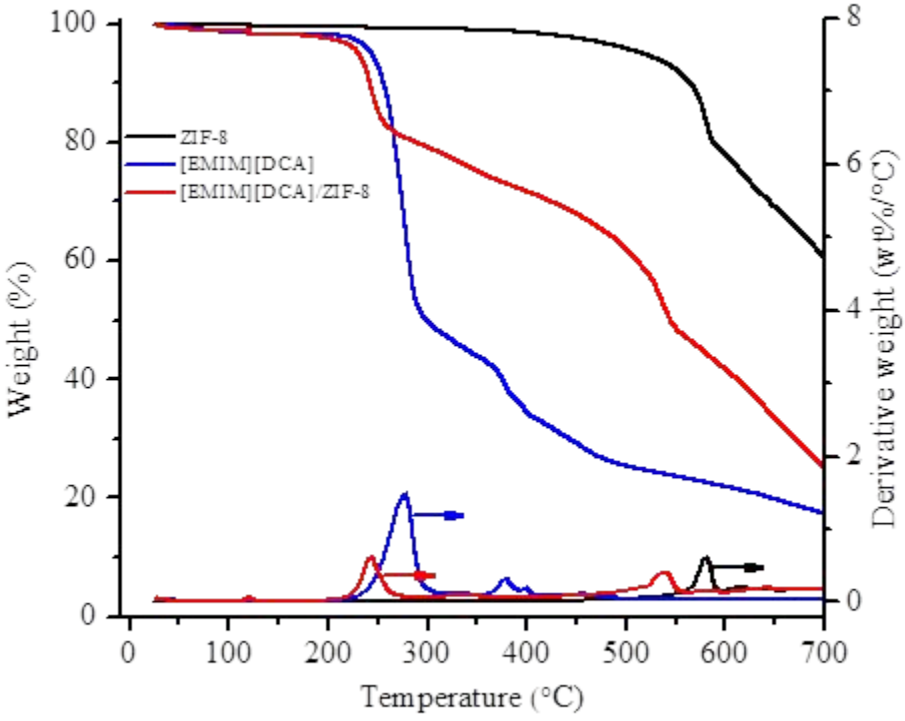

Figure S58. Thermal stability of pristine ZIF-8, bulk [EMIM][DCA], and [EMIM][DCA]/ZIF-8.

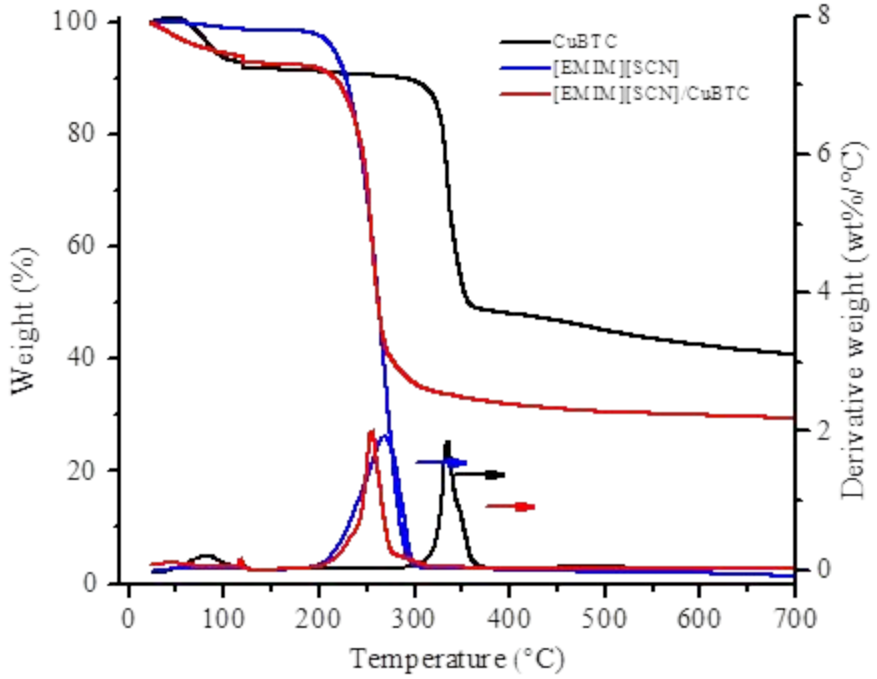

Figure S59. Thermal stability of pristine CuBTC, bulk [EMIM][SCN], and [EMIM][SCN]/CuBTC.

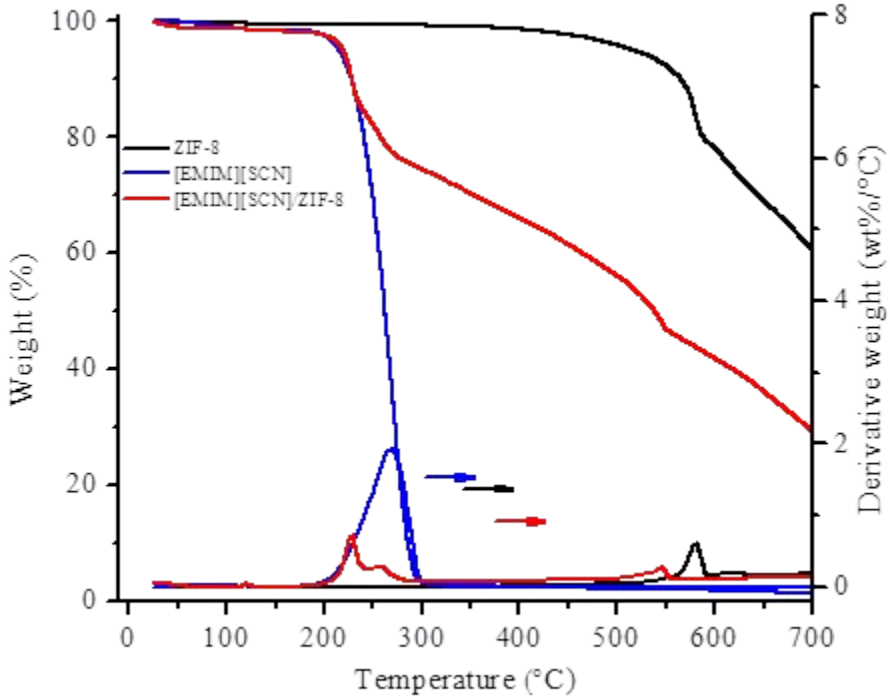

Figure S60. Thermal stability of pristine ZIF-8, bulk [EMIM][SCN], and [EMIM][SCN]/ZIF-8.

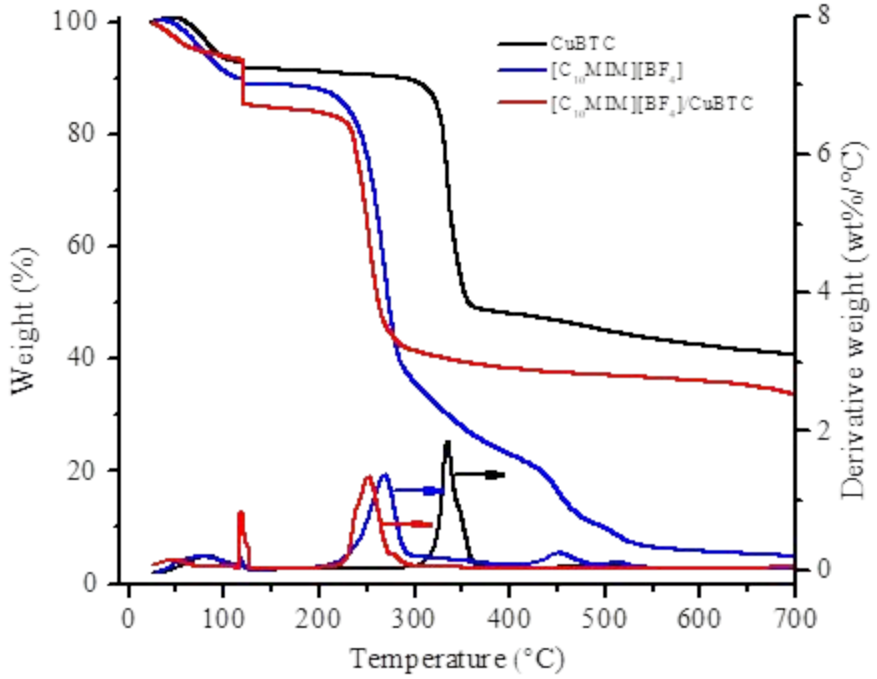

Figure S61. Thermal stability of pristine CuBTC, bulk $[C_{10}MIM][BF_4]$, and $[C_{10}MIM][BF_4]$/CuBTC.

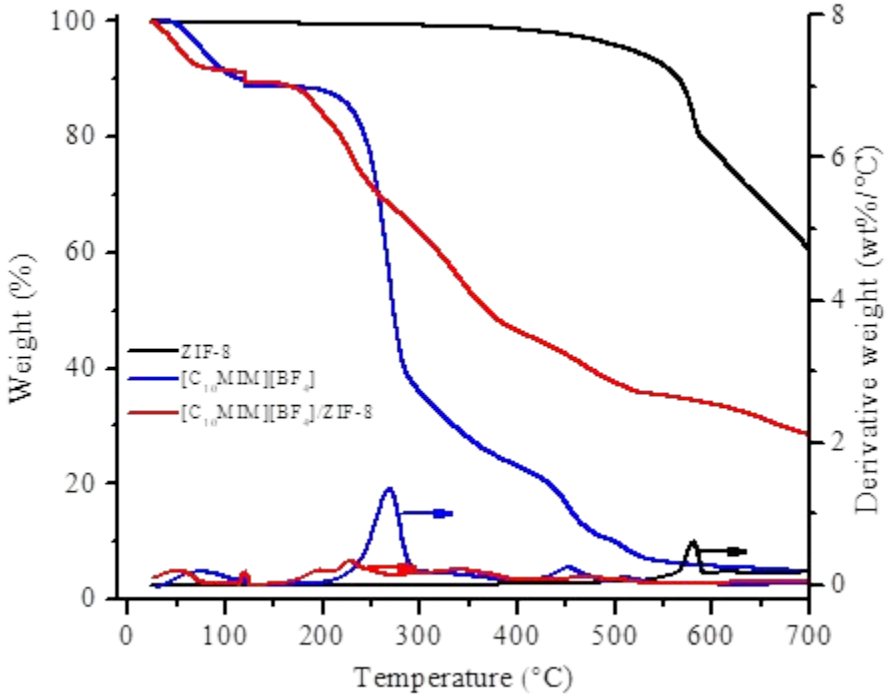

Figure S62. Thermal stability of pristine ZIF-8, bulk $[C_{10}MIM][BF_4]$, and $[C_{10}MIM][BF_4]$/ZIF-8.

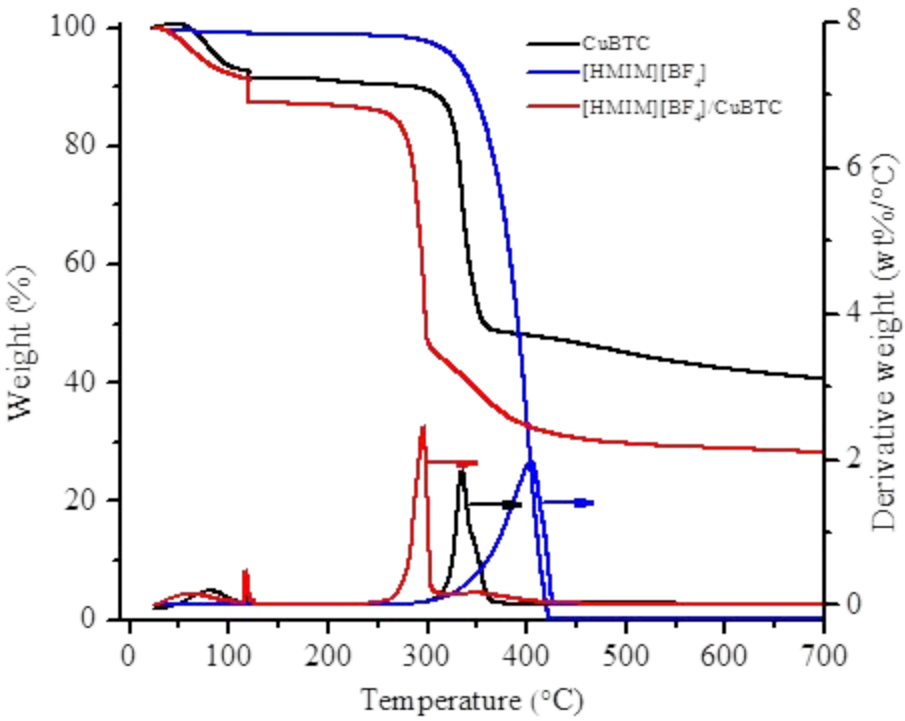

Figure S63. Thermal stability of pristine CuBTC, bulk [HMIM][BF_4], and [HMIM][BF_4]/CuBTC.

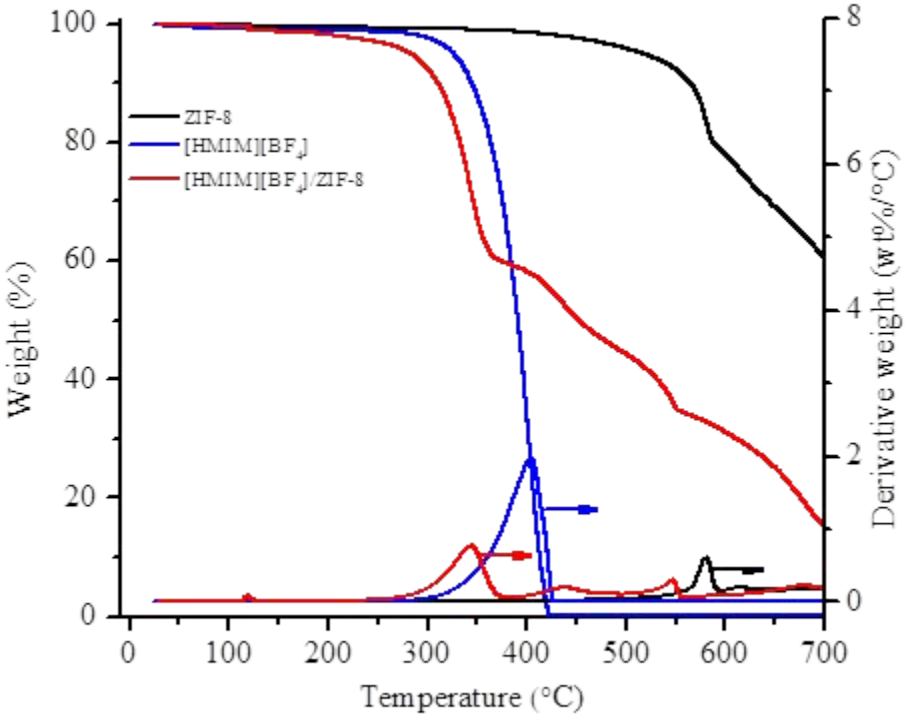

Figure S64. Thermal stability of pristine ZIF-8, bulk [HMIM][BF_4], and [HMIM][BF_4]/ZIF-8.

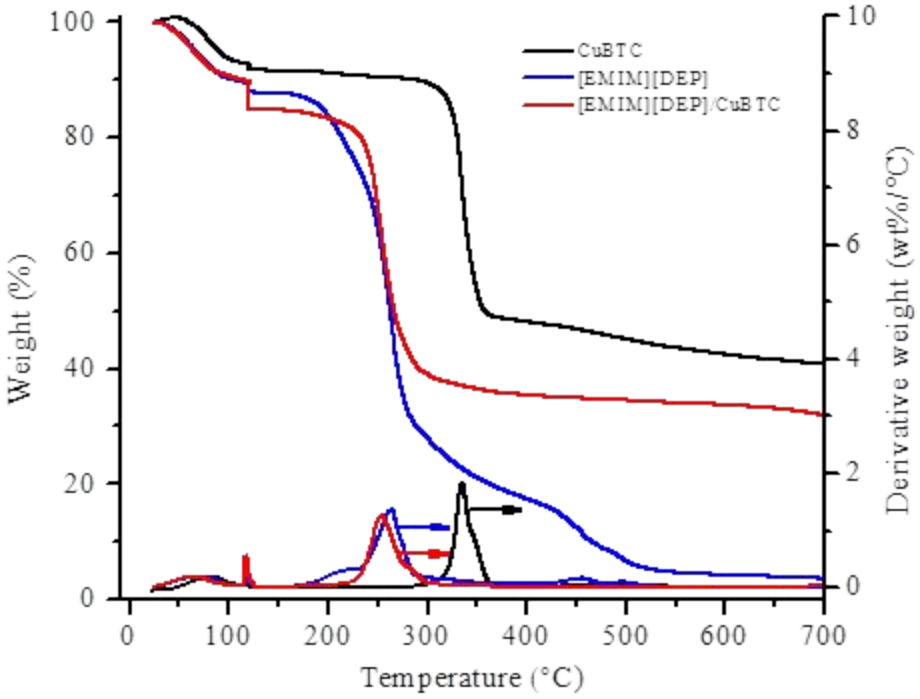

Figure S65. Thermal stability of pristine CuBTC, bulk [EMIM][DEP], and [EMIM][DEP]/CuBTC.

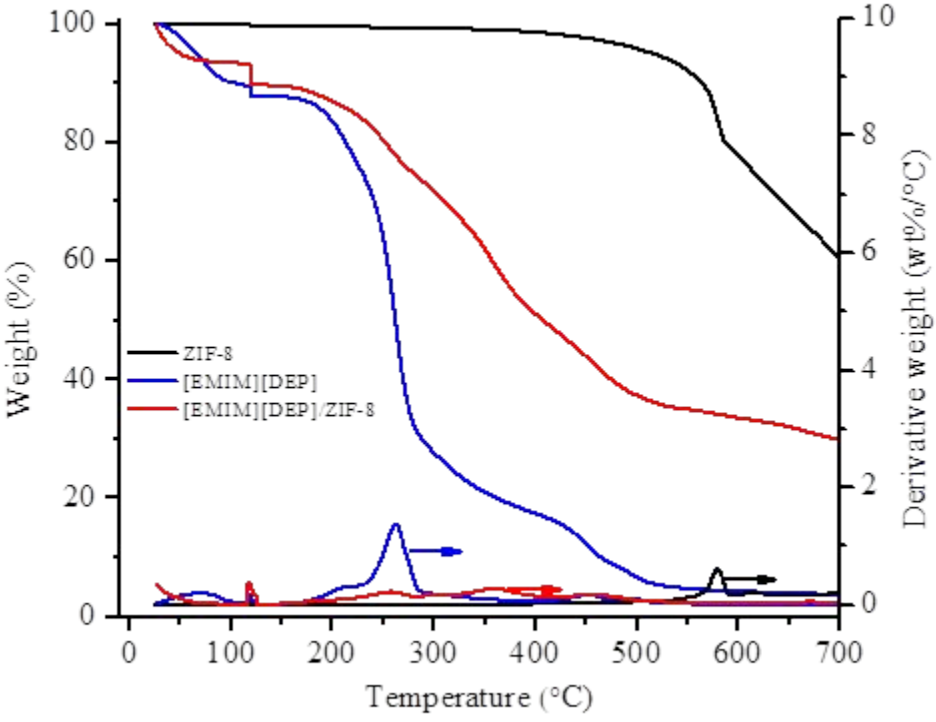

Figure S66. Thermal stability of pristine ZIF-8, bulk [EMIM][DEP], and [EMIM][DEP]/ZIF-8.

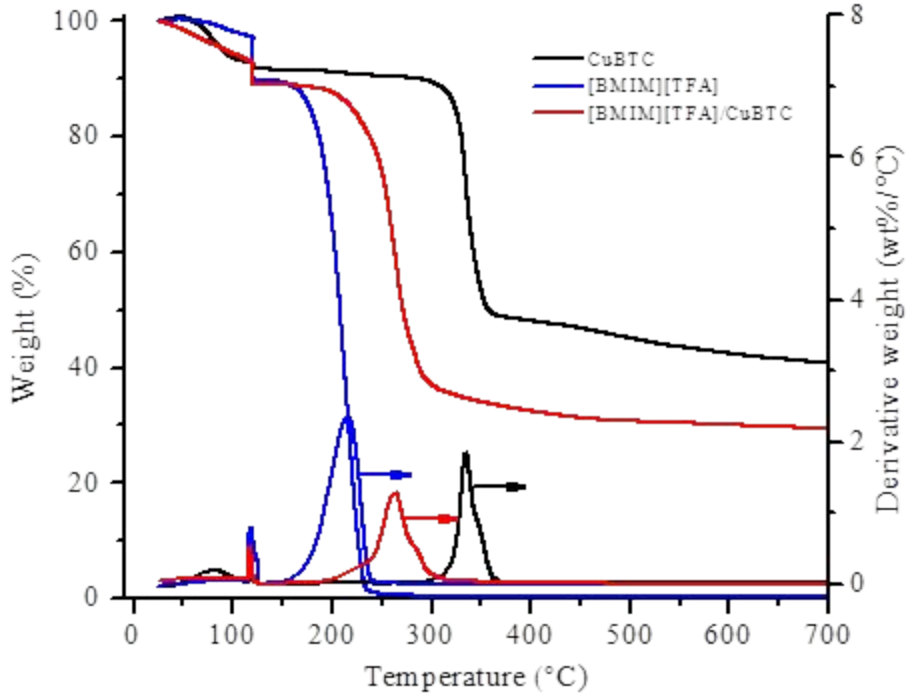

Figure S67. Thermal stability of pristine CuBTC, bulk [BMIM][TFA], and [BMIM][TFA]/CuBTC.

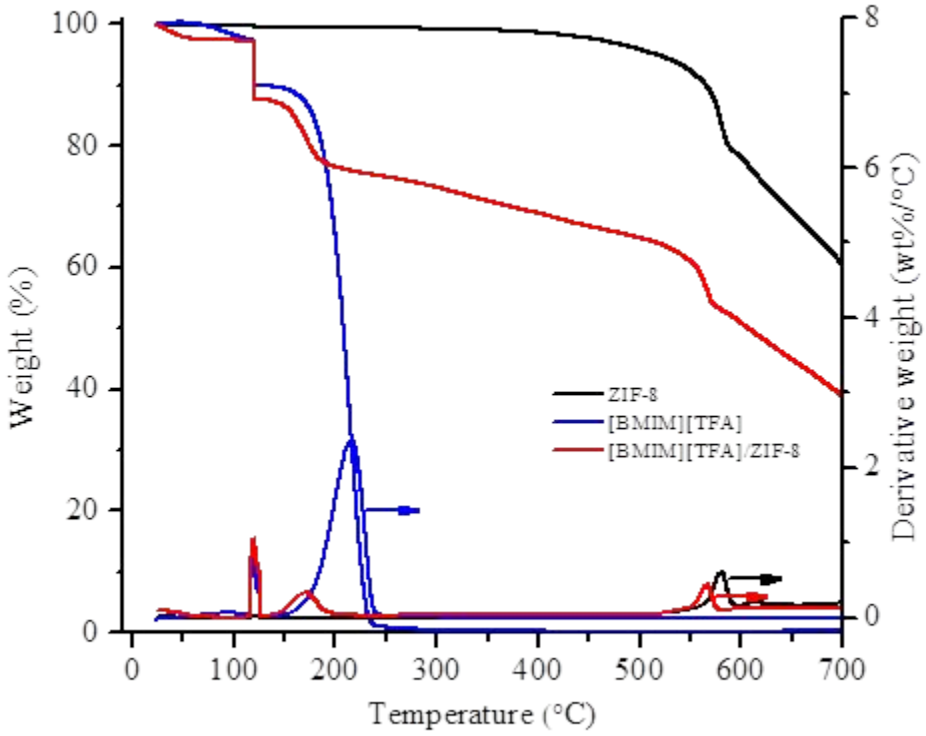

Figure S68. Thermal stability of pristine ZIF-8, bulk [BMIM][TFA], and [BMIM][TFA]/ZIF-8.

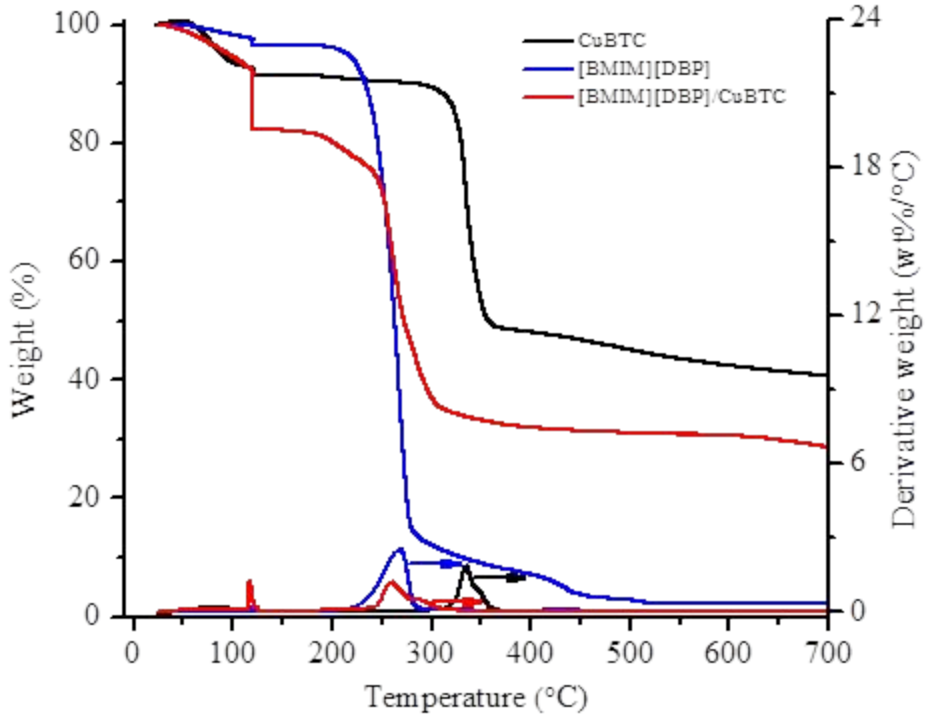

Figure S69. Thermal stability of pristine CuBTC, bulk [BMIM][DBP], and [BMIM][DBP]/CuBTC.

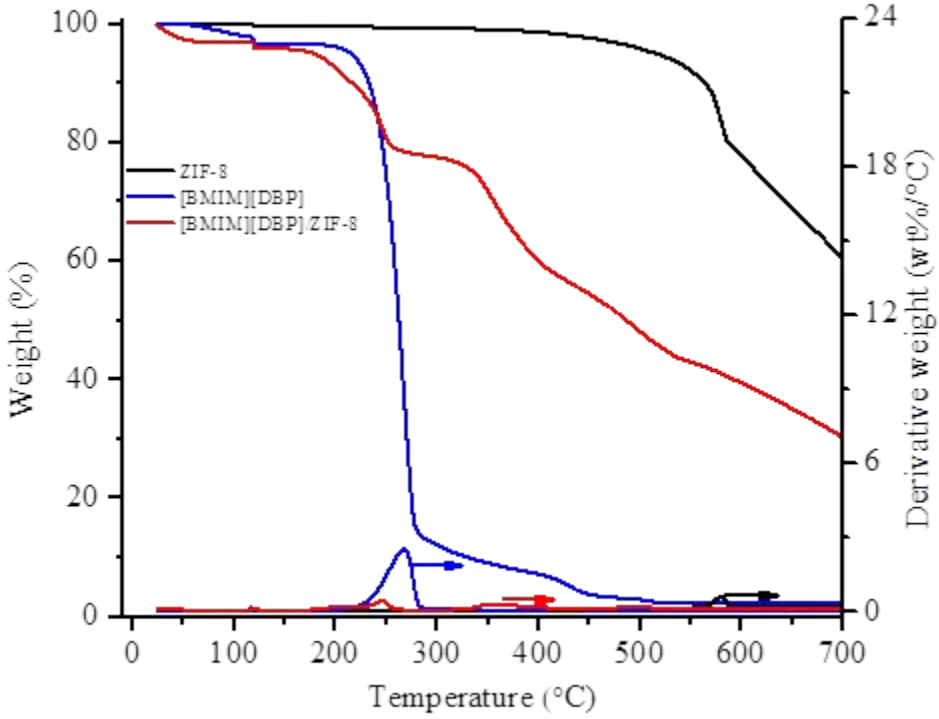

Figure S70. Thermal stability of pristine ZIF-8, bulk [BMIM][DBP], and [BMIM][DBP]/ZIF-8.

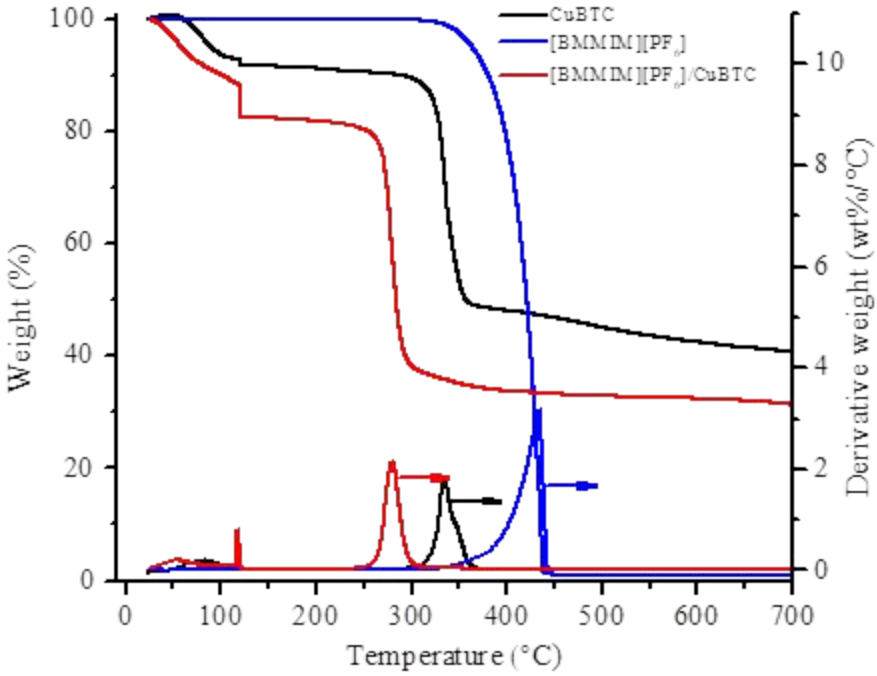

Figure S71. Thermal stability of pristine CuBTC, bulk [BMMIM][PF_6], and [BMMIM][PF_6]/CuBTC.

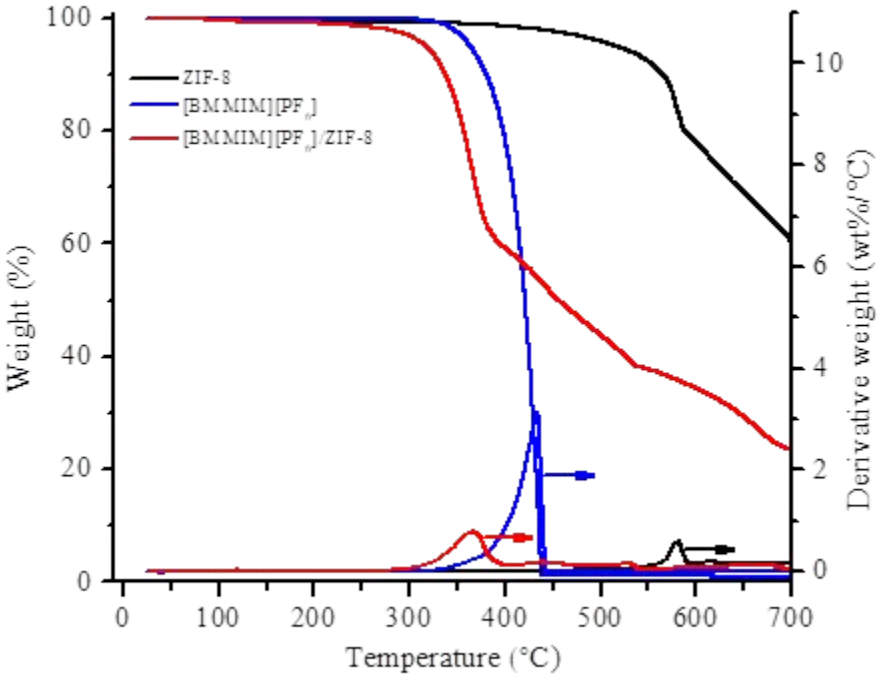

Figure S72. Thermal stability of pristine ZIF-8, bulk [BMMIM][PF_6], and [BMMIM][PF_6]/ZIF-8.

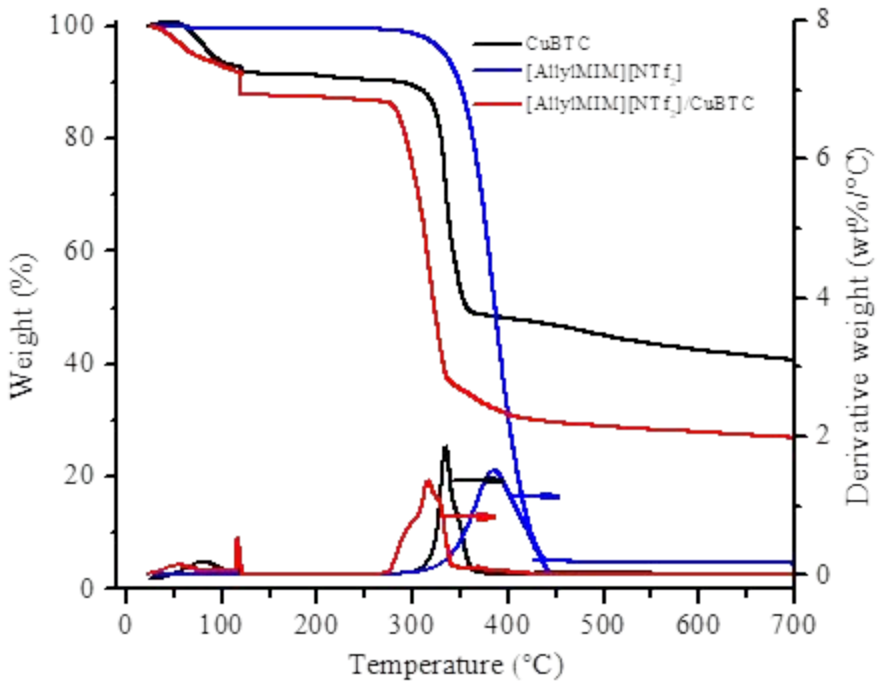

Figure S73. Thermal stability of pristine CuBTC, bulk [AllylMIM][NTf_2], and [AllylMIM][NTf_2]/ CuBTC.

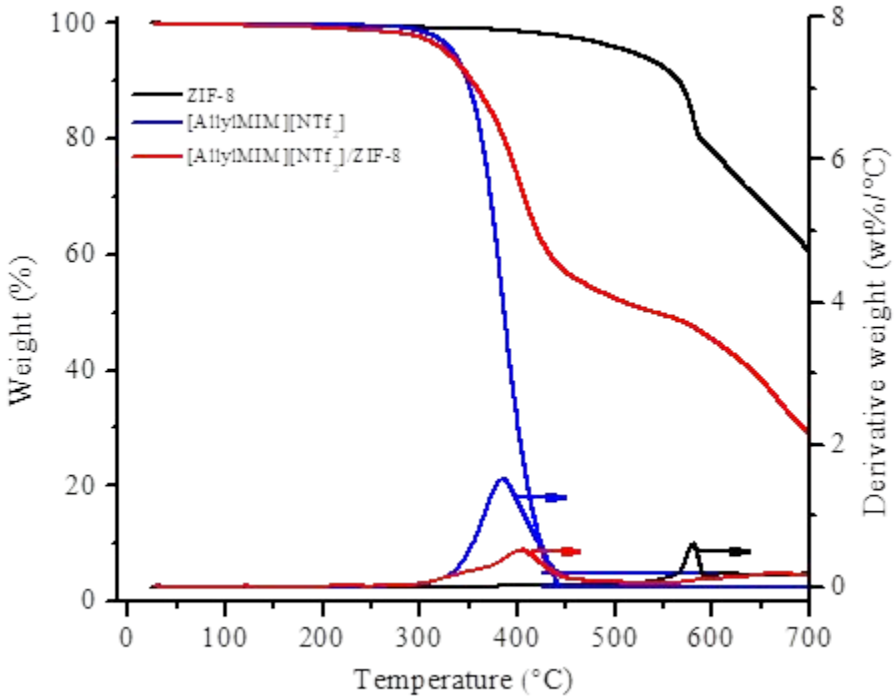

Figure S74. Thermal stability of pristine ZIF-8, bulk [AllylMIM][NTf_2], and [AllylMIM][NTf_2]/ZIF-8.

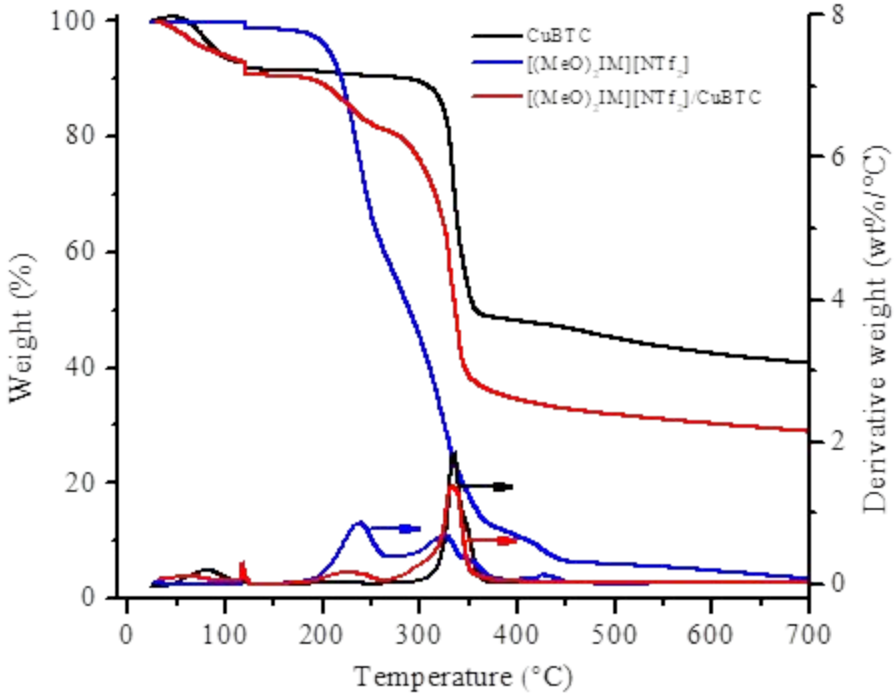

Figure S75. Thermal stability of pristine CuBTC, bulk [(MeO)2IM][NTf_2], and [(MeO)2IM][NTf_2]/CuBTC.

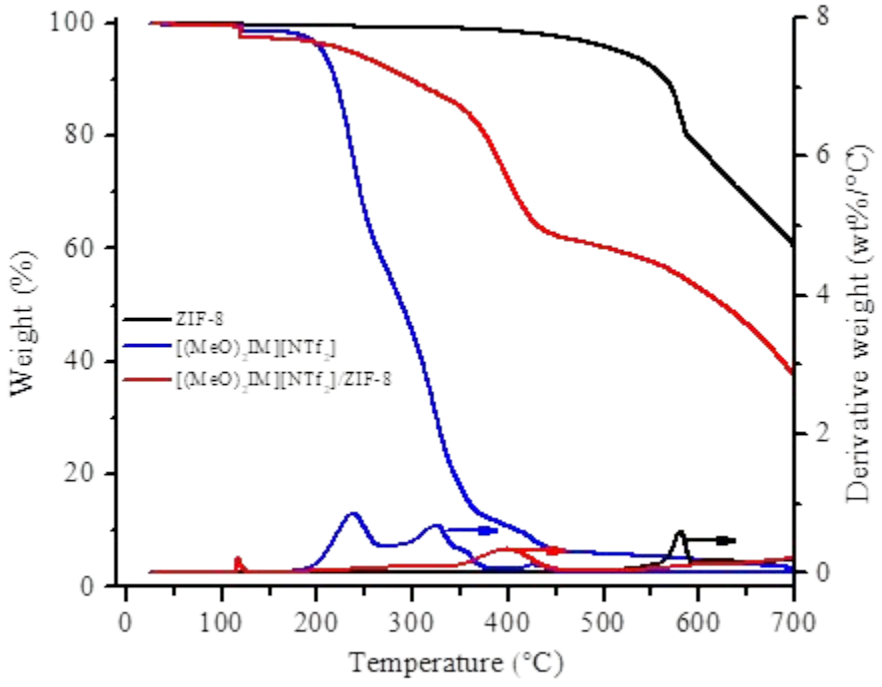

Figure S76. Thermal stability of pristine ZIF-8, bulk [(MeO)2IM][NTf_2], and [(MeO)2IM][NTf_2]/ZIF-8.

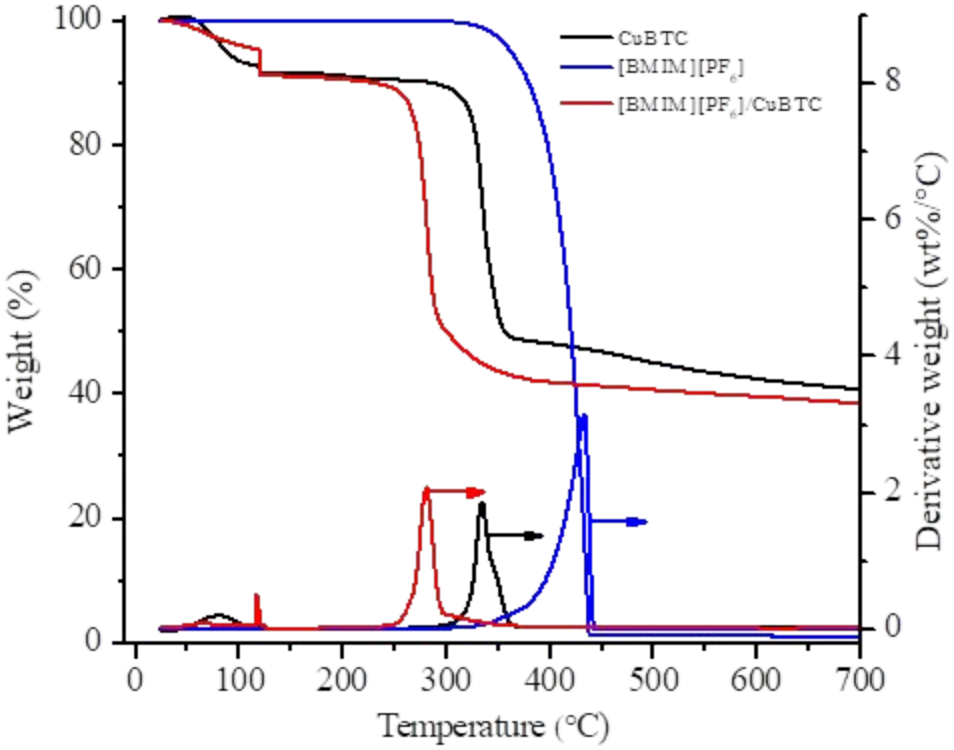

Figure S77. Thermal stability of pristine CuBTC, bulk [BMIM][PF_6], and [BMIM][PF_6]/CuBTC.

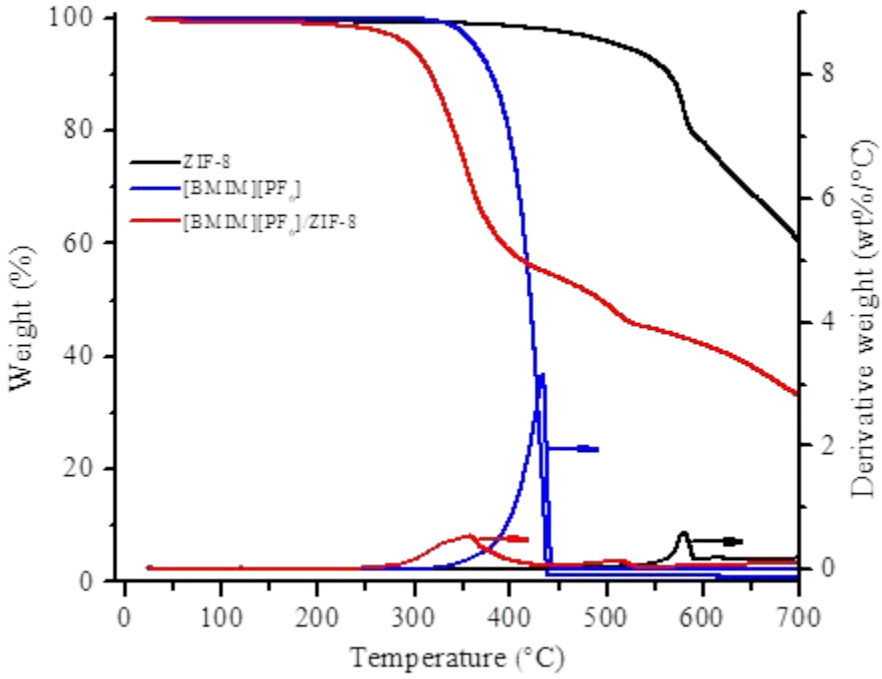

Figure S78. Thermal stability of pristine ZIF-8, bulk [BMIM][PF_6], and [BMIM][PF_6]/ZIF-8.

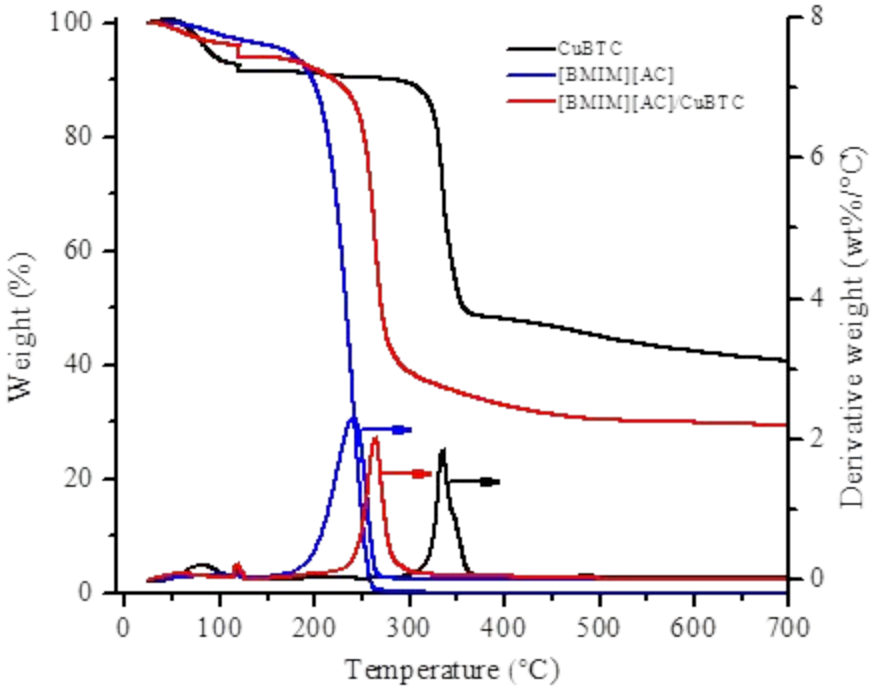

Figure S79. Thermal stability of pristine CuBTC, bulk [BMIM][AC], and [BMIM][AC]/CuBTC.

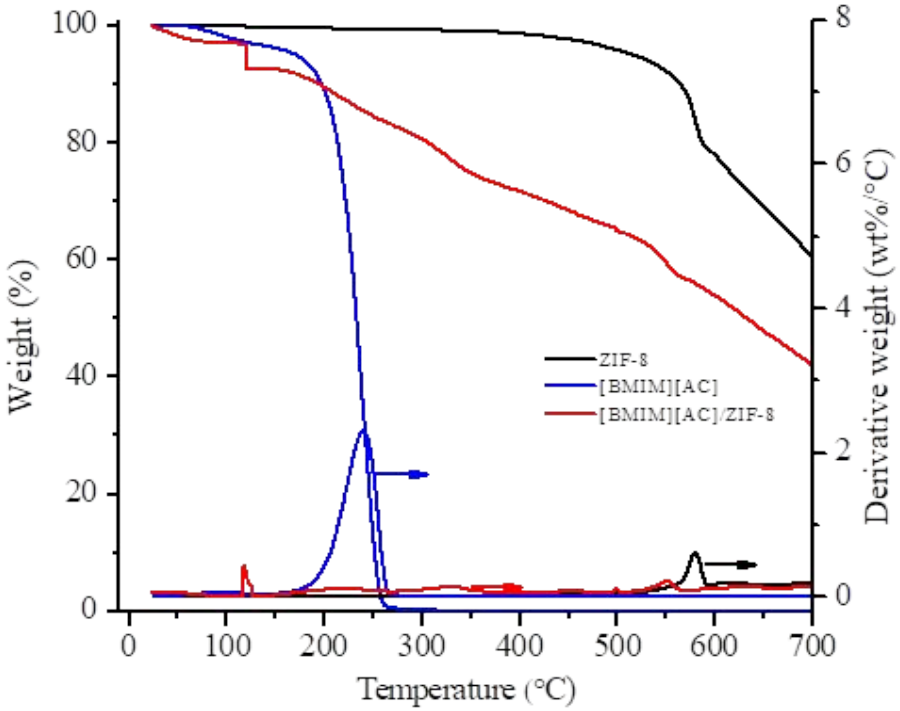

Figure S80. Thermal stability of pristine ZIF-8, bulk [BMIM][AC], and [BMIM][AC]/ZIF-8.

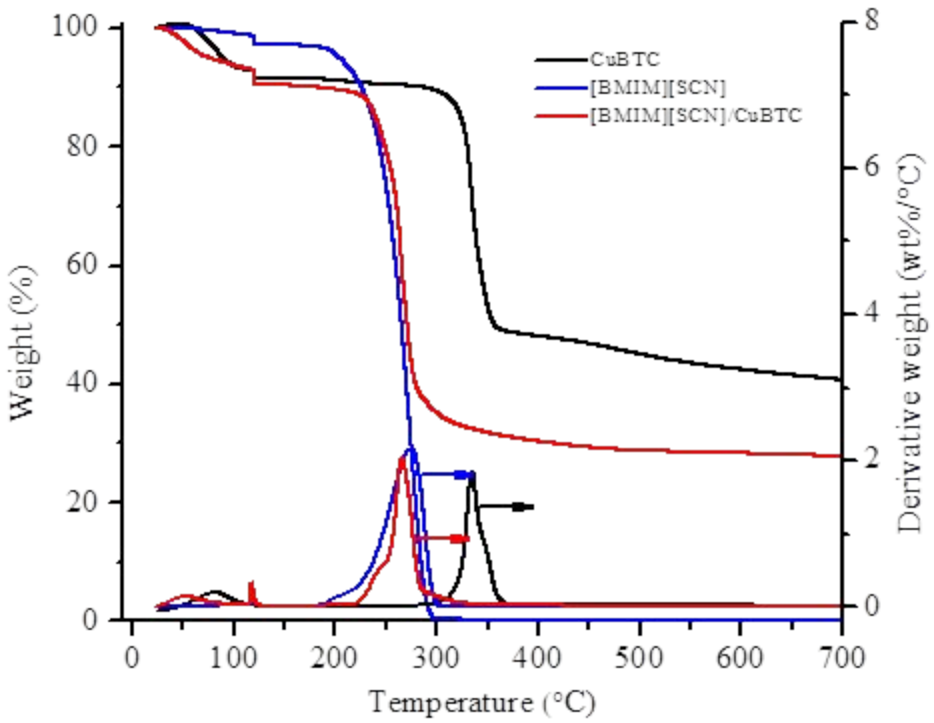

Figure S81. Thermal stability of pristine CuBTC, bulk [BMIM][SCN], and [BMIM][SCN]/CuBTC.

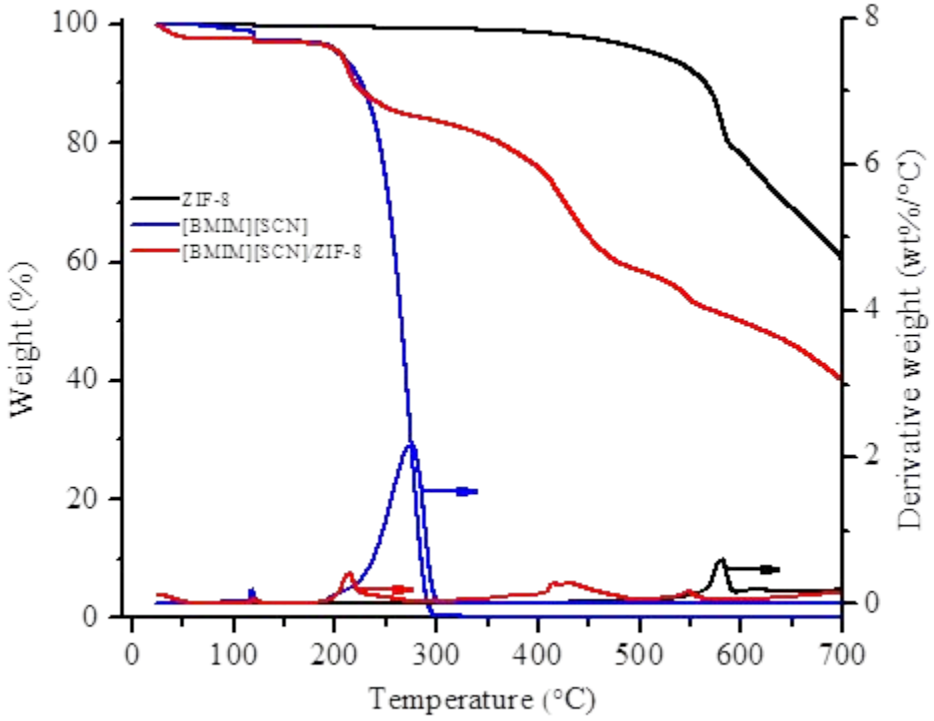

Figure S82. Thermal stability of pristine ZIF-8, bulk [BMIM][SCN], and [BMIM][SCN]/ZIF-8.

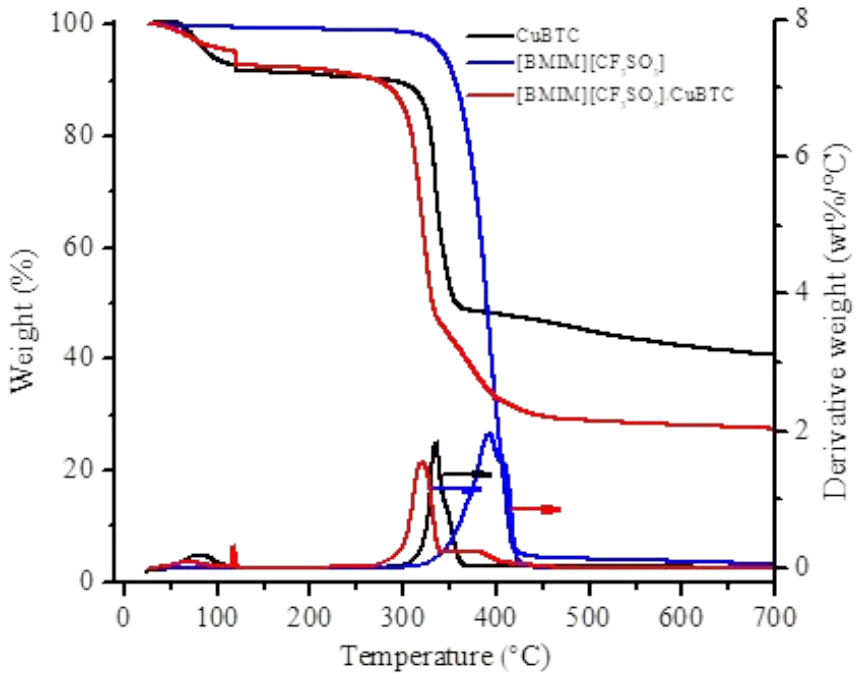

Figure S83. Thermal stability of pristine CuBTC, bulk [BMIM][CF_3SO_3], and [BMIM][CF_3SO_3]/CuBTC.

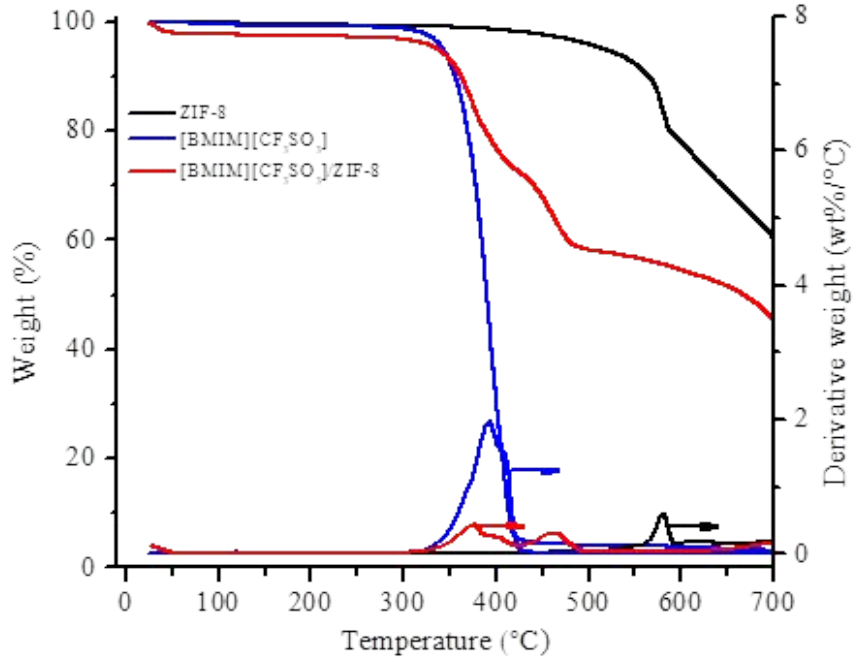

Figure S84. Thermal stability of pristine ZIF-8, bulk [BMIM][CF_3SO_3], and [BMIM][CF_3SO_3]/ZIF-8.

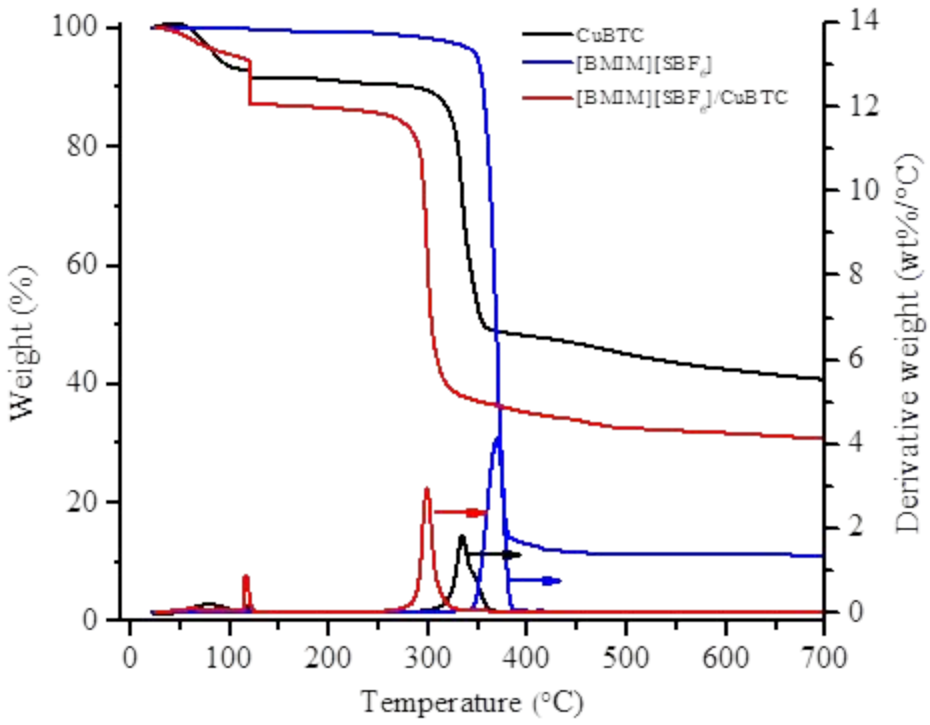

Figure S85. Thermal stability of pristine CuBTC, bulk [BMIM][SbF_6], and [BMIM][SbF_6]/CuBTC.

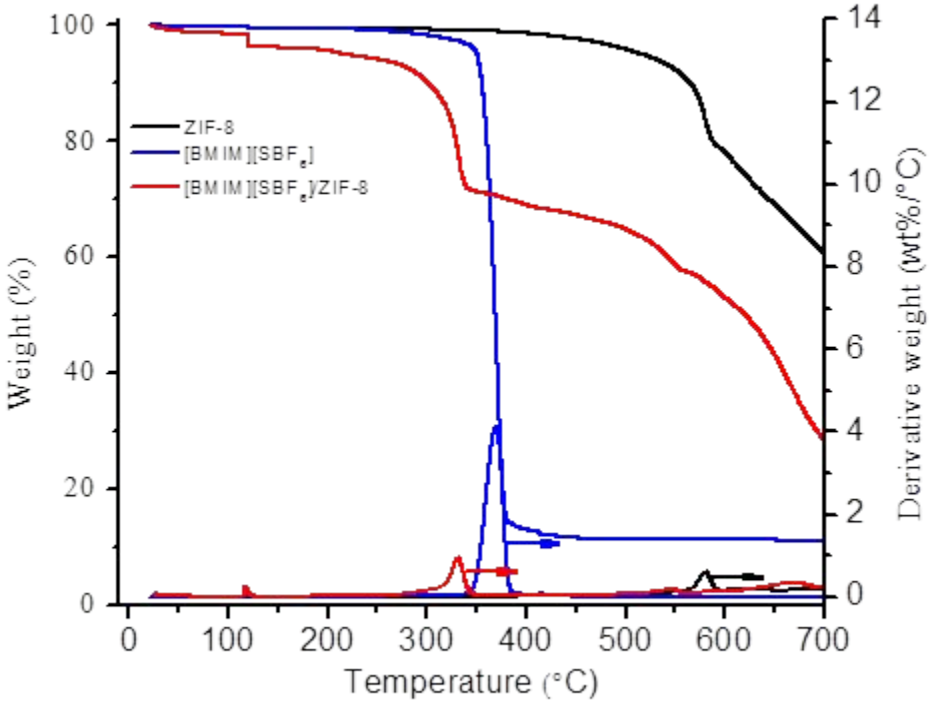

Figure S86. Thermal stability of pristine ZIF-8, bulk [BMIM][SbF_6], and [BMIM][SbF_6]/ZIF-8.

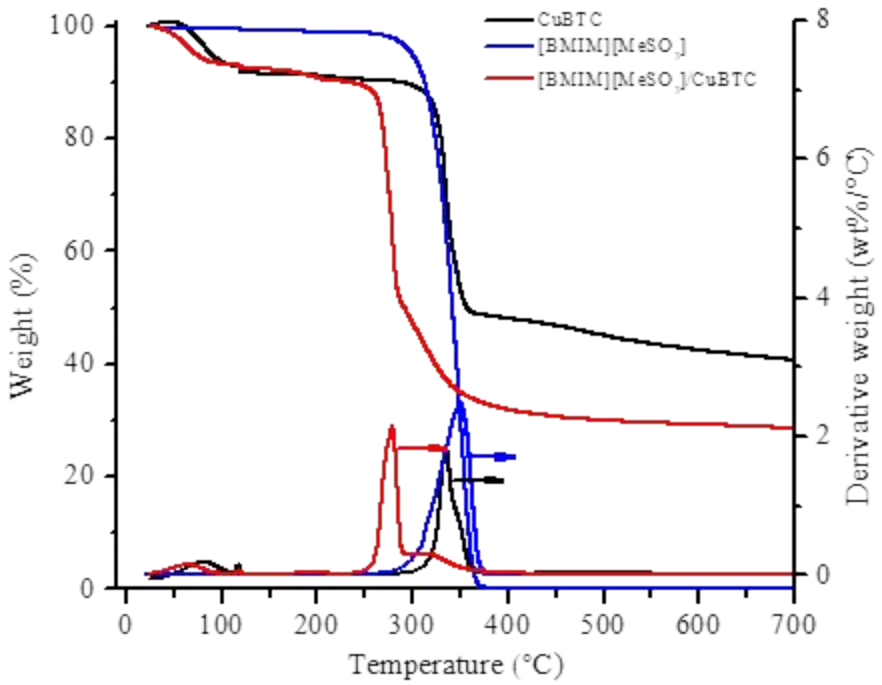

Figure S87. Thermal stability of pristine CuBTC, bulk [BMIM][$MeSO_3$], and [BMIM][$MeSO_3$]/CuBTC.

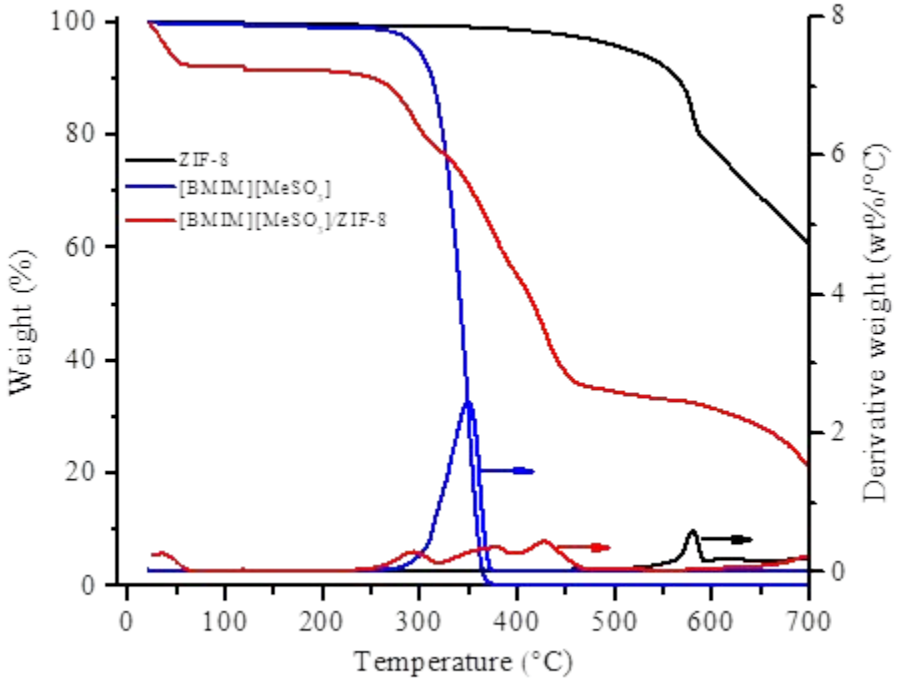

Figure S88. Thermal stability of pristine ZIF-8, bulk [BMIM][$MeSO_3$], and [BMIM][$MeSO_3$]/ZIF-8.

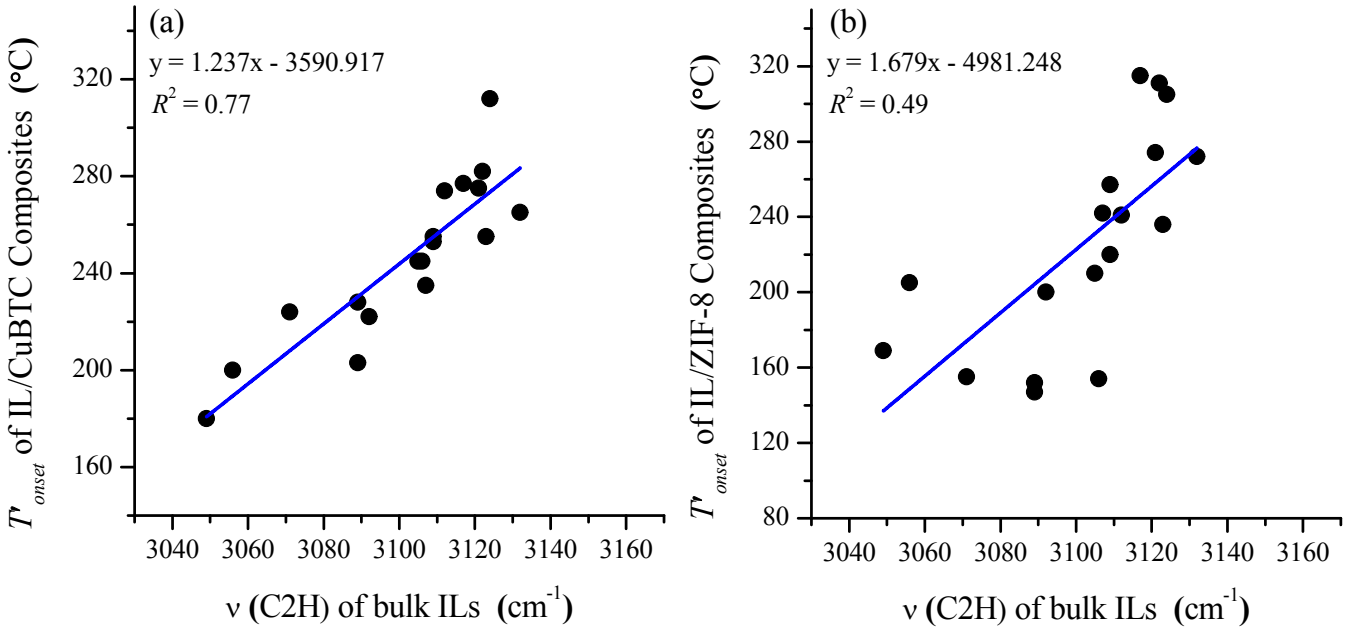

Figure 89. Relation between T'_{onset} of IL/MOF composites and ν(C2H) of bulk ILs: (a) IL/CuBTC composites; (b) IL/ZIF-8 composites.

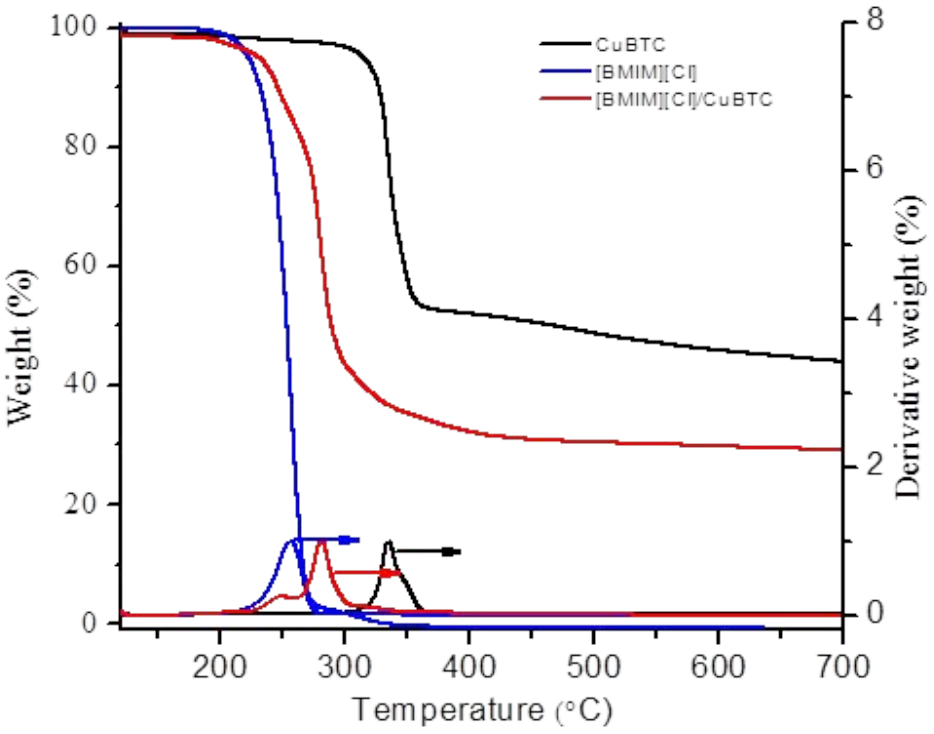

Figure 90. Thermal stability of pristine CuBTC, bulk [BMIM][Cl], and [BMIM][Cl]/CuBTC.

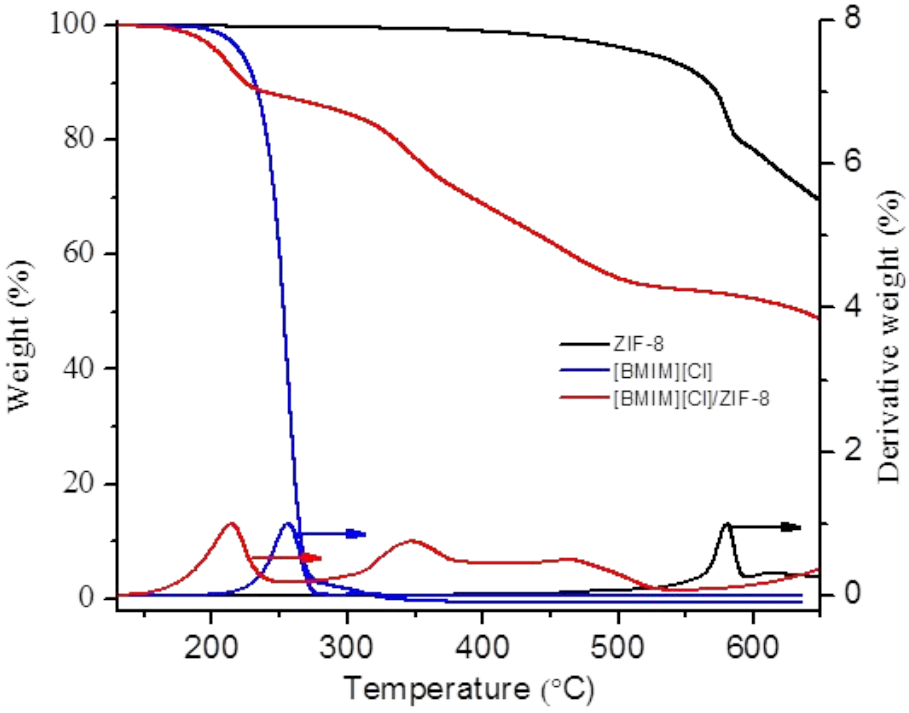

Figure 91. Thermal stability of pristine ZIF-8, bulk [BMIM][Cl], and [BMIM][Cl]/ZIF-8.

Table S4. Structural descriptor of cations considered for QSPR analysis.

Cations	E_{HOMO} (eV)	E_{LUMO} (eV)	Dipole (debye)	CPK Area (Å²)	CPK Ovality	CPK Volume (Å³)	Polarizability (m^3)	ZPE (kJ/mol)
EMIM	-11.91	-5.23	1.67	160.59	1.26	135.44	50.78	442.07
BMIM	-11.8	-5.14	5.67	201.11	1.34	172.26	53.77	591.36

Table S5. Structural descriptor of anions considered for QSPR analysis.

Anions	E_{HOMO} (eV)	E_{LUMO} (eV)	Dipole (debye)	CPK Area (Å²)	CPK Ovality	CPK Volume (Å³)	Polarizability (m^3)	ZPE (kJ/mol)
PF_6	-5.54	4.06	0	103.96	1.21	75.2	45.21	47.57
$MeSO_3$	-1.97	3.4	4.12	97.76	1.18	71.05	45.87	130.54
CF_3SO_3	-2.93	3.78	4.11	115.64	1.23	85.53	46.73	69.45
Ac	-0.97	3.78	3.85	81.54	1.11	59.49	45.07	125.67
TFA	-2.26	4.12	4.7	99.24	1.16	73.96	45.86	66.24
$OcSO_4$	-2.52	1.57	20.43	250.73	1.47	208.61	57.33	660.84
SbF_6	9.68	-11.56	0	115.97	1.26	83.4	43.21	42.39
$MeSO_4$	-2.45	3.28	4.06	108.48	1.21	79.61	46.48	142.68
DCA	-1.79	3.76	1.02	86.61	1.12	64.27	45.28	55.33
SCN	-1.09	3.98	1.66	69.54	1.07	49.4	44.18	22.6
BF_4	-4.55	4.45	0	77.27	1.1	55.06	43.72	36.26
NTf_2	-4.37	3.04	0.24	203.57	1.44	157.62	52.41	137.09
DEP	-2.51	2.83	6.88	177.75	1.35	141.69	51.6	390.72
Cl	-0.74	6.2	0	39.9	1	23.7	41.65	0

Table S6. Coefficients of the multiple linear regression models.

Composite	b_0	*CPK ovality* *(cation)*	*Dipole* (cation)	$E_{HOMO\ (anion)}$	$E_{LUMO\ (anion)}$	*CPK area* *(anion)*
IL/CuBTC	-61.305779	141.584973	-	-1. 078196	-	8.233680
	CPK volume *(anion)*	*Polarizability* (anion)	*ZPE* *(anion)*	R^2	Multiple R	Adjusted R^2
	-9.535733	-	-	0.99	0.99	0.99
IL/ZIF-8	b_0	*CPK ovality* *(cation)*	*Dipole* (cation)	$E_{HOMO\ (anion)}$	$E_{LUMO\ (anion)}$	*CPK area* *(anion)*
	-123.204190	-	6.495490	-17.891239	-20.423683	-
	CPK volume *(anion)*	*Polarizability* (anion)	*ZPE* *(anion)*	R^2	Multiple R	Adjusted R^2
	-	8.071835	-0.280061	0.99	0.99	0.96

Units= *Dipole (debye)*; E_{HOMO} *(eV)*; E_{LUMO} *(eV)*; *CPK volume* ($Å^3$); *CPK Area* ($Å^2$); *Polarizability* (m^3); *ZPE (kJ/mol)*.

Multiple R is the correlation coefficient and shows how strong the linear relationship between dependent and independent variables. R^2 values generally increased when a new parameter is added to the model, while adjusted R^2 values only increase when the newly added parameter improves the quality of the fit.

References:

(1) Sezginel, K. B.; Keskin, S.; Uzun, A. Tuning the Gas Separation Performance of CuBTC by Ionic Liquid Incorporation. *Langmuir* **2016**, *32* (4), 1139–1147.

(2) Koyuturk, B.; Altintas, C.; Kinik, F. P.; Keskin, S.; Uzun, A. Improving Gas Separation Performance of ZIF-8 by [BMIM][BF_4] Incorporation: Interactions and Their Consequences on Performance. *J. Phys. Chem. C* **2017**, *121* (19), 10370–10381.

(3) Nozari, V.; Keskin, S.; Uzun, A. Toward Rational Design of Ionic Liquid/Metal-Organic Framework Composites: Effects of Interionic Interaction Energy. *ACS Omega* **2017**, *2* (10), 6613–6618.

(4) Zeeshan, M.; Keskin, S.; Uzun, A. Enhancing CO_2/CH_4 and CO_2/N_2 Separation Performances of ZIF-8 by Post-Synthesis Modification with [BMIM][SCN]. *Polyhedron* **2018**, *155*, 485–492.

(5) Nozari, V.; Zeeshan, M.; Keskin, S.; Uzun, A. Effect of Methylation of Ionic Liquids on the Gas Separation Performance of Ionic Liquid/Metal-Organic Framework Composites. *CrystEngComm* **2018**, *20* (44), 7137–7143.

(6) Kinik, F. P.; Altintas, C.; Balci, V.; Koyuturk, B.; Uzun, A.; Keskin, S. [BMIM][PF_6] Incorporation Doubles CO_2 Selectivity of ZIF-8: Elucidation of Interactions and Their Consequences on Performance. *ACS Appl. Mater. Interfaces* **2016**, *8* (45), 30992–31005.